Experimental investigation of the spatial and temporal variation of rocking armour units

Rocking revisited V

Daan Houtzager

Master thesis

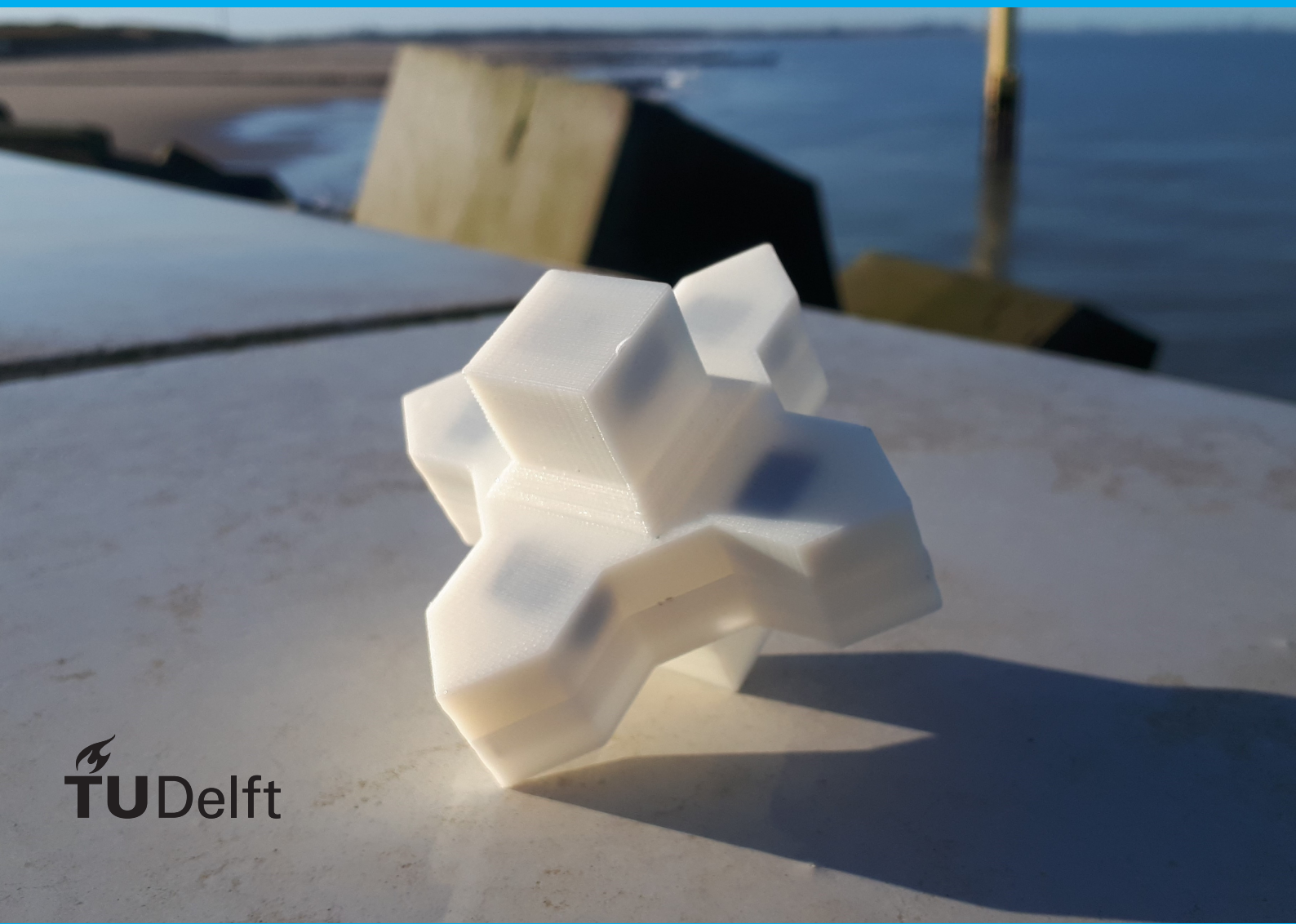

TU Delft

Experimental investigation of the spatial and temporal variation of rocking armour units
Rocking revisited V

by

Daan Houtzager

at the Delft University of Technology,

Student number:	4248031	
Project duration:	September, 2019 – July, 2020	
Thesis committee:	Dr. ir. B. Hofland	TU Delft, supervisor
	Dr. ir. A. Antonini	TU Delft
	Dr. ir. R.W. Hut	TU Delft
	Dr. ir. M.R.A. van Gent	Deltares
	Ir. J.C. van der Lem	Royal HaskoningDHV
	Ir. P. Bakker	Delta Marine Consultants

TU Delft

Preface

Deze thesis vormt het laatste onderdeel van mijn master hydraulic engineering, met een specialisatie in coastal engineering. Tevens markeert dit het einde van mijn mooie studententijd aan de TU Delft. Het onderzoek naar rocking Xbloc units was een leerzaam, uitdagend en motiverend project. waarbij ik de kennis van mijn studie en vaardigheden zoals organiseren en problemen oplossen, heb kunnen combineren tot een afstudeeronderzoek waar ik zeer tevreden over ben. Een groot project als dit is natuurlijk niet iets wat je alleen kunt doen en daarom wil ik graag nog wat mensen bedanken voor hun hulp en ondersteuning.

Allereerst wil ik mijn afstudeercommissie, bestaande uit: Bas Hofland, Alessandro Antonini, Rolf Hut, Marcel van Gent, Cock van der Lem en Pieter Bakker bedanken voor hun ondersteuning en positiviteit gedurende het onderzoek. In het speciaal wil ik Bas bedanken voor de mogelijkheid om te werken aan het rocking onderzoek van de TU Delft.

Daarnaast wil ik graag Sander de Vree, Jaap van Duin, Arno Doorn, Pieter van der Graag en Frank Kalman bedanken voor de ondersteuning bij het voorbereiden en uitvoeren van de experimenten in het Waterlab.

Verder wil ik Rutger en Laurens bedanken voor hun hulp met het 3D printen en de software van de Smart Xbloc. En bedankt aan: Almaz, Daniël, Gijs van G, Gijs V, Ingo, Jarl, Joëll, Ruben, Stach, Tim B, Tim R, Willie & Zach voor het lezen van en de feedback op het geschreven gedeelte van mijn Thesis.

Als laatste wil ik mijn ouders, broer en zussen: Marc, Hennie, Isabelle, Frederique en Karel bedanken voor hun ondersteuning in het algemeen.

Daan Houtzager
Delft, juli 2020

Summary

This section summarizes the master thesis by Daan Houtzager (2020), titled: Experimental investigation of the spatial and temporal variation of rocking armour units. The focus of this research is on rocking of armour units, applied in a single layer on a breakwater. The development of the smart Xbloc makes it possible to measure accelerations and angular velocity with a stand alone sensors at a sampling frequency of around 100 Hz.

Armour units under wave loading can sometimes start to move back and forth, this phenomenon is known as rocking. Rocking can lead to significant impacts between armour units, which can result in breakage. This is especially important for single layer armour units, like the Xbloc. The current literature does not provide the spatial distribution of the number of impacts and the impact velocities due to rocking. Furthermore, only limited knowledge is available on the distribution in time. The research aim of this thesis is:

- Determining the spatial and temporal distribution of the number of moving armour units, the number of impacts and the impact velocity of rocking armour units.

To achieve this aim the following innovations have been made compared to previous rocking studies: The number of sensors was increased, allowing to measure rocking with 10 smart Xbloc units during the model tests. An auto-calibration method for the accelerometer has been implemented to the smart Xbloc. A tool has been developed to visualize the rotations of the smart Xbloc in 3D to validate the movements. The executed test program consists of a large number of repetitions to capture a wide range of data to determine the spatial variation of rocking. The measurement data has been used to calculate new parameters like the linear velocity and the angle of rotation. An observation form was created and used to do visual observations during testing. The angle of rotation is compared to the visual observations.

A physical scale model was set up at the Hydraulic Engineering Laboratory of the TU Delft. A section of a breakwater, situated in deep water, was created in a wave flume and loaded with irregular waves. The model was built with an impermeable core and large water depth to ensure some rocking of the armour units. Ten smart Xbloc units were embedded in the armour layer of the breakwater model. Due to the large number of sensors and many repetitions with the same wave conditions enough data has been collected to accurately measure the variation of rocking. During testing, the sensors were placed at still water level (SWL) and $2d_n$ above and below SWL. The collected data has been processed to find all separate movements, called events. Over 45.000 of these events were found, for each event the impact velocity has been determined.

During testing each smart Xbloc measured at least some movements, the number of impacts can be used to describe the spatial variation of rocking. The number of moving units is much higher than previously reported, which is attributed to the use of the smart Xbloc because it provides much more detailed measurements than conventional measurement techniques.

The number of impacts can be described with a lognormal distribution, depending on the location on the slope as well as on the stability number. The number of impacts per 1000 waves is found to vary between less than 10 up to almost 1000, a typical rocking motion consists of tho impacts. This indicates that the number of impacts depends not only on wave condition but is dominated by the movement space of the armour unit. At still water level the largest number of impacts per 1000 waves was found. Also, at SWL the number of impacts increased during the first test runs but it decreased significantly after around 4800 waves, while the wave height was increased.

It has been found that the impact velocity, exceeded by 2% of the events ($v_{i,2\%}$), is strongly dependent on the location on the slope. At SWL the impact velocity ($v_{i,2\%}$) increases with increasing wave height. While, above and below the SWL the impact velocity ($v_{i,2\%}$) is more or less constant for increasing wave heights. The highest impact velocities are found at SWL.

The collected data, analysis and results provide a unique look into the behaviour of single layer armour units. The results can be used to validate rocking models and provide valuable statistical information on the number of impacts and the impact velocities.

List of symbols and abbreviations

A	Acceleration vector	-
a	Acceleration	m/s^2
a	Acceleration vector	-
a_x,a_y,a_z	Acceleration in x, y and z direction	m/s^2
$alpha$	Rotation angle	deg
b	Acceleration vector	-
C	Correction factor	-
c	Wave celerity	m/s
CDF	Cumulative density function	-
d	Water depth	m
D_n or d_n	Nominal diameter	m
DMC	Delta Marine Consultants	-
E	Cumulative error	-
e_k	Error of measurement k	-
E_i	Error due to a rotation within an event (m/s) for one axis, with i=x,y,z	-
$E_{k,n}$	Kinetic energy of the impact per event	J
$E_{k,total}$	Total kinetic energy from all events	J
E_t	Error per time step	m/s
E_T	Cumulative error	m/s
$F(v_i)$	Cumulative density of the impact velocity	m/s
g	Gravitational acceleration	9.81 m/s^2
GPD	Generalized Pareto distribution	-
h	Wave height	m
h	Height of Xbloc	m
H_s	Significant wave height	m
$H_{m0,i}$	Incoming significant wave height	m
k	Wave number	m^{-1}
k	Index parameter	-
L_0	Deep water wave length	m
m	Mass of smart Xbloc	0.141 kg
N	Number of waves	-
N	Number of orientations	-
N_E	Number of events	-
n	Number of events	-
n	Number of data points of an event	-
N_s	Stability number	-
O	Bias vector	-
p	Percentage exceedance probability	%
r	Rotation during event	deg
r_i	Rotation at point i	deg
$r_{tot,i}$	Total rotation at point i	deg
ρ_s	Density stone	kg/m^3
ρ_w	Density water	kg/m^3
S	Scale factor matrix	-

s_{0p}	Wave steepness	-
$S_{i,i}$	Scale factor, i = x,y,z	-
SWL	Still water level	-
t	Time	s
T_p	Peak period	s
V	Acceleration vector	-
v_i	Velocity at point i	m/s or rad/s
$v_{i,angular}$	Angular impact velocity	m/s
$v_{i,linear}$	Linear impact velocity	m/s
$v_{x,i}, v_{y,i}, v_{z,i}$	Velocity in x y and z direction for point i	m/s
$v_{i,p\%}$	Impact velocity given probability of exceedance p	m/s or rad/s
$v_{res,i}$	Resultant linear velocity at point i	m/s
v_x, v_y, v_z	Velocity in x y and z direction	m/s
V_{Xbloc}	Volume Xbloc	m^3
W	Weight	kg
Δ	Relative density	-
Δt	Time interval	s
ξ	Iribarren number	-
μ	Mean	-
ω	Total angular velocity	rad/s
$\omega_x, \omega_y, \omega_z$	Angular velocity around x, y and z axes	rad/s
σ	Standard deviation	-
θ	Location parameter	-
θ	Angle	rad

Contents

Preface iii

Summary v

List of symbols and abbreviations vii

1 Introduction 1
- 1.1 Background . . . 1
- 1.2 Problem description . . . 2
- 1.3 Objective . . . 3
- 1.4 Approach . . . 3
- 1.5 Research Method . . . 3
  - 1.5.1 Physical modelling . . . 3
  - 1.5.2 Research plan . . . 4
- 1.6 Definition of frequently used terms . . . 4

2 Literature Review 5
- 2.1 CUR-70 . . . 5
  - 2.1.1 Test program . . . 5
  - 2.1.2 Number of rocking armour units and impacts . . . 6
  - 2.1.3 Distribution of number of impacts along the slope . . . 6
  - 2.1.4 Distribution of peak accelerations . . . 6
  - 2.1.5 Distribution of impact velocities . . . 7
  - 2.1.6 Review . . . 8
- 2.2 Rocking Revisited I . . . 9
  - 2.2.1 Test Program . . . 9
  - 2.2.2 Number of impacts . . . 9
  - 2.2.3 Probability distribution of impact velocities . . . 9
  - 2.2.4 Additional conclusions of the Thesis . . . 10
- 2.3 Rocking Revisited II . . . 11
  - 2.3.1 Test program . . . 11
  - 2.3.2 Number of rocking units and impacts . . . 11
  - 2.3.3 Impact velocities . . . 11
- 2.4 Smart Rocking Armour Units . . . 12
  - 2.4.1 Physical model tests . . . 12
- 2.5 Rocking revisited III . . . 13
  - 2.5.1 Model Setup . . . 13
  - 2.5.2 Model Tests . . . 13
  - 2.5.3 Conclusion . . . 13
- 2.6 Rocking revisited IV . . . 14
  - 2.6.1 Impact velocity . . . 14

3 Model setup 15
- 3.1 Main dimensions . . . 15
  - 3.1.1 Breakwater base . . . 15
  - 3.1.2 Freeboard . . . 15
  - 3.1.3 Under layers . . . 16
- 3.2 Placement and packing density armour layer . . . 16
- 3.3 Hydrodynamic conditions . . . 16
  - 3.3.1 Stability number . . . 16
  - 3.3.2 Breaker type . . . 17
  - 3.3.3 Wave period . . . 18

3.4 Number of waves . . . 18
3.5 Breakwater state . . . 18
3.5.1 Number of test runs in a test series . . . 19
3.6 Test program . . . 19

4 Model testing **21**
4.1 Testing facility . . . 21
4.2 Breakwater model . . . 21
4.2.1 Under layer . . . 21
4.2.2 Armour layer . . . 22
4.3 Coordinate system armour layer . . . 23
4.4 Sensors . . . 23
4.4.1 Smart Xbloc . . . 23
4.4.2 Mass Smart Xbloc . . . 23
4.4.3 Smart Xbloc validation . . . 24
4.4.4 Camera . . . 24
4.4.5 Wave gauges . . . 25
4.4.6 Visual observations . . . 25
4.5 Measurement overview . . . 25

5 Accelerometer calibration **27**
5.1 Calibration method . . . 27
5.2 Calibration measurement . . . 27
5.3 Data processing . . . 27
5.4 Autocalibration method . . . 30
5.5 Error estimate accelerometer . . . 31

6 Data post-processing **33**
6.1 Coordinate system smart Xbloc . . . 33
6.2 Methodology . . . 34
6.3 Data-transfer errors . . . 36
6.4 Extracting separate test runs . . . 36
6.5 Gyroscope bias correction . . . 36
6.6 Detecting motion events . . . 37
6.6.1 Modulus angular velocity . . . 37
6.6.2 Event extraction . . . 37
6.7 Distribution number of events . . . 38
6.7.1 95% confidence boundary . . . 39
6.8 Angular impact velocity . . . 39
6.8.1 Kinetic energy of the impact . . . 40
6.9 Linear impact velocity . . . 40
6.9.1 Remove gravitational acceleration . . . 40
6.9.2 Linear impact velocity . . . 41
6.10 Distribution impact velocity . . . 42
6.10.1 Angular impact velocity in m/s . . . 44
6.10.2 95% confidence boundary . . . 44
6.11 Differential rotation . . . 45
6.12 Rotation during event . . . 46
6.13 Wave characteristics . . . 47

7 Results **49**
7.1 Number of impacts . . . 49
7.2 Impact velocity . . . 50
7.3 Differential rotation . . . 51
7.4 Rotation during event . . . 51
7.5 Wave conditions . . . 52

8 Analysis **53**
8.1 Number of moving armour units . . . 53
8.2 Number of impacts . . . 53
8.2.1 Mean number of events . . . 54
8.2.2 Spatial variation number of events . . . 54
8.2.3 Extreme values number of events . . . 55
8.3 Impact velocity . . . 55
8.3.1 Extreme values . . . 56
8.3.2 Angular versus Linear impact velocity . . . 56
8.4 Rotation during an event . . . 58
8.4.1 Visual observations . . . 58
8.5 Visual observable rotations . . . 59
8.5.1 Rotation and impact velocity . . . 60

9 Discussion **61**
9.1 Number of impacts . . . 61
9.2 Impact velocity . . . 61
9.2.1 Angular versus linear impact velocity . . . 62
9.3 Visual observations and the Smart Xbloc . . . 62
9.4 Number of events versus number of impacts . . . 63
9.5 Confidence level number of events . . . 63
9.6 Confidence level impact velocity . . . 64
9.7 Spatial and temporal distribution . . . 65
9.8 Literature . . . 65
9.8.1 Number of impacts . . . 65
9.8.2 Impact velocity . . . 65

10 Conclusion **69**

11 Recommendations **71**
11.1 Settlement analysis . . . 71
11.2 Angular and linear velocity . . . 71
11.3 Rocking revisited IV . . . 71
11.4 Smart Xbloc . . . 71

Bibliography **73**

A Measured wave conditions per test series **75**

B Measurement overview **77**

C Calibration values accelerometer **79**
C.0.1 Results calibration . . . 79

D Exceedance curves angular impact velocity **81**

E Differential rotation results **83**

F Extreme value distribution impact velocity **85**
F.1 Angular impact velocity in radians per second . . . 85
F.2 Linear impact velocity . . . 86
F.3 Angular velocity exceedance curves SWL . . . 87
F.4 Angular velocity exceedance curves SWL+2dn . . . 89
F.5 Angular velocity exceedance curves SWL-2dn . . . 91
F.6 Linear velocity exceedance curves SWL . . . 93
F.7 Linear velocity exceedance curves SWL+2dn . . . 95
F.8 Linear velocity exceedance curves SWL-2dn . . . 97

G Impact velocity confidence boundary **99**

H Distributions number of events **101**

I Observations forms **111**

1

Introduction

In January and February 2020, lab experiments were executed in a wave flume at the Hydraulic Engineering Laboratory of the TU Delft. Smart Xbloc sensors were applied in a scale model of a breakwater to measure rocking. This section will give background information on breakwaters and rocking, as well as the problem description, objective and approach to the problem.

1.1. Background

Around the world breakwaters are used to protect coastlines and harbours against waves and currents. The cross section of a rubble mound breakwater is typically composed of several layers of stones, increasing in size. The core is constructed of the smallest stone size and layers of larger stones are placed on top of the core to prevent the smaller stones from washing away. A typical cross section of a breakwater is shown in Figure 1.1.

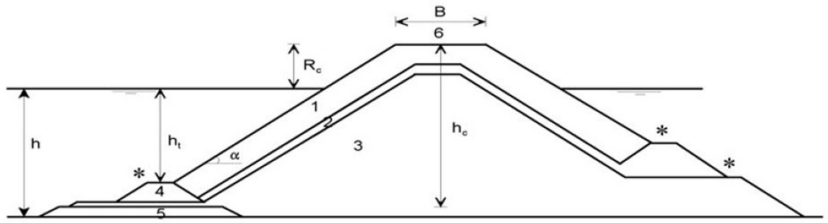

Figure 1.1: Typical cross section of a rubble mound breakwater (van den Bos and Verhagen, 2018)

With ever increasing cargo vessels and larger port sizes, breakwaters are constructed that extend into deeper waters with higher waves. With limited availability of large natural rocks, special concrete blocks, like the Xbloc, were developed for the armour layer, see Figure 1.2. The slender shape of these armour units increases the stability by interlocking and to minimize the volume of concrete needed. To increase the effectiveness of interlocking, the armour units are generally applied on a relatively steep slope. These types of interlocking armour units can be applied in a single layer, which is economically beneficial compared to a double layer.

Under wave loading, armour units can start to move back and forth. This process is called rocking and results in collisions between units, which eventually can lead to breakage. In the period from 1978 to 1980, several well designed breakwaters with a double armour layer failed along the coast of the Mediterranean sea and the Atlantic ocean. An analysis of the damage showed that substantial percentages of the concrete armour units were broken. These events raised awareness of rocking and sparked the first research into this phenomenon. Especially for breakwaters with a single armour layer, the effects of rocking are of importance. As only some damage can be allowed to these structures. Nowadays, breakwaters are still constructed with single layer concrete armour units like the Xbloc, and rocking can still lead to breakage of armour units. The available knowledge on the rocking mechanism

is limited, which makes predicting rocking difficult. The development of a new sensor, as described by Hofland et al. (2018), makes it possible to measure accelerations and angular velocity with a sample rate of around 100 HZ. These sensors are implemented in smart Xbloc units, allowing to measure the rocking behaviour in scale models.

Figure 1.2: Concrete Xbloc armour unit at the Dutch coast

1.2. Problem description

Breakwaters with concrete armour units are designed and constructed all over the world. With the growing size of single layer randomly-placed concrete armour units, rocking is still often the governing failure mechanism (Hofland et al., 2018). Rocking is usually quantified with three parameters:

- The number of rocking armour units
- The number of impacts between armour units
- The impact velocity

The parameters are stochastic, and show variations in both space and time. The number of rocking armour units is often based on visual observation. However, tests with instrumented armour units have shown that this method is underestimating the actual number of rocking armour units and number of impacts. Measurements with instrumented small scale armour units have shown a large variation in the number of impacts, ranging from almost none up to impacts for almost every single wave. The aim of previous studies have been mainly to measure the impact velocities during rocking. Therefore, normal armour units that were rocking visually, were replaced with an instrumented unit. While this method provides statistical data on the variation of rocking in time, the selection of locations does not represent the variation in space. The spatial and temporal variation of rocking armour units on a breakwater are important engineering parameters in order to understand and model breakwaters under wave loading. The current literature does not provide in depth information on the variation of the three mentioned parameters in space and time.

1.3. Objective

The objective of this thesis is to gain knowledge on the spatial and temporal variation of rocking armour units by measuring rocking using the smart Xbloc sensor. From this objective and the problem statement the following research objective for this thesis was formulated:

- Determining the spatial and temporal distribution of the number of moving armour units, the number of impacts and the impact velocity of rocking armour units.

The following sub-objectives have been formulated:

- Comparison of linear and angular impact velocity. The impact velocity can be determined with two methods. The first method is to integrate the acceleration which results in the linear velocity. The second method is to read the impact velocity directly from the gyroscope data.
- Increase the accuracy, confidence and robustness of the smart Xbloc as a tool for measuring rocking by:
  - improving the data processing to extract more parameters like the rotation and differential rotation.
  - Defining event characterization to extract impacts from a large amount of data.
  - Integration of accelerometer data to determine the linear velocity.
  - Validating the sensor using a 3D visualization tool.
  - Implementing a calibration method for the accelerometer to make an error estimation.

The following research questions have been formulated:

- How many impacts does a single armour unit experience and how does the number of impacts depend on the location and the stability number?
- What are the impact velocities and how do the impact velocities vary for different locations and stability numbers?
- How large is the angle of rotation per movement and how does this rotation compare to the visual observations?

1.4. Approach

The approach to the problem is summarized in the following steps.

- Analysis of the available literature on rocking of armour units and the stability of Xbloc armour units.
- Creating a physical scale model of a breakwater and measuring accelerations and angular velocity, using 10 smart Xbloc units.
- Analysis of the measurement data to determine the variation of the three parameters.

1.5. Research Method

First, the motivation for using a physical model will be discussed. The second part will provide the research plan.

1.5.1. Physical modelling

Physical modelling is a tool that is widely used in hydraulic engineering. There are many engineering problems that cannot be simulated with numerical models. For this research, it was decided to set up a physical model because of the following reasons:

- Physical modelling allows insight in the rocking behaviour of armour units, without simplifying assumptions, that would have to be made for analytical or numerical models. Also, there is no data available to verify if the assumptions would be justified.

- The Smart Xbloc is a new sensor that is capable of measuring rocking with a sample frequency of around 100 Hz and without any wires attached during testing. It has never before been possible to do these kind of measurements.
- An analytical model for rocking Xbloc units has been developed by Goud, (2020). This model is based on assumed distributions for several parameters, some of these assumptions can be verified using data from a physical model.

1.5.2. Research plan

Based on the above described steps a research plan has been designed to execute the experiments. The research plan consists of the following steps:

- A setup for the model will be made, considering the main dimensions of the breakwater and the placement and design of the armour layer. Also, a test program for the model tests is made, containing the hydraulic conditions, like the significant wave height, number of waves and wave steepness.
- 10 smart Xbloc units will be built and used to measure rocking. It is believed that, by using in the order of ten instrumented armour units, a sensible estimate of the spatial statistics of the variation in rocking can be made (Hofland et al., 2018).
- Several sensors are used during the model testings. To measure rocking, the smart Xbloc is used; the hydraulic conditions are measured with three wave gauges; a camera is placed to measure the settlements after each test run; an observations form is created to keep track of visual observations.
- The test program will be executed by doing several repetitions with the same test conditions. Repetitions are necessary to measure a wide range rocking and capture the spatial distribution.
- The data from the model tests will be analyzed, calculating the impact velocity and determining the number of impacts. These results will be used to determine the temporal and spatial variation of rocking.
- The auto-calibration method, as proposed by Frosio et al. (2009), for an accelerometer, will be implemented to be used for the smart Xbloc.

1.6. Definition of frequently used terms

Some of the frequently used terms might cause confusion. Therefore, the following definitions will be used in this thesis.

- Test series: a test series consists of 5 test runs.
- Test run: a test run is one test in the lab with one wave series.
- Wave series: a wave series consists of around 1200 waves. 5 wave series with increasing wave height have been used during each test series.

2

Literature Review

This chapter describes the outcome of the literature review, about research on rocking of armour units.

2.1. CUR-70

In the period from 1978 to 1980, several well designed breakwaters failed along the coast of the Mediterranean sea and the Atlantic ocean. An analysis of the damage showed that substantial percentages of the concrete armour units were broken. These events showed that the design guidelines fell short and led to a multidisciplinary research, where both the hydraulic and the concrete aspects were integrated. This research project was coordinated by the Centre for Civil Engineering Research and Codes work-group C70 (CUR, 1990).

A model was created and scale tests were performed with instrumented Cube and Tetrapod armour units. The number of moving armour units, the number of collisions and the impact velocity were measured. As it was not possible to recreate the impact characteristics properly, the acceleration signal was integrated to find the impact velocity, which can be scaled to be used for prototype conditions (Van der Meer and Heydra, 1991).

2.1.1. Test program

The number of moving units was recorded by overlay and single frame technique. The impact velocities at a number of locations were measured with instrumented units. Measurements were performed at four depths, $y/d_n = +2, 0, -2, -4$, where d_n is the nominal diameter and y is the vertical distance to the still water line (SWL). An example of an acceleration measurement can be found in Figure 2.1.

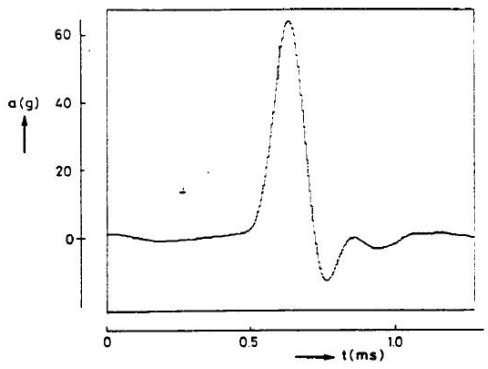

Figure 2.1: Example of an acceleration measurement (Tetrapod) (CUR, 1990).

During testing, the location of the instrumented unit was chosen as a location where a rocking movement did occur at that moment. This was done to ensure a reading of the accelerometer. An extreme value in terms of spatial distribution was chosen, without specification of the spatial exceedance value that was chosen. Therefore, the data represents the variation of rocking in time, but not in space.

2.1.2. Number of rocking armour units and impacts

To determine the number of moved units $N_{o,mov}$, a curve was created from the measurements and compared it to the curve of the general stability formula by van der Meer (1988). This resulted in the following equations:
For Cubes in a double layer:

$$H_s/(\Delta D_n) = b(6.7N_{o,mov}^{0.4}/N^{0.3} + 1.0)s_m^{-0.1} - 0.5 \tag{2.1}$$

For Tetrapodes:

$$H_s/(\Delta D_n) = b(3.75N_{o,mov}^{0.5}/N^{0.25} + 0.85)s_m^{-0.2} - 0.5 \tag{2.2}$$

Where N is the number of waves and S_m is the wave steepness. The total number of impacts $N_{o,imp}$ was assumed to be roughly three times the number of movements.

$$N_{o,imp} = 3N_{o,mov} \tag{2.3}$$

2.1.3. Distribution of number of impacts along the slope

Using the single-frame-technique, it was found that most units moved in a wide band around still water level (SWL). However, it was not possible to measure movements below $0.5 - 1.0H_s$. The distribution of the number of impacts was assumed to be more or less uniform from SWL to the toe (Van der Meer and Heydra, 1991). From the analysis it was concluded that the upper level of movement was around $1H_s$ above SWL. Also, it was (arbitrarily) assumed that the number of impacts above SWL was linearly decreasing from SWL to $1H_s$ above SWL. This resulted in an assumed distribution of impacts along the slope as shown in Figure 2.2.

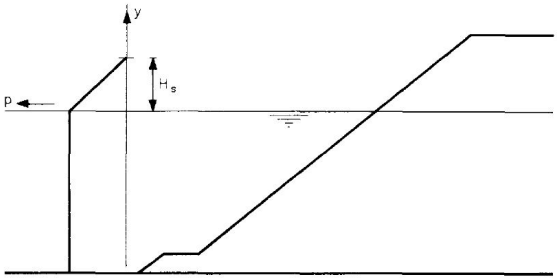

Figure 2.2: Assumed distribution of number of impacts along the slope (Van der Meer and Heydra, 1991).

2.1.4. Distribution of peak accelerations

Multiple exceedance curves were created, as shown in Figure 2.3. An exponential distribution with a threshold level describes the type of curves in Figure 2.3. The general expression for the probability of exceedance, Equation 2.4, was proposed (Van der Meer and Heydra, 1991).

$$p(a/g) = exp[-(a/g - c)/b] \tag{2.4}$$

- $p(a/g)$ = probability of exceedance
- c = threshold level
- b = scale parameter
- a = peak acceleration (m/s^2)
- g = gravitational acceleration ($9.81 m/s^2$)

The proposed threshold level c, Equation 2.5, was applied because low wave heights produced not only impacts, but also small peaks caused by small movements without impacting another unit. Therefore, it was assumed that an impact was only present if a certain threshold value c was exceeded. This value c was assumed independent of the wave height and only dependent on the location of the unit.

$$c = 10exp[-d_1|y/D_n|] \tag{2.5}$$

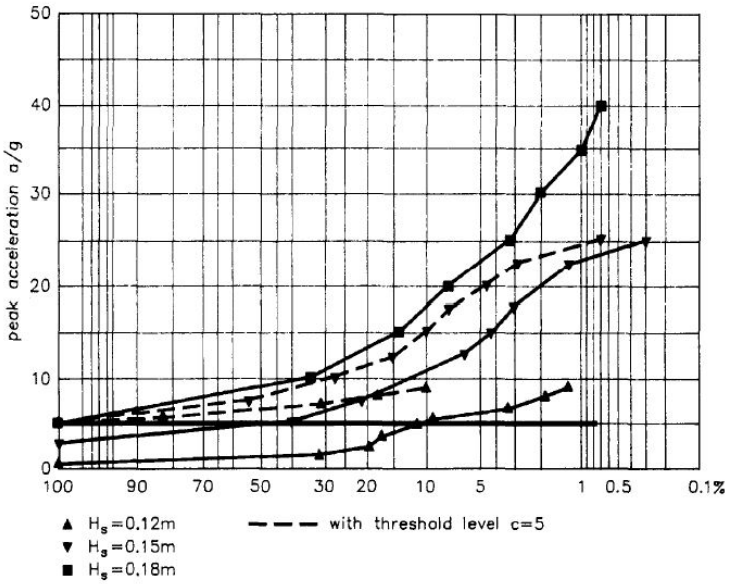

Figure 2.3: Example of exceedance curves for the peak acceleration (Van der Meer and Heydra, 1991).

The parameter b in Equation 2.4, determines the location of the curve and depends on the wave height, or the stability number $H_s/\Delta D_n$. A linear relation between b and H_s/D_n was assumed and can be calculated using Equation 2.6, Van der Meer and Heydra (1991).

$$b = 5H_s/\Delta D_n exp(-d_2|y/D_n|) \tag{2.6}$$

Because the peak accelerations did not show large differences between Cubes and Tetrapods, Equation 2.4, 2.5 and 2.6 are valid for both Cubes and Tetrapods applied in a double layer.

2.1.5. Distribution of impact velocities

Substitution of the relationship between peak acceleration and impact velocity, gave the following expressions for the distribution of the impact velocities at the centre of the units (Van der Meer and Heydra, 1991).
For Cubes:

$$p\left(\frac{v}{\sqrt{gD_n}}\right) = exp\left(\left(-\frac{v}{\sqrt{gD_n}} - c\right)/b\right) \tag{2.7}$$

with:

$$c = 0.049exp\left(-d_1\left|\frac{y}{D_n}\right|\right) \tag{2.8}$$

$$b = 0.025\frac{H_s}{\Delta D_n}exp\left(\left|\frac{y}{D_n}\right|\right) \tag{2.9}$$

For Tetrapods:

$$p\left(\frac{v}{\sqrt{gD_n}}\right) = exp\left(\left(-\frac{v}{\sqrt{gD_n}}^{1.43} - c\right)/b\right) \tag{2.10}$$

with:

$$c = 0.0103exp\left(-d_1\left|\frac{y}{D_n}\right|\right) \tag{2.11}$$

$$b = 0.0051\frac{H_s}{\Delta D_n}exp\left(-d_2\left|\frac{y}{D_n}\right|\right) \tag{2.12}$$

2.1.6. Review

The CUR C70 is a very extensive research on rocking covering both on the strength of the material as well as the forcing. The following remarks were made after the analysis:

- Measuring the number of rocking units was done by overlay- and single-frame-technique. The accuracy of this method is low, as was shown with measurements from Le (2016). This technique was not capable of measuring all the way down to the toe. The formula to determine the total number of moved units, Equation 2.3, is therefore not accurate.
- The location of the instrumented unit was changed to a location where movement did occur. Therefore it gives statistical data on the temporal distribution of the accelerations. However, it does not provide information on the spatial distribution of impacts.
- During testing the instrumented unit was connected to a computer via a wire. This wire could influence the movements. This problem can be solved with the development of a stand alone instrumented unit.
- The instrumented unit could only measure accelerations in one direction. Therefore the rocking movement could not be captured completely. Also, no distinction between translational and rotational motions could be made.
- The measurements were done with a single instrumented unit in each test. Therefore, the results probably do not cover the whole range of possible impact velocities.

2.2. Rocking Revisited I

At the TU Delft research on rocking was continued by Tuan Le (2016) in his master thesis: Rocking of a Single Cube on a Breakwater Slope. The objective of the thesis was:

- Obtaining knowledge on, and measurements of the rocking behaviour and failure mode of single layer armour units.

For this purpose, an analytical model was created and scale model tests were performed. A big difference with previous research was the method of finding the impact velocity, which was not based on measuring the accelerations of the impact directly, but by measuring the angular velocity ω. This method was expected to be more reliable and required a much lower sample frequency, the approach is illustrated in Figure 2.4.

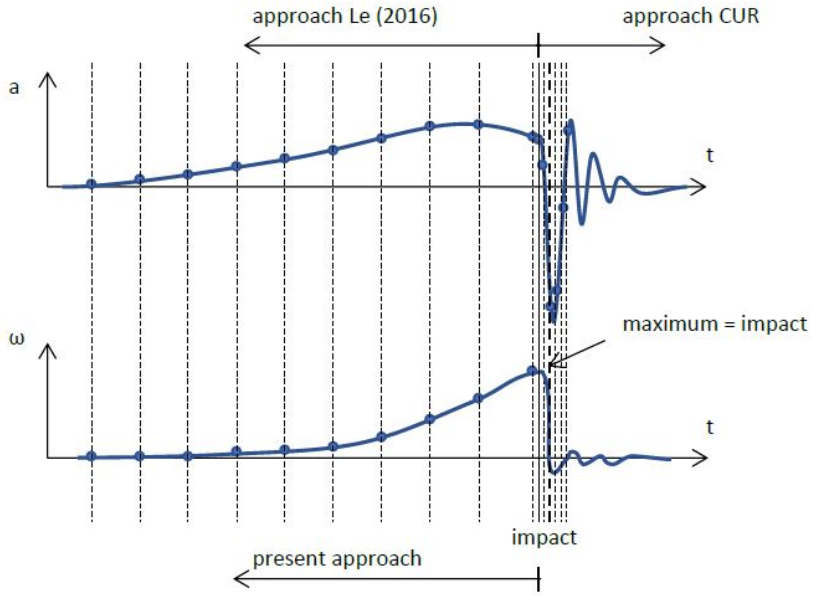

Figure 2.4: Schematic representation of the time variations of acceleration α and angular velocity ω during rocking and collision (Hofland et al., 2018).

2.2.1. Test Program

The setup for for the experiments consisted of two configurations: a single cube on a slope and a cube that is embedded in a slope of multiple cubes. One cube was fitted with an accelerometer with a high sampling frequency. The cube was connected to the slope with a hinge and connected to a computer via a wire. A second cube was attached to the slope (static), and fitted with a pressure sensor. The cubes were located at the same levels as the CUR C70 research program.

2.2.2. Number of impacts

The CUR C70 research assumed an average of three collisions per cube, this was found to be inaccurate. The number of collisions appeared to depend on many parameters such as wave height, wave steepness, position on slope and degree of exposure of the cube to wave attack. For some of the tested conditions the number of collisions was very high (Le, 2016). For further research, it was proposed to take the number of collisions into account as a variable that is dependent on the hydraulic and geometric conditions.

2.2.3. Probability distribution of impact velocities

It was found that the data could be described by a Weibull distribution. This is different from the CUR C70 research, where an exponential distribution was proposed. This was addressed to the fact that the wave steepness parameter was not used in the CUR C70 research. However, the difference between the exponential and Weibull distribution was small.

2.2.4. Additional conclusions of the Thesis

- The location $y/D_n = -2$ is normative in terms of design because it resulted in the lowest stability number (Le, 2016).
- The output of the analytical model was compared with the test results of the regular wave series, and showed that the analytical model has similar dependencies regarding the wave height and wave steepness. It was found that the model is too conservative, and the order of magnitude of the velocities are overestimated.
- The new approach, measuring the impact velocity directly using a gyroscope was successful in determining the impact velocity.

2.3. Rocking Revisited II

The research on rocking was continued by S.S. Arefin (2017) in his masters's thesis: Measurement on Rocking of cubes in a Double Layer on a Breakwater. The objective of the research was:

- Determination of spatial and stochastic distribution of rocking behavior of armour units.

This problem was approached by designing a representative model breakwater, measuring the rocking behavior of cubes and analyzing the impact/collision of the armor units.

2.3.1. Test program

The hydraulic conditions for the tests consisted of three wave heights, and the wave steepness was varied between $S_{m-1.0} = 0.02$ and 0.04. Eight instrumented cubes were used with a sample frequency of $50Hz$, and were placed at the same depths as the CUR C70 research. During testing the cubes were connected to a computer with a wire.

As was also found by Le (2016), measuring the angular velocity from the gyroscope provides more distinctive data than using the accelerometer. This technique was validated, as it gave impact velocities of the same order of magnitude as was found by integrating the accelerometer signal.

2.3.2. Number of rocking units and impacts

The results from the analysis were compared with the CUR C70 research and the following observations were done:

- The threshold for rocking as proposed by the CUR C70 research was wrong. The test results showed that there was movement with stability numbers as low as $H_s/\Delta D_n = 0.9$ and 1.1.
- It was assumed that the number of impacts is equal to the number of peaks in the angular velocity signal. The resulting number of impacts was not around three times the number of movements, but continuous and increasing with increasing wave heights (Arefin, 2017). No clear distinction between a movement, a collision and rocking was made.
- The number of collisions divided by the number of waves ranges between 0 and 0.9 and is dependent on the wave height, wave steepness and the position of the cube on the slope (Arefin, 2017).
- The maximum number of collisions was found at a depth of $y/D_n = -2$, the minimum number of collisions was found at $y/D_n = -4$.

2.3.3. Impact velocities

The data from the gyroscope was used for the calculation of the impact velocity, and gives a much more precise result than the acceleration data from the accelerometer (Arefin, 2017). The results showed that the maximum impact velocity was at a depth of $y/D_n = -2$ for a wave steepness of $s_{m-1.0} = 0.04$. Therefore, it was concluded that the wave steepness should also be incorporated in future design formulas.

2.4. Smart Rocking Armour Units

Smart Rocking Armour Units (Hofland et al., 2018), describes the method to measure rocking motions of lab-scale armour units, as was used by Le (2016) and Arefin (2017).

2.4.1. Physical model tests

Miniature 9-axis Inertial Measurement Unit (IMU) sensors were tested for their practical applicability in breakwater research. The IMU is capable of measuring acceleration, rotation rate (gyroscope) and magnetic field (compass). The maximum sampling frequency of the sensors is 100 Hz (Hofland et al., 2018). Instead of using the CUR approach, by integrating the acceleration signal during impact, the approach as used by Le (2016), using the acceleration before impact, can be used to determine the impact velocity v_i. Because the impact duration is in the order of $1ms$, while the acceleration before impact are related to the wave period, around $1s$, at a 100 Hz sampling frequency could suffice (Hofland et al., 2018). Another method was applied by Arefin (2017), where the gyroscope was used instead of the accelerometer. The gyroscope measures the angular velocity ω so no integration of the signal is needed, but rather a single velocity measurement just before the impact. The absolute value of the angular velocity can be obtained from the three measured angular velocity components with Equation 2.13 (Hofland et al., 2018).

$$|\omega| = \sqrt{\omega_x^2 + \omega_y^2 + \omega_z^2} \tag{2.13}$$

The impact velocity v_i can be estimated by assuming a pure rotational motion of the cube with a diameter d_n. The following equation can be used:

$$v_i \approx d_n |\omega| \tag{2.14}$$

The gyroscope measurements have been validated, by placing them on a bar that was rotated 90 degrees, the result is shown in Figure 2.5. The gyroscope measurements show less noise than the accelerometer, but they contain a slight underestimation (bias) of 0.7 degree over the full 90 degrees. During testing, four of the eight cubes began to malfunction, so during the last few tests only four were

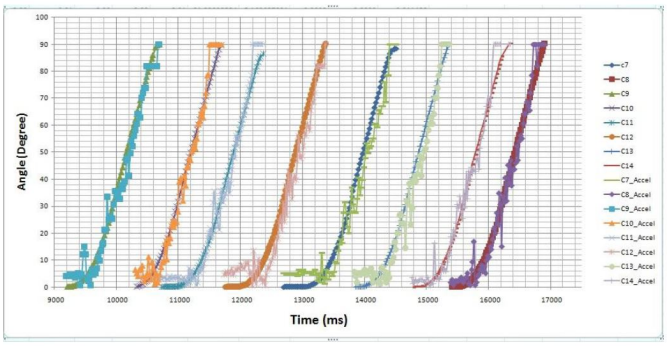

Figure 2.5: 90 degrees rotation test of the sensors (Arefin, 2017).

still functioning. It is believed that only when in the order of ten cubes can be instrumented, a sensible estimate of the spatial statistics can be made (Hofland et al., 2018). After experiments were performed, it was concluded that using the gyroscope measurements can provide a straightforward measurement of the impact velocity magnitude, caused by the impact of a rocking armour unit against an adjacent unit.

2.5. Rocking revisited III

The study on rocking at the TU Delft was continued by Ganga Caldera (2019) as part of her master thesis on Rocking of single layer armour units. The big difference was that the research was now focusing on single layer armour units. The aim of this thesis was:

- Determining magnitude, spatial and stochastic distribution of impact velocities of Xblocs, that are rocking under the wave action.

To achieve this aim the following sub-objectives were defined:

- Further improve and validate the dedicated measurement technique for rocking analysis.
- Determine the parameters related to rocking of Xblocs and methods to derive these parameters efficiently and accurately from these devices.
- Compare and validate the parameters with previous studies.

Until this point, the bottleneck in measuring rocking was the sampling frequency. Therefore, the sensor had to be improved, to make it able to record data with a sampling frequency of around 100 Hz. This led to the development of the smart Xbloc, which can measure at a sampling frequency of around 100 Hz (Caldera, 2019). Two instrumented smart Xbloc units were produced.

2.5.1. Model Setup

The slope and wave conditions were designed in such a way that acceptable rocking motion could be expected. The following choices were made for the setup of the model.

- For the breaker type surging waves with an Iribarren number larger than 3.2 were used during testing.
- To increase the probability of rocking a relative mild slope of 2 (vertical) in 3 (horizontal) $2V : 3H$ was used.
- An impermeable slope was used to reduce the stability of the structure and increase the forces on the Xbloc units. This slope also reduced the setup time of the model allowing for efficient measuring.

2.5.2. Model Tests

Multiple visual observations were made regarding the interlocking and settlement, during each test. These observations suggest that there is a relation between rocking, packing density, interlocking capacity and settlement (Caldera, 2019). During testing the instrumented Xbloc units were relocated to the location of armour units that was rocking.

2.5.3. Conclusion

After successfully updating the measuring technique, performing multiple measurements and analyzing the results the following points were concluded.

- The rocking motions are captured well with a sample frequency of $100Hz$, with 5 to 10 data points per rocking event. It is now possible to interpret the complete rocking motion (Caldera, 2019).
- The magnitude of impact velocity and number of impacts depend not only on the wave characteristics but also on the effectiveness of interlocking (Caldera, 2019).
- Settlements can significantly affect the amount of rocking. Settlement of the top rows can result in extra pressure on the lower rows increasing the effectiveness of interlocking.
- Both the horizontal and the vertical position of the armour unit on the slope influences the amount of rocking.
- Comparing the results from the gyroscope and the accelerometer, it was observed that the gyroscope has less noise in the signal. Also, the analysis to obtain the impact velocity is less prone to errors, as no integration is needed. However, the accelerometer measurements resulted in higher impact velocities for the same peaks compared to the gyroscope. It is recommended to use the impact velocity from the gyroscope (Caldera, 2019).

2.6. Rocking revisited IV

The research on rocking was continued by Thomas Goud (2020) in his thesis about the analysis of rocking-induced stresses for concrete breakwater armour units. A probabilistic method to predict breakage of armour units is created for the Xbloc armour unit. The model uses the impact velocity as input, and determines in a probabilistic manner if the event will lead to breakage of an armour unit. Many of the stochastic variables were estimated as no data was available.

2.6.1. Impact velocity

The impact velocity can be calculated using Formula, 2.15 (Goud, 2020).

$$v = f_{cor} * \sqrt{2s * \left(k_1 \frac{C_D u^2}{(\Delta + 1)\, d_n} - k_2 \left[1 - \frac{1}{\Delta + 1} \right] g \right)} \tag{2.15}$$

Where

f_{cor}	empirical correction factor, $f_{cor} = 1 - \frac{\sqrt{s}}{4}$ for Xbloc
s	available space between the blocks
C_D	drag coefficient
u	run-up velocity of the wave
d_n	nominal diameter of the armour unit
H_s	significant wave height
Δ	relative density
g	gravitational acceleration
k_1 and k_2	dimensionless variables

The model does not take the number of impacts of an individual armour unit into account. The impact velocity is assumed to be 0 for 50% of the waves. This assumption has been made implicitly because the distribution for the travelled distance s is 0 for 50% of the cases. In Figure 2.6 the probability of exceedance for the impact velocity is shown, the velocity has been determined for an Xbloc with the same size as was used by (Caldera, 2019).

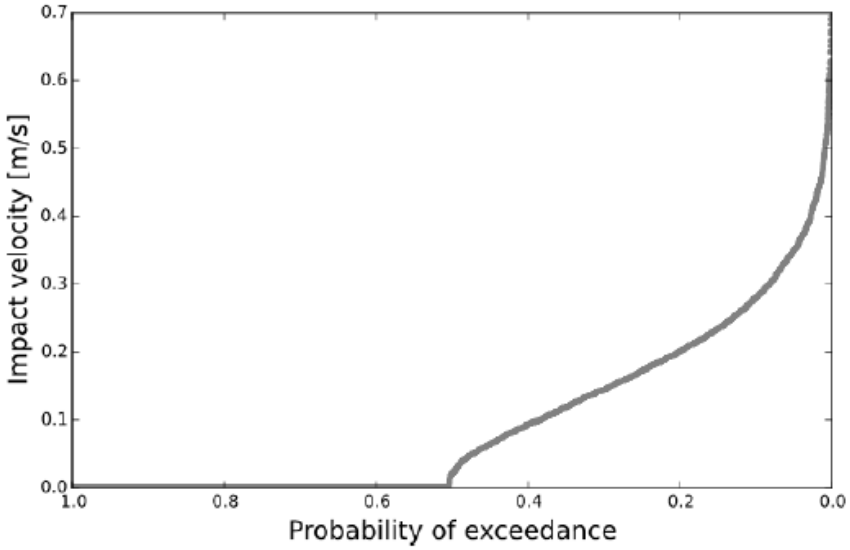

Figure 2.6: Probability of exceedance impact velocity for $H_s = 11.5cm$ and $d_n = 3.91cm$ as used by Goud (2020).

A functional model has been made, which is capable of estimating the number of armour units that will fail. The model is very complex and many simplifications had to be made. The impact velocity could be verified by the lab experiments.

3

Model setup

The overall aim for the design of the model setup is to represent a section of a breakwater situated in deep water. To ensure some rocking of the armour units an impermeable core was applied as well as a large number of rows on a relatively long slope without a toe structure. In this section the main dimensions of the breakwater model are discussed. For each parameter the design rules or common design choices are discussed as well as their (expected) effect on rocking. Finally the design choice for the parameter is given.

3.1. Main dimensions

3.1.1. Breakwater base

The slope on which a filter and armour layer will be placed, consists of a wooden impermeable base, see Figure 3.1. The base has a slope of 2V:3H which is a typical, but relative mild slope for a rubble mound breakwater with Xbloc armour units (DMC, 2018). The slope of the breakwater affects the interlocking between the Xbloc armour units. A steeper slope results in more pressure from the rows of armour units on each other, increasing the interlocking effect. Therefore, a steeper slope is more stable and rocking is less likely to occur. To increase the probability of measuring rocking a relative mild but typical slope of 2V:3H is used.

The base of the structure is fitted with a wooden elevation at the base, on which the first row of Xbloc armour units is placed. No toe structure was implemented to represent a breakwater in deep water. See Figure 3.1 for the cross section of the design.

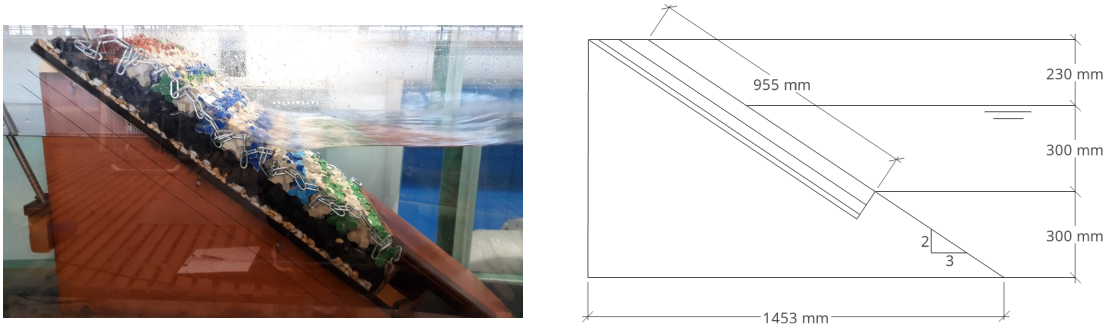

Figure 3.1: Cross section of the model layout

3.1.2. Freeboard

The freeboard of a breakwater is determined by overtopping criteria. The freeboard has two effects on the stability of the armour units. The first effect is that a higher freeboard results in more horizontal rows of armour units, thus increasing the pressure on the lower layers. This extra pressure will increase

the interlocking between the armour units. Second, a higher freeboard increases the forces on the armour units during wave run-down (DMC, 2003). Finally, a higher freeboard requires more materials and is less economical. Therefore, the choice of freeboard is a balance between these effects, also the dimensions of the wave flume play an important role. Taking the previous points into account a freeboard of 0.83 meter has been used.

3.1.3. Under layers

A typical breakwater consists of an armour layer, one or multiple filter layers and a core. The wooden base represents the core and is applied with a layer of glued stones $d = 0.02m$, to represent the roughness of core material. The filter layer affects the run up and run down of the waves. A thin layer results in higher velocities thus inducing higher forces on the armour units. A thicker layer dampens the run up and run down and thus reduces the forces. The filter layer has a thickness of $0.04m$ and consists of loose rock. For practical reasons the material for the underlayer will be prepared as a composition with the following characteristics:

- 15% of $16mm$ sieve passing and $11mm$ sieve retained
- 70% of $22mm$ sieve passing and $16mm$ sieve retained
- 15% of $25mm$ sieve passing and $22mm$ sieve retained

3.2. Placement and packing density armour layer

There are two placement possibilities for Xbloc armour units in a single layer, placement in a random pattern or placement in regular patterns (DMC, 2003). The Xbloc armour units will be placed in a predefined pattern with random orientation. It is important that the armour units on the slope are secured by the 2 units placed above and the unit should be in contact with the under layer (DMC, 2019). The placement of the first armour layer has been carried out under supervision of DMC.

The effect of the packing density on rocking is expected to be of major importance. A higher packing density increases the interlocking between units and reduces the movement space of the unit. In practice, a high packing density is more stable and would be preferred for high stability. The packing density for the model was determined in collaboration with DMC and is based on the recommended packing density of at least 1.20 $(units/D^2)$. With $D = 5.64cm$ the distance between the center of gravity of each unit in x and y direction is determined. This was done using a calculation tool for Xbloc placement provided by DMC. The average horizontal distance should be $1.30 * D = 7.47cm$, and the average vertical distance should be no less than $0.64 * D = 3.57cm$.

Xbloc units will be placed in a tessellated grid with random orientations. The armour layer will consist of alternating rows of 11 and 10 units, see Figure 4.4. During placement the packing density is checked using a custom ruler, showing the theoretical horizontal and vertical distance between the blocks.

3.3. Hydrodynamic conditions

In this section the hydraulic test program will be discussed. Each parameter will first be discussed separately, giving the design rules and considerations. Also, other factors like the breakwater state and research objective will be discussed. At the end of this section the test program is provided including wave conditions as well as practical considerations. The measured wave conditions during each test are shown in the appendix, Table A.1.

3.3.1. Stability number

The stability number N_s, Equation 3.1 is often used in hydraulic engineering. The effect on the slope and the armour layer for different stability numbers, depending on the gradient of the slope, can be determined with Table 3.1. However, observations by Caldera (2019) suggested that the given stability numbers are too conservative. Therefore, it was decided to run three tests with different stability numbers, and use the results from those tests to determine from what stability number a reasonable amount of rocking armour units could be expected. The stability numbers that were used in the final test program can be found in Table 3.2.

$$N_s = \frac{H_s}{\Delta D_n} \tag{3.1}$$

$$V_{Xbloc} = (H_s/N_s * \Delta)^{1/3} * C \tag{3.2}$$

$$\Delta = \rho_s/\rho_w - 1 \tag{3.3}$$

where

N_s	Stability number
H_s	Significant wave height (m)
Δ	Relative density
D_n	Nominal diameter of the armour unit (m)
V_{Xbloc}	Volume of the armour unit (m^3)
C	Correction factor ($C = 2$ for an impermeable core)
ρ_s	Density of Xbloc ($2341 kg/m^3$)
ρ_w	Density of water ($1000 kg/m^3$)

Table 3.1: The effect of the slope for the stability number as observed by DMC (2003). And the adapted stability number for an impermeable core and milder slope.

Effect on the slope	Stability number (N_s) (3V:4H)	Adapted stability number (N_s) (2V:3H)
Stable slope	2.77	2.20
Start rocking	3.10	2.46
Start of damage	3.50	2.78
Start of failure	3.96	3.14

3.3.2. Breaker type

The breaker type can be predicted with the Iribarren number ξ or surf similarity parameter, see Equation 3.4. The breaker type affects the way the forces of the wave act on the breakwater and armour units. For an impermeable core and surging waves ($\xi > 3.2$), the waves will slowly run up and down the slope leading to fairly high run-up (van den Bos and Verhagen, 2018). Because of this reason, a breaker parameter of $\xi = 3.2$ will be used. This will result in both surging and collapsing breakers. The wave steepness s_{op} is 4% for this condition.

$$\xi = \frac{tan(\alpha)}{\sqrt{s_{0p}}} \tag{3.4}$$

$$s_{op} = H_s/L_0 \tag{3.5}$$

3.3.3. Wave period

The wave period is based on a constant wave steepness of 4%, which is used to determine the wave length L_0. With the wave length the wave period is determined using Equation 3.6. The wave period of the test program can be found in Table 3.2.

$$T_p = c/L_0 \tag{3.6}$$

$$c = \sqrt{g/k * tanh(kd)} \tag{3.7}$$

T_p Peak period (s)
c Wave celerity (m/s)
L_0 Deep water wave length (m)
g Gravitational constant 9.81 (m/s^2)
k Wave number $2\pi/L$
d Water depth [m]

3.4. Number of waves

The number of waves for a test run has to be large enough in order to produce statistically reliable test results. This is usually between 500 to 3000 waves for the physical modelling of breakwaters (Kirkegaard et al., 2011). There are two aspects to keep in mind when choosing the number of waves. Rocking is expected to decrease during testing due to an increase of the packing density. Therefore, the number of waves should not be chosen too large. Also, in order to do a full test series, consisting of 5 test runs, the number of waves should not be too large because this takes too much time. For the model tests the number of waves N = 1200 is used.

3.5. Breakwater state

Under wave loading, the strength of the armour layer changes due to settlements. Because of this change the ”state” of the breakwater with respect to the packing density has to be considered. Common practice in testing a scale model of a breakwater, is to use 5 test runs with stepwise increasing wave height. The first test run is generally a settling or shake down test, consisting of low energy waves (Garcia et al., 2013). The main purpose of this test is to compensate for the construction of the breakwater in dry conditions, and to reproduce the natural evolution and initial settlements of the armour layer, prior to the first storm. The following observations can be expected during a test series according to Garcia et al. (2013).

- During the first test the units located under the SWL are rearranged and an overall ”uniform” settlement of the layer is taking place.
- During the lower storm conditions some slight differential settlements of the layer can be observed and some units may be seen to be occasionally rocking. The packing density below SWL increases slightly.
- During design conditions no damage (unit extractions) is observed as the armour layer has been strengthened during previous tests. Fewer movements (rocking or rotation) should be observed.
- During the overload test we would expect to make similar observations to those of the design wave condition but with more settlement permitted.

In the past, several breakwaters failed due to breakage of armour units during the first storm. Therefore, doing a shake-down test, increasing the strength of the armour layer, is not a realistic scenario for failure due to breakage. Therefore, it was decided not to do a shake-down test and start measuring from the first wave.

3.5.1. Number of test runs in a test series

Rocking is expected to decrease during testing due to settlements and an increase in interlocking. Therefore, the slope should be rebuilt after a number of test runs. It was decided that a test series consists of five test runs with increasing wave height. After each test series the armour layer is completely removed and rebuild for the next test series.

3.6. Test program

The following test program is applied, Table 3.2, taking into account the different findings of the sections in this chapter. The test program consists of five test runs each with an increasing wave height. The practical considerations are:

- Instead of a shake-down test, the test will start with a mild condition, $N_s = 1.91$. The wave height will be increased to heavy storm conditions $N_s = 3.43$. See Table 3.2.
- The waves will be irregular, and are based on a JONSWAP spectrum.
- The breaker type will be between collapsing and surging breakers $\xi = 3.2$. With a constant wave steepness $s_{0p} = 0.04$.
- Each test run contains $N = 1200$ waves.
- All tests will be executed with a constant water depth of $0.6m$.
- After each test series, consisting of the five test runs the armour layer will be rebuilt.
- The first 5 test series will be applied with 10 sensors placed at SWL. A quick analysis of these first test series will be carried out to determine if enough data has been collected to continue and measure at $SWL + 2d_n$ and $SWL - 2d_n$.

Table 3.2: Test program for one test series.

Test run	Significant wave height H_s (m)	Stability number N_s	Wave steepness S_{op}	Peak period T_p (s)	Number of waves N
1	0.10	1.91	0.04	1.26	1200
2	0.12	2.29	0.04	1.42	1200
3	0.14	2.67	0.04	1.68	1200
4	0.16	3.05	0.04	1.75	1200
5	0.18	3.43	0.04	1.92	1200

4

Model testing

This chapter will discuss the actual model testing in the lab. The model set-up can be found in the previous chapter.

4.1. Testing facility

All tests were carried out in the Hydraulic Engineering Laboratory at the TU Delft. The wave flume has a length of 40 m, a width of 0.8 m and a height of 1.0 m. Waves are generated with the wave paddle which has an active absorption system. The breakwater model was located 20 meters from the wave paddle.

4.2. Breakwater model

The breakwater model represents a section of a breakwater situated in deep water. The dimensions of the breakwater model as used during testing can be found in Figure 4.1.

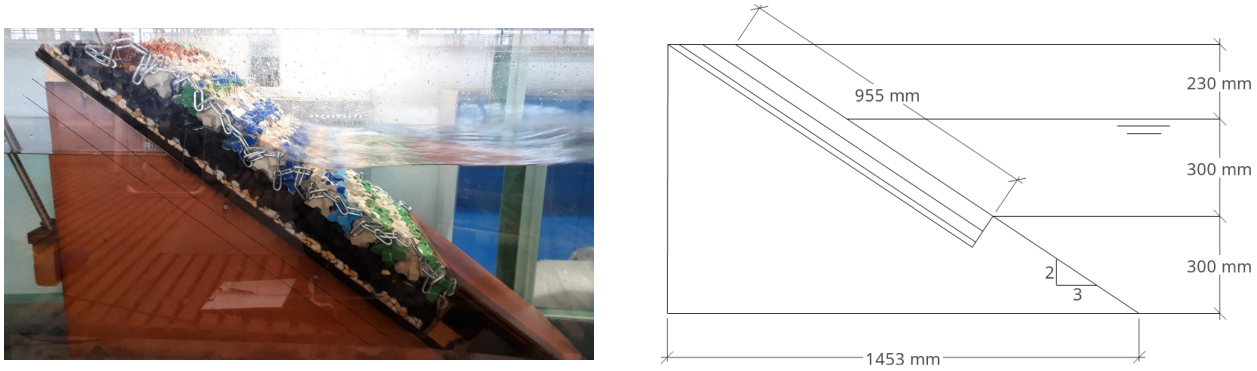

Figure 4.1: Side view of the model and dimensions.

4.2.1. Under layer

On the glued layer of the base, an under layer with a thickness of 4 cm was placed. A sample of 100 stones from the under layer was analyzed to determine the weight and density of the material, these values were used to construct a sieve distribution graph, see Figure 4.2. The nominal diameter d_n was calculated using Equation 4.1. The nominal diameter d_{n50} of the under layer is 15.19 mm, the density of the material ρ_s is 2970 (kg/m^3).

$$d_n = \sqrt[3]{(W/\rho_w)} \tag{4.1}$$

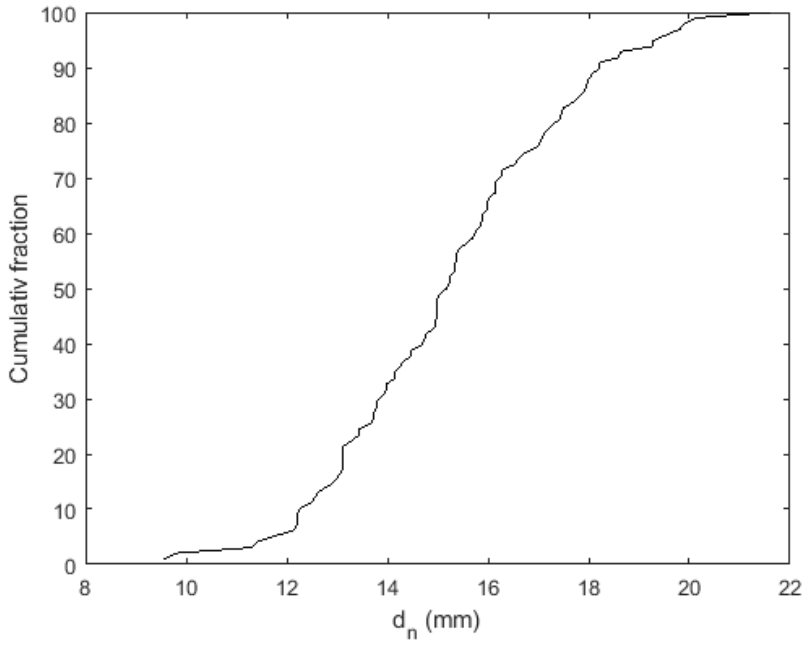

Figure 4.2: Sieve distribution of the under layer, based on a sample of 100 stones.

4.2.2. Armour layer

The armour layer was constructed using Xbloc armour units provided by BAM. The Xbloc units have a height of 5.6 cm and a nominal diameter d_n of 4 cm. The first row contains 11 Xbloc units placed in a regular pattern, the rows above it are alternating between 10 and 11 armour units per row. The full armour layer consists of 26 rows. The first placement of the armour layer was carried out under supervision of a DMC employee, for later tests digital feedback was given on the slope construction to ensure the slope was build to a high standard.

When the armour layer was finished, two iron chains were placed to secure the Xbloc units positioned against the walls of the flume, see Figure 4.3. This is recommended because at the boundaries the Xbloc units are not properly supported. Data from units against the side of the flume were not used in the analysis.

Figure 4.3: Scale model under wave attack with the iron chain placed between the outer column and the flume.

4.3. Coordinate system armour layer

The coordinate system for the armour layer, see Figure 4.4, is defined with a row number and a location number. The bottom row is given number one and the row above it number two. For each row the armour units are given a numbered from left to right. Before each test the location of the sensors are written down using this coordinate system, as part of the visual observations form. The row number of the smart Xbloc unit for each test can be found in Appendix I.

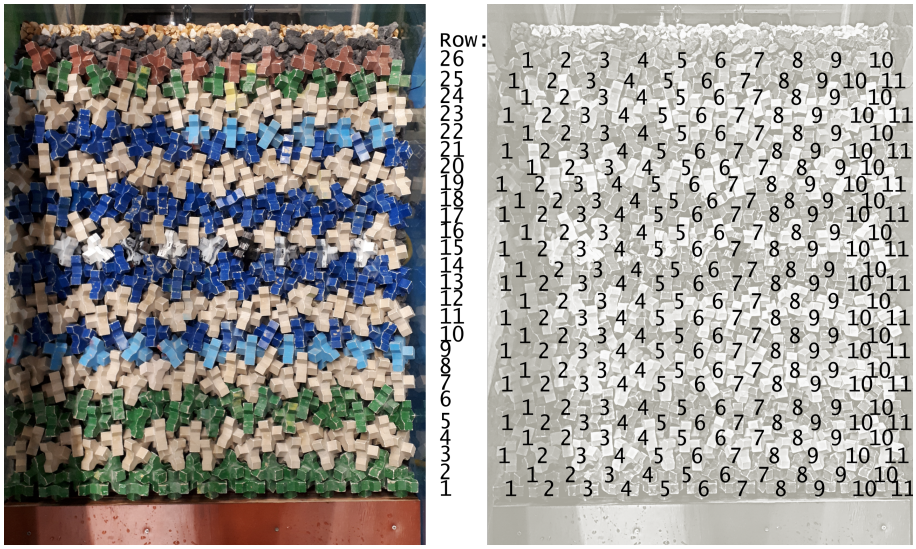

Figure 4.4: Coordinate system of the armour units in the armour layer.

4.4. Sensors

During each test run multiple sensors were used to collect data. The accelerations and angular velocity were measured with 10 smart Xbloc units. A camera was used to take a photograph before and after each test run to analyze the along slope settlements. The wave conditions were measured with three wave gauges. Visual observations were carried out to observe the movements of all the Xbloc units in the armour layer. This section provides information about the different sensors that have been used.

4.4.1. Smart Xbloc

The smart Xbloc units, used for this research were made according to the design of the smart Xbloc by Caldera (2019). The design is made to fit in a hollow 3D printed Xbloc unit and is capable to collect data at a sample rate of around 100 Hz. Two smart Xbloc units were created and tested by Caldera (2019). For this project, 9 new sensors were made and the two sensors from the previous project have been used. The sensors have been labelled 1 to 11. The sensors produced by Caldera (2019) were given number 10 and 11.

The smart Xbloc contains a ST LSM9DS1 sensor, featuring a 3D digital linear acceleration sensor and a 3D digital angular rate sensor. The sensor has an USB connection, which is used to charge the device and retrieve data. The sensors can be turned on and off with a reed switch. The electronics are placed inside a 3D printed Xbloc unit. Lead weights were carefully positioned in the arms of the Xbloc, to represent the same dynamic behaviour as a normal Xbloc unit. The 3D printed units have been filled with a waterproof compound to prevent water from damaging the electronics.

4.4.2. Mass Smart Xbloc

The mass of the Smart Xbloc units was measured and compared with the normal scale models, that were provided by BAM. The average mass of the Smart Xbloc units is 141.0 grams, which is 1.3 grams more than the average weight of the Xbloc units provided by BAM. The mass for each sensor can be found in Table 4.1. It should be noted that the variation in mass was much larger for the smart Xbloc units, when compared to the normal Xbloc units. This could be because the lead weights were not cut

properly, but also due to pockets of air inside the Xbloc unit. The difference in weight compared to the standard Xbloc units is small and can be neglected.

Table 4.1: Mass of the smart Xbloc units.

Sensor number	Weight (grams)
1	136.2
2	143.5
3	147.3
4	144.6
5	139.6
6	148.9
7	136.2
8	140.0
9	142.9
10	127.0
11	144.8

4.4.3. Smart Xbloc validation

To validate the sensor a validation measurement was performed and filmed. In this validation measurement the sensor was rotated in multiple orientations. The data was visualized with a Matlab script showing the rotation of in 3D. The result was synced to the video and it was found that the data represents the actual movement of the armour unit very closely. A screenshot of the video is shown in Figure 4.5.

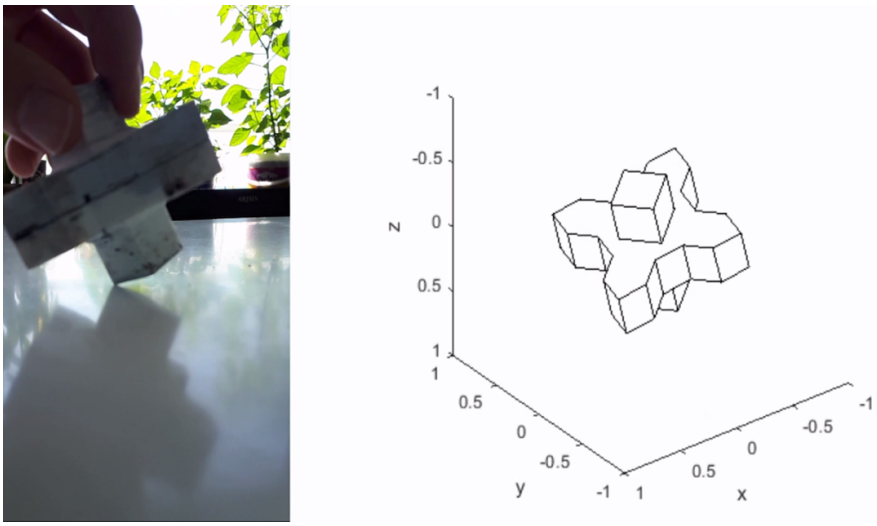

Figure 4.5: Screenshot of the validation video.

4.4.4. Camera

A photograph was taken before and after each test run, these images can be used to analyze the along slope settlements. To reduce the error of this technique, the camera has to be placed at a high location (Hofland and van Gent, 2016). Therefore, a custom wooden frame was built, placing the camera 2.8 m above the wave flume, see Figure 4.6. The camera was connected to a computer to take photographs remotely, an example of a photograph can be found in Figure 4.6. Due to limited time the data from the camera has not been analyzed. All data has been stored and can be obtained for further processing.

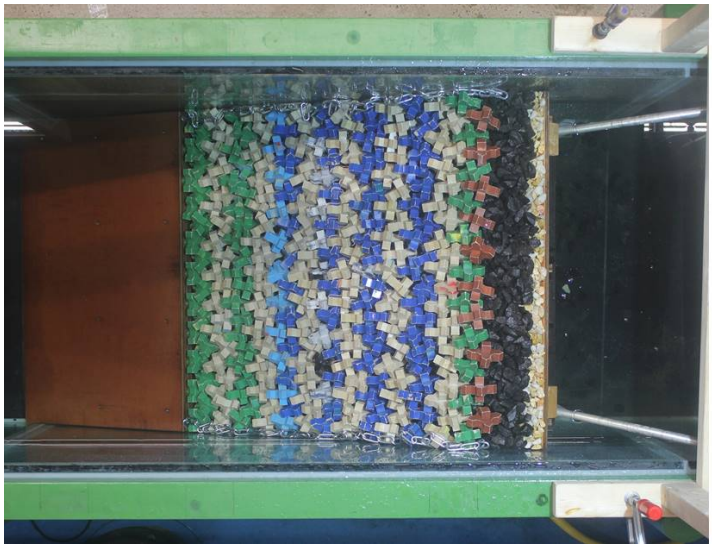
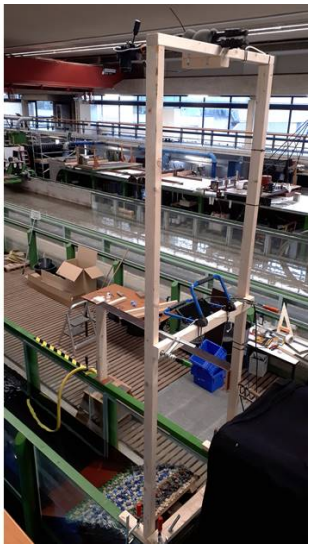

Figure 4.6: Example of a photograph after a test run and the camera frame.

4.4.5. Wave gauges

Three wave gauges were used to measure the waves. The wave gauges were located halfway the wave flume at 10 meters from the wave paddle. The distance between wave gauges 1 and 2 was 30 cm, between 2 and 3 it was 40 cm. The data was analyzed using a script that was provided by the TU Delft. This script uses the method of Zelt and Skjelbreia (1992), and was used to calculate the incoming significant wave height ($H_{m0,i}$). The results for each test series can be found in Appendix A, Table A.1.

4.4.6. Visual observations

Besides the Smart Xbloc measurements, rocking was also observed visually during each test. To do this in a consistent way, an observation form was created, see Appendix I, Figure I.1. In this form, all the relevant information was written down: date, test number, water depth and smart Xbloc locations. Also, start and end time for each test run were noted. This made it possible to retrace irregularities in data and ensured a consistent work flow. The forms for each test series are shown in Appendix I.

4.5. Measurement overview

24 test series were carried out in the lab. The test series were labelled chronologically starting at T1 for the first test series. The date, sensor location, water depth and wave steepness for each test series can be found in Appendix B Table B.1.

The first three test series were used to evaluate the setup and determine the wave conditions for the later tests. During two of these tests, the base structure was unstable and moved for the largest waves. This problem was solved by adding extra steel supports attaching the structure to the wave flume. Because of this, the results of the first three tests are not considered valid measurements. The data from these tests were not used for further processing or analysis.

During test series T4 to T22 only the location of the sensors were variable, all the other variables were kept constant. The two final test series, T23 and T24, were performed with a lower wave steepness of $S_{0p} = 0.02$. Due to the limitations of the wave flume, only three test series were used during the last two tests, see Table A.1. An overview of all the tests containing the location of the sensors, the water depth and the wave steepness can be found in Table B.1. The sensor location is given with respect to still water level (SWL).

During each test the waves were measured with three wave gauges. There were around 1200 waves per test run. The waves were irregular and based on a standard JONSWAP spectrum. Table A.1 gives an overview of the measured wave conditions, the wave height is the incoming significant wave height ($H_{m0,i}$) and was analyzed using the method of Zelt and Skjelbreia (1992). The average measured wave conditions per test run can be found in Table 7.1.

5

Accelerometer calibration

To improve the accuracy of the smart Xbloc, the calibration method for an accelerometer by Frosio et al. (2009), has been implemented to be used for the sensor. Only two calibration measurements were done during the test period. Large deviations between the results of those two measurements were found. Therefore, the calibration values have only been used to estimate the error, which is around 5% for the linear velocity.

5.1. Calibration method

The accelerometer is calibrated using the auto-calibration method for MEMS accelerometers by Frosio et al. (2009). This method can be used to determine the scale factors for the Main and Cross-axis and the bias for each axis. These calibration values can be used to correct for the misalignment of the sensor axis. The method is based on the assumption that an inertial sensor, in static condition, is subjected only to the gravitational force (Frosio et al., 2009). To use the method a calibration measurement has to be done. A Matlab script was written which extracts the static measurements from the calibration measurement and calculates the calibration values. The results of the calibrations are shown in Table C.1 and C.2.

The calibration method has only been used to make an estimate of the error, which is around 5% of the calculated impact velocity. For the analysis, the non-calibrated data has been used because the difference between the results of two calibration measurements was significantly large. Therefore, the calibration values cannot be considered valid for all test series. For future use of the smart Xbloc, it is recommended to use this method and do a calibration measurement before and after every test series, to improve the accuracy of the measurement. The following sections will provide an outline of the calibration method as implemented for the smart Xbloc. The last section covers the error estimate.

5.2. Calibration measurement

The first step to calibrating the smart Xbloc is to do a calibration measurement, the data form this measurement is used to determine the calibration values. This measurement must feature data from at least nine random static orientations (Frosio et al., 2009). The procedure is to place all the sensors on a stable platform. The sensors are rotated in different orientations and left motionless for about 25 seconds before rotating again. In total the Smart Xbloc units were placed in 22 orientations. An example of data from a calibration measurement is shown in Figure 5.1.

5.3. Data processing

The data from the calibration measurement does not have a constant sampling frequency due to the way it is programmed (Caldera, 2019). The smart Xbloc is always measuring with a sample rate of around 100 Hz. However, when the sensor is motionless only every 0.5 seconds a data point is saved, this has been done to save storage space on the smart Xbloc. Only when the smart Xbloc measures a rotation above the threshold level of 0.05 rad/s, or an acceleration above the threshold level of $1.01g$, the data is saved at the high sampling frequency of around 100 Hz. After the smart Xbloc has collected

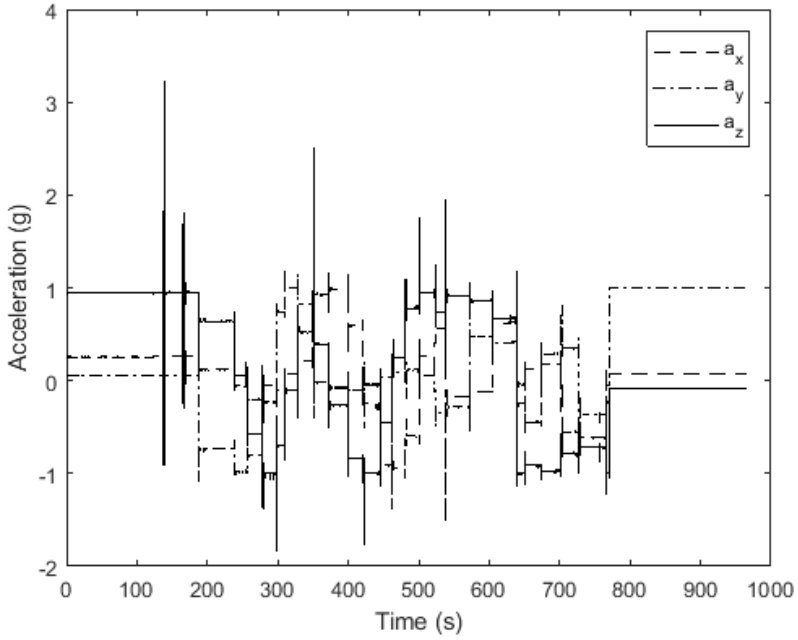

Figure 5.1: Example of a calibration measurement, showing the acceleration in three axes (a_x, a_y, a_z), for multiple orientations.

10 samples the data is saved from the random access memory to the main storage of the device. During these moments, the sample frequency is also lowered to around 2 Hz (Caldera, 2019).

These changes in sample frequency are used to extract the motionless data in the calibration measurement. The sample frequency is calculated, if the sample frequency is higher than 5 Hz the data point corresponds to a motion and is removed from the data. By removing all the high frequency data, the remaining data points are either motionless or correspond to a data transfer from the random access memory to the main storage. The result of this step is shown in Figure 5.2.

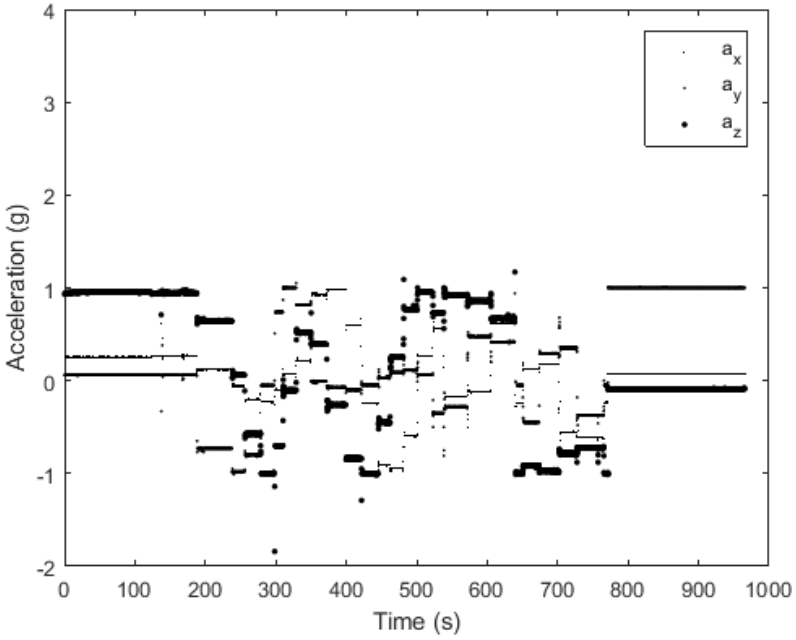

Figure 5.2: Example of a calibration measurement after data points with a high frequency have been removed.

The next step is to extract the actual motionless data from the low frequency data points. This has been done with an algorithm that finds successive measurements that are exactly the same for the three axes. The algorithm searches for successive low frequency measurements in the original data set, including the high frequency data points. If two or more successive low frequency measurements are found, they must come from a moment where the sensor is motionless. For these data points, the three axis of the accelerometer measure only the gravitational acceleration. Those points are saved in a separate list containing the values that will be used as input for the calibration method, these are called the calibration points and are shown in Figure 5.3.

Due to a small movement or a small irregularity in the stable platform, there could be two calibration points that are very close to each other. In this case they are not used for the calibration, because the input should only contain data from different orientations (Frosio et al., 2009). In Figure 5.1, the calibration points used to determine the calibration values are noted with a filled marker. The empty markers are motionless or static data points that are too close to each other.

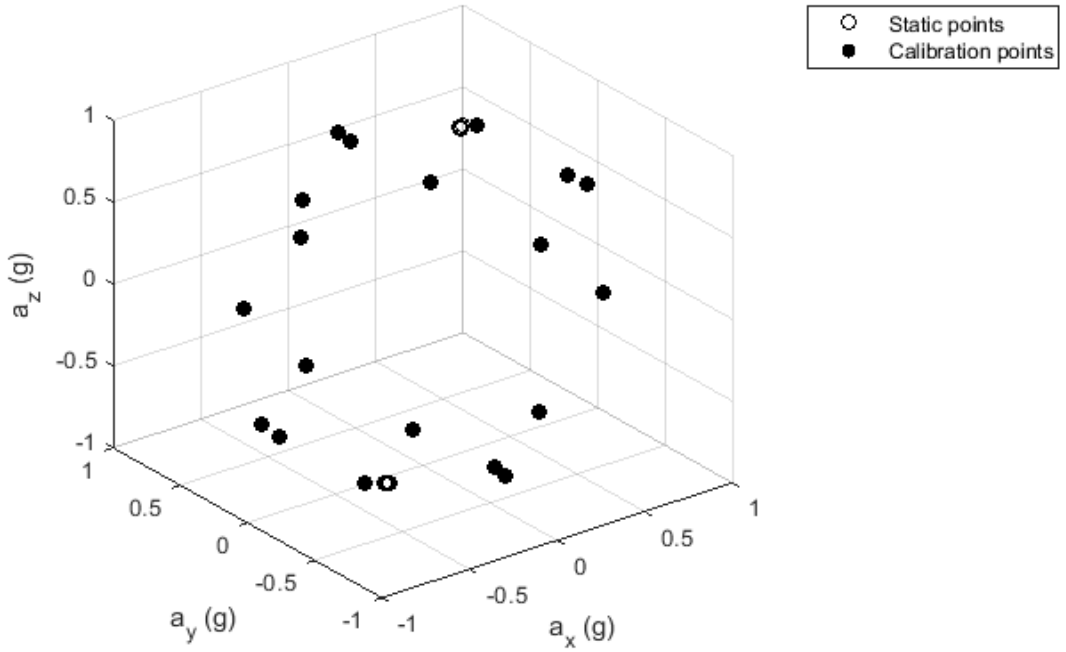

Figure 5.3: Example of the calibration points extracted from a calibration measurement. The filled markers are used for the calibration, the empty markers are too close to each other and not used in the calibration.

5.4. Autocalibration method

The sensor is represented mathematically by Equation 5.1 (Frosio et al., 2009). This expression describes the relation between the accelerometer output $V^T = [v_x, v_y, v_z]$ and actual acceleration vector $A^T = [a_x, a_y, a_z]$. The diagonal of matrix S represents the scale factors along the three axes, the other elements of S represent the cross-axis factors. The bias is represented by the vector O.

$$A = S(V - O) \tag{5.1}$$

Where

$$S = \begin{bmatrix} \mathrm{S}_{xx} & \mathrm{S}_{xy} & \mathrm{S}_{xz} \\ \mathrm{S}_{yx} & \mathrm{S}_{yy} & \mathrm{S}_{yz} \\ \mathrm{S}_{zx} & \mathrm{S}_{xy} & \mathrm{S}_{zz} \end{bmatrix}, O = \begin{bmatrix} \mathrm{O}_x \\ \mathrm{O}_y \\ \mathrm{O}_z \end{bmatrix} \tag{5.2}$$

The auto calibration method is based on the fact that the modulus of the acceleration vector, in static conditions, is equal to the gravity acceleration g.

$$\sqrt{a_x^2 + a_y^2 + a_z^2} = g \tag{5.3}$$

To find the calibration values the sensor is placed in N different random orientations. The solution is found by calculating the error e_k, Equation 5.4, for each static orientation and minimizing the cumulative error E, Equation 5.5 (Frosio et al., 2009). The resulting system of equations is used to iteratively minimize the cumulative error E, using Newton's Method. The resulting calibration values are shown in Table C.1 and Table C.2.

$$e_k = a_x^2 + a_y^2 + a_z^2 - g^2 \tag{5.4}$$

$$E = \frac{\sum_{k=1}^{N} e_k^2}{N} \tag{5.5}$$

5.5. Error estimate accelerometer

The accelerometer data is used to find the linear velocity. Therefore, an error estimate for the linear velocity has been made.

To estimate the error of the non-calibrated data from the accelerometer the calibration values from Table C.2 have been used to correct the raw data, using Equation 5.1. With the corrected data the linear impact velocity for all events has been calculated, using the method explained in section 6.9. This has been done for 10 randomly selected test series. The impact velocity for all events with an impact velocity higher than 0.1 m/s is shown in Figure 5.4. The error has been determined by calculating the absolute difference in linear impact velocity between the calibrated data and non calibrated data for each event. The average deviation per event in percentage is determined. Taking the mean of all the average deviations per event resulted in the average error of the raw data. It was found that the mean error due to using the non-calibrated values is 5.6% with a standard deviation of 3.6% for the calculated linear impact velocity.

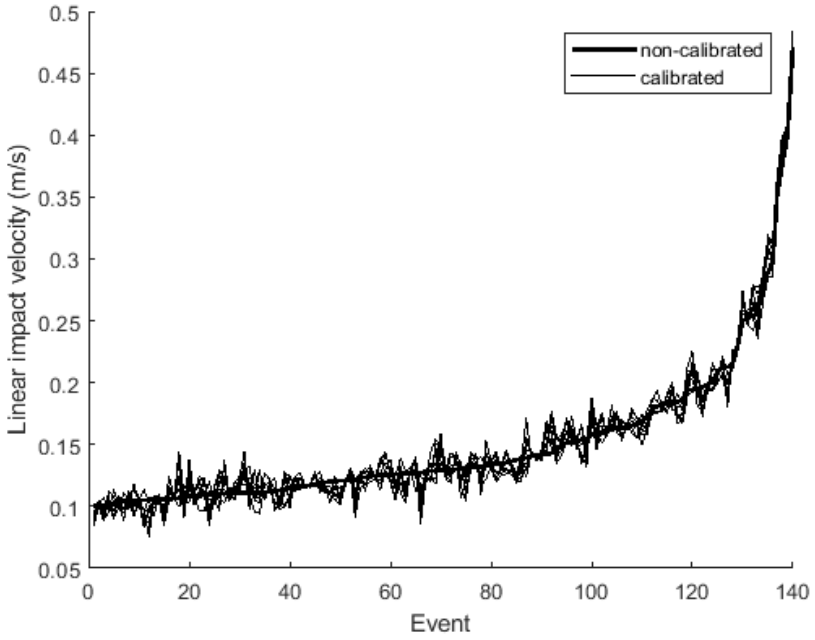

Figure 5.4: The linear impact velocity as calculated with the raw data and with the calibrated accelerations with the calibration values from C.2.

Comparing the calibration results shown in Table C.1 and Table C.2, a significant difference between two calibration measurements for the same sensor was found. This could be caused by the fact that the output of an accelerometer depends on the temperature (Frosio et al., 2009). Therefore, the calibration values from two calibration measurements cannot be considered valid for all test series. Because of this reason, the raw accelerometer data is used in the data processing and analysis.

6

Data post-processing

The raw data from the sensors is processed to find the values of interest. All data has been processed using Matlab.

6.1. Coordinate system smart Xbloc

The main axes of the smart Xbloc are shown in figure 6.1. The accelerometer measures accelerations in three axes (x,y,z), the positive direction is marked with an plus (+) and the negative direction is marked with a minus (-). The gyroscope measures rotation around three axes in radians per second, the right hand rule can be used to determine the positive rotational direction: the thump points in the positive direction, when you close the other fingers they will move in the positive direction. The actual orientation of the axis as shown in Figure 6.1 might be slightly different for each sensor because the electronics were not placed perfectly in the 3D printed Xbloc. The velocities calculated in this chapter are in the local coordinate system of the smart Xbloc.

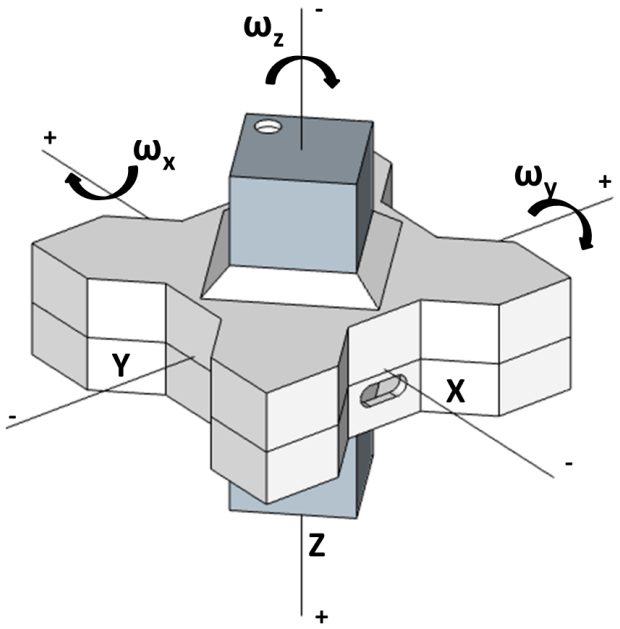

Figure 6.1: Main axes of the smart Xbloc sensor and the positive directions of the accelerometer and gyroscope.

6.2. Methodology

In this section the methodology for the calculation of the different parameters of interest is summarized. This is done for the following sections:

- Gyroscope bias correction
- Extracting motion events
- Distribution function number of events
- Angular impact velocity
- Linear impact velocity
- Distribution function impact velocity
- Differential-rotation
- Rotation during event

Gyroscope bias correction

Sometimes there is small bias in one of the axis of the gyroscope data. This bias is expressed by a constant measurement of ±0.01 rad/s when the sensor is stationary. The bias is corrected for each axis separately with the following steps:

1. Movements are removed from the gyroscope data by only taking the data between +0.03 rad/s and -0.03 rad/s.
2. The bias is determined by taking the mean of the data between the thresholds.
3. If the mean is nonzero, the mean value is subtracted from all the data to correct for the bias.

Extracting motion events

To analyze the number of impacts, separate movements are detected in the data. Different movements are separated by a period without rotational movement. These separate movements are called events. For each event the impact velocity is found by taking the maximum resultant velocity. Usually two events, and thus two impacts, are found per wave period. The technical definition of an event is: a number of consecutive gyroscope measurements for which the total rotation rate (ω) is larger than 0.011 rad/s and at least once exceeding the value of 0.051 rad/s. The value of 0.051 rad/s has been chosen because this value is larger than the noise level of the data. Therefore, no noise will be marked as a motion event. The value of 0.011 rad/s is used to distinguish between separate motion events, the value of 0 rad/s might be more logical to mark the beginning and end of an event, but it was found that for this value the distinction between events was not clear due to noise in the data. The following steps have been executed to extract the motion events:

1. The total angular velocity (ω) is calculated by taking the modulus of the angular velocity vector with the three components: ω_x, ω_y, ω_z.
2. All data points for which the total angular velocity (ω) exceeds the threshold value of 0.051 rad/s are marked.
3. All data points for which the total angular velocity (ω) exceeds the threshold value of 0.011 rad/s are marked, if one of the consecutive data points above this value also exceeds the other threshold value (ω = 0.051 rad/s) the consecutive measurements are marked as an event.
4. The star and end time of the event are listed in a separate matrix and used as boundaries of an event during further processing.
5. The number of events per 1000 waves (N_E) is determined for each test run separately by dividing the total number of events by the number of waves and multiplying it by 1000.

Distribution number of events
The distribution of the number of events (N_E) can be determined for two variables: the location on the slope and the stability number. The following steps have been executed to find a distribution function to describe the number of events per 1000 waves:

1. The empirical probability density function, probability plot and cumulative density function have been plotted for each combination of the two variables.
2. Using the Matlab toolbox for distribution fitting, several commonly used distributions were fitted and evaluated visually and with the Kolmogorov-Smirnov test. The best fit was found for the lognormal distribution.
3. The parameters (σ, μ) for the lognormal distribution were determined for each combination of variables.

Angular impact velocity
The angular impact velocity ($v_{i,angular}$) is determined from the gyroscope data. It is determined for each event separately, with the following steps:

1. For each event with n data points the maximum angular velocity (ω) is determined. It is assumed that there is only one impact per event, which is equal to maximum rotational velocity within that event.
2. The angular impact velocity (ω_i) is in radians per second. The impact velocity ($v_{i,angular}$) in meters per second is estimated by multiplying ω_i with the height h of the Xbloc ($h = 0.056m$).

Linear impact velocity
The linear impact velocity is calculated by integrating the accelerometer data. Before the data can be integrated the gravitational acceleration has to be removed from the data to obtain the wave induced accelerations. This is executed with the following steps for each axis separately:

1. Between each event the mean of the acceleration is taken. This value represents the gravitational acceleration.
2. the mean of the acceleration is subtracted from the data between the events, with this step the gravitational acceleration is removed from the data.
3. For each event, the mean of the data between that event en the one before it, is subtracted to remove the gravitational acceleration during the event. The rotation during the event has been neglected because the rotations are small.

After the gravitational acceleration is removed the linear impact velocity ($v_{i,linear}$) can be calculated for each event separately. This is executed with the following steps:

1. For the number of data points in an event (n) the linear velocity ($v_{x,i}$, $v_{y,i}$, $v_{z,i}$) for each axis at each data point i (i=1,2,3,...,n) is calculated by integration of the accelerometer data. Integration is executed for each event separately, using the midpoint rule with a special condition for the time interval to reduce errors.
2. The resultant linear velocity for each data point ($v_{res,i}$) is determined by taking the modulus of the velocity vector, with the three velocity complements ($v_{x,i}$, $v_{y,i}$, $v_{z,i}$).
3. The linear impact velocity ($v_{i,linear}$) is assumed to be equal to the maximum linear velocity ($v_{res,i}$) during the event.

Distribution impact velocity
The distribution function for the impact velocity was found to be bimodal. Therefore, only a distribution fit was made for the extreme values of the impact velocities using the generalized Pareto distribution (GPD). This is executed with the following steps:

1. The probability of exceedance curve for the impact velocities has been constructed for each combination of location on the slope and stability number.
2. All data with a smaller probability of exceedance than 5% is selected and the parameters for the GPD have been determined.

Differential rotation event
During a movement the smart Xbloc might obtain a different orientation. The difference between a new orientation and the old orientation is called the differential rotation (θ). For each event the differential rotation is determined by executing the following steps:

1. The gravitational acceleration before and after an event are determined and stored in vector a and b.

2. Using the dot-product between vector a and b the differential rotation angle (θ) per event is calculated.

Rotation during event
Within an event the armour unit is rotating, due to the angular velocity. The rotation angle (r) is defined as the maximum rotated angle with respect tot the starting position. This rotation angle is determined with the following steps:

1. For each axis separately the angular velocity of an event, with n data points, is integrated using the midpoint rule for each data point i. This gives the total rotation per data point ($r_{x,i}$, $r_{y,i}$, $r_{z,i}$) around each axis (i=1,2,3,...,n).

2. The total rotation ($r_{tot,i}$) for each time step is calculated by taking the modulus of the rotation vector.

3. The rotation angle during the event (r) is determined by taking the maximum value of the total rotation ($r_{tot,i}$) of all time steps within the event.

6.3. Data-transfer errors
After each test series, a script is uploaded to the processor of the sensor enabling the transfer of the collected data to a computer. The program Coolterm (Version 1.6.0) is used as serial port terminal to collect and save the transferred data from the sensor. During the data transfer reading errors occur creating a gap in the data. The data from each sensor is uploaded twice, after which the data sets are compared. Gaps due to the reading errors are repaired by taking data from the other upload to fill the gaps in the data.

6.4. Extracting separate test runs
The uploaded data from the sensor contains a complete test series with 5 separate test runs, between each test run the smart Xbloc is turned on and off. When the smart Xbloc is activated, the time is reset and the smart Xbloc starts to measure. The resetting of the time is used to distinguish between separate test runs of the different measurements. A Matlab script was used to separate and extract the test runs from the main file and store each test run in a separate matrix.

6.5. Gyroscope bias correction
The gyroscope measures angular velocity in three axes; when the sensor is at rest the angular velocity reading should be zero. This was observed to be true for most of the measurements. However, due to a small drift, the gyroscope sometimes reads an angular velocity of ±0.01 rad/s, while stationary. This is a bias in the measurement and needs to be corrected. An example of the angular velocity in three axes is shown in Figure 6.2, where ω_y has a bias of -0.01 rad/s. The bias correction is done for each axis of the gyroscope separately, see Figure 6.3 for only the bias in ω_y. To calculate the bias, the mean of the data between two threshold values is taken, see Figure 6.3. The threshold values are used to exclude peaks and find the mean of just the bias. The gyroscope measures in steps of 0.01 m/s, therefore the calculated mean is rounded to two decimals and subtracted from the data to correct for the bias; Figure 6.4 shows the data after it is corrected for the bias in ω_y. This method for correcting the bias in the gyroscope has been applied to all data. The gyroscope bias is assumed to be constant. This assumption can be made because the measurement duration is short (20 to 30 minutes), therefore the drift in the sensor during the measurement is small.

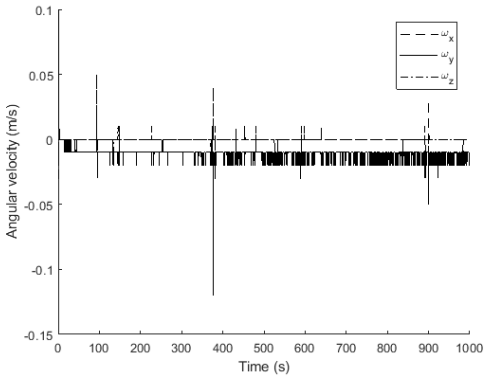

Figure 6.2: Gyroscope data for three axis, ω_y has a bias of -0.01 rad/s.

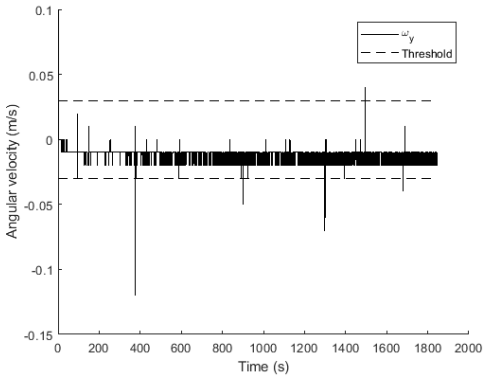

Figure 6.3: Bias in ω_y of -0.01 rad/s and the two threshold values to exclude peaks.

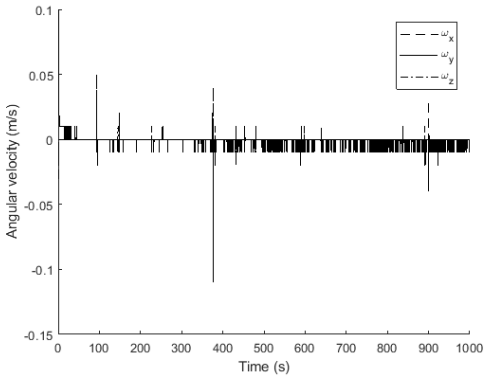

Figure 6.4: Gyroscope data for three axis after bias correction for ω_y.

6.6. Detecting motion events

6.6.1. Modulus angular velocity

The gyroscope in the smart Xbloc measures angular velocity in three axes (ω_x,ω_y,ω_z), the resultant angular velocity ω in rad/s is calculated using Equation 6.1.

$$\omega = \sqrt{\omega_x^2 + \omega_y^2 + \omega_z^2} \tag{6.1}$$

6.6.2. Event extraction

Events with rotational motion are detected in the data. To do so, the data is analyzed using two threshold values. Threshold 1 is used to find events without capturing noise of the sensor as an event. Threshold 2 is used to determine the duration of the event. These threshold values have been applied to the resultant angular velocity ω.

In Figure 6.5, an example of two events is given. On the left, the data before the events analysis can be seen; all the data points are marked with an x. On the right, the data after extracting the event is given; the data points within an event are now marked with an o. The boundaries of the event are marked with a vertical line.

The value for threshold 1 is 0.051 rad/s. This value has been chosen because the sensor measures angular velocity in steps of 0.01 rad/s, which is also the typical noise level found in the data. For the situation that all three axes would measure a noise of 0.01 rad/s at the same time, the resultant angular velocity would still be well below the value of 0.051 rad/s. Therefore, all events will be detected with this threshold, without capturing noise as event.

The value for threshold 2 is 0.011 rad/s. This value has been chosen because it is just above the noise level of 0.01 rad/s. Different values were tried and it was found that 0.011 rad/s, was most effective for detecting the duration of an event.

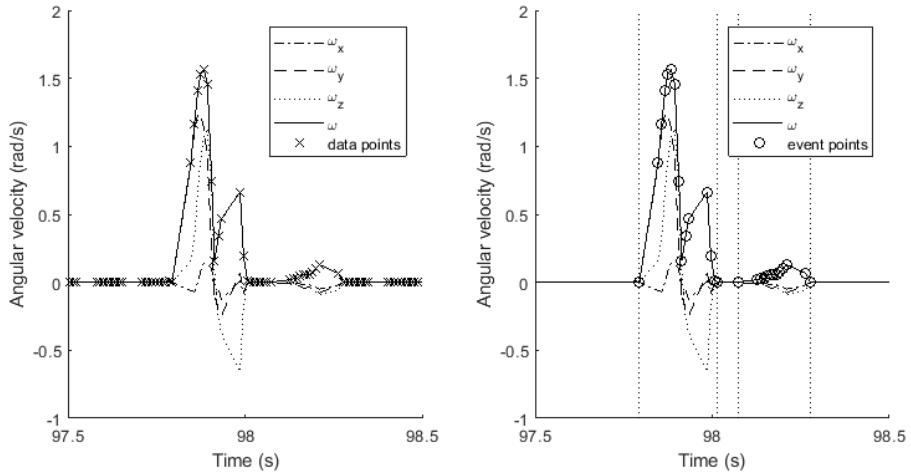

Figure 6.5: Example from the gyroscope data showing two event before and after extraction.

6.7. Distribution number of events

To describe the distribution of the number of events, several commonly used distribution functions were fitted through the data. After visual inspection, the log-normal distribution seemed to best describe the data. Therefore, the Kolmogorov-Smirnov test with a 1% significance level was used to check the null-hypothesis. It was found that for all the combinations of wave height and location on the slope the null-hypothesis could not be rejected. As the log-normal distribution could not be rejected with the Kolmogorov-Smirnov test and was also visually observed to give the best fit, it is reasonable to conclude that the number of events per 1000 waves can be described with the log-normal distribution, Equation 6.2. The mean and the standard deviation for each combination of the wave condition and location on the slope are shown in Table 6.1. The empirical cumulative density function and the fit using the parameters from Table 6.1 are shown in Appendix H.

$$f(N_E) = \frac{1}{\sigma N_E \sqrt{2\pi}} e^{-\frac{(ln(N_E)-\mu)^2}{2\sigma^2}} \tag{6.2}$$

where

N_E	number of events per 1000 waves
$f(N_E)$	probability of N_E
σ	standard deviation of $Ln(N_E)$, see Table 6.1
μ	mean of $Ln(N_E)$, see Table 6.1

Table 6.1: Mean (μ) and standard deviation (σ) for the natural logarithm of the number of events per 1000 waves, for different stability numbers and locations on the slope with respect to still water level.

Stability number	1,85		2,21		2,58		2,92		3,32	
	μ	σ	μ	σ	μ	σ	μ	σ	μ	σ
SWL$+2d_n$	3,10	1,03	3,54	1,07	3,02	1,55	2,78	1,46	3,00	1,54
SWL	3,05	1,30	3,22	1,52	3,53	1,55	3,46	1,77	2,93	1,49
SWL$-2d_n$	2,82	1,18	2,34	1,38	2,50	1,66	2,96	1,65	2,65	1,84

6.7.1. 95% confidence boundary

The 95% confidence boundary for the empirical cumulative density is calculated using the ecdf() function in Matlab. This function uses Greenwoods method for determining the lower and upper 95% confidence boundary of the empirical cumulative density function. This method can be used as a variance estimation of an empirical cumulative density function (Lawless, 2003). The empirical cumulative density function, the log-normal distribution fit and the empirical 95% confidence boundary are shown in Appendix H.

6.8. Angular impact velocity

The angular impact velocity is determined as the maximum value in the angular velocity ω_j of an event with n data points (j=1,2,3,...,n). The angular velocity is measured in radians per second and therefore also the impact velocity is given in radians per second. The impact velocity in meters per second can be estimated by multiplying the angular velocity in radians per second with the height of the unit, Equation 6.4. For each event, a maximum velocity is found. The exceedance curve per wave condition for three locations on the slope is shown in Appendix D.

$$\omega_i = max(\omega_j) \tag{6.3}$$

$$v_{i,angular} = \omega_i * h \tag{6.4}$$

where

ω_i	impact velocity of an event (rad/s)
ω_j	angular velocity at point j (j=1,2,3,...,n)
$v_{i,angular}$	estimated angular impact velocity in meters per second
h	height of the smart Xbloc (h = 0.056 m)

An example of the impact velocity from the data is shown in Figure 6.6. This figure shows a couple of rocking movements, the impact velocity per event is also shown. It can be observed that during one wave period two events and two impact velocities are detected by the method as discussed in Section 6.6.

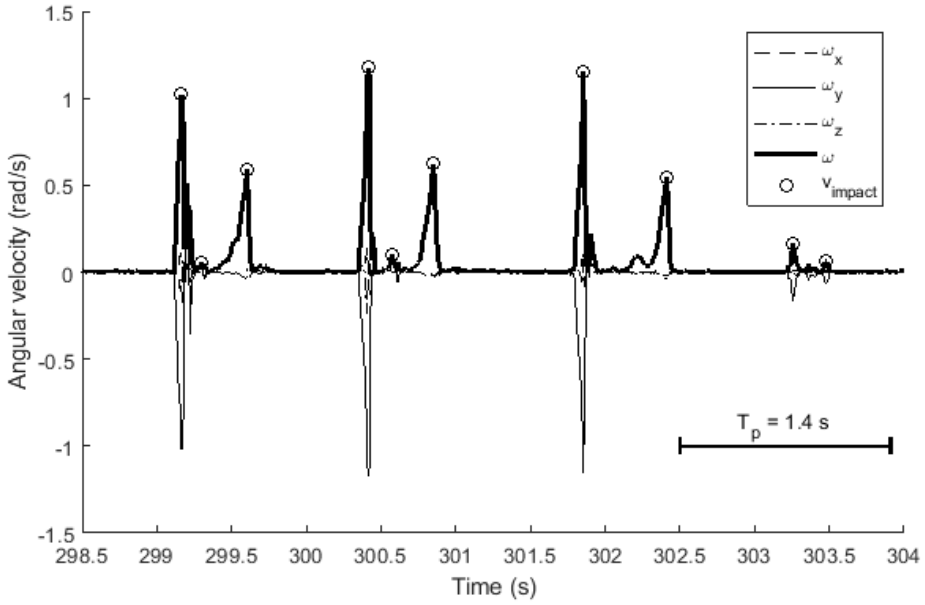

Figure 6.6: Example from the data, showing the total rotation ω and the detected impacts

6.8.1. Kinetic energy of the impact

The kinetic energy due to an impact can be estimated with Equation 6.5. The total energy due to all the impacts at a certain depth, with a number of impacts n is calculated with Equation 6.6. The results have been used in the analysis to compare the kinetic energy for different rotations.

$$E_{k,i} = \frac{1}{2} m v_{im,i}^2 \tag{6.5}$$

$$E_{k,total} = \sum_{i=1}^{n} E_{k,i} \tag{6.6}$$

where

$E_{k,i}$	kinetic energy of the impact per event (J)
n	number of events
m	mass of smart Xbloc (m = 0.141 kg)
$v_{im,i}$	Impact velocity per event (m/s)
$E_{k,total}$	Total kinetic energy from all events (J)

6.9. Linear impact velocity

The linear impact velocity can be calculated by integrating the accelerometer data. Before this is possible, the acceleration due to rocking has to be determined by removing the gravitational acceleration from the data.

6.9.1. Remove gravitational acceleration

To find the linear velocity, the acceleration due to gravity is removed from the accelerometer data. The accelerometer measures acceleration in three axes. When the sensor is not moving, the three axes of the accelerometer measure the gravitational acceleration, due to a change in orientation the three axes measure a different value, as can be seen in the left part of Figure 6.7. During events, as discussed in Section 6.6, the sensor might obtain a new orientation. Therefore, the average gravitational acceleration between events is determined for each axis. This value is subtracted from the data between the two events and the event right after this interval, with this step the gravitational acceleration is removed from the data. The result of these steps can be found on the right of Figure 6.7.

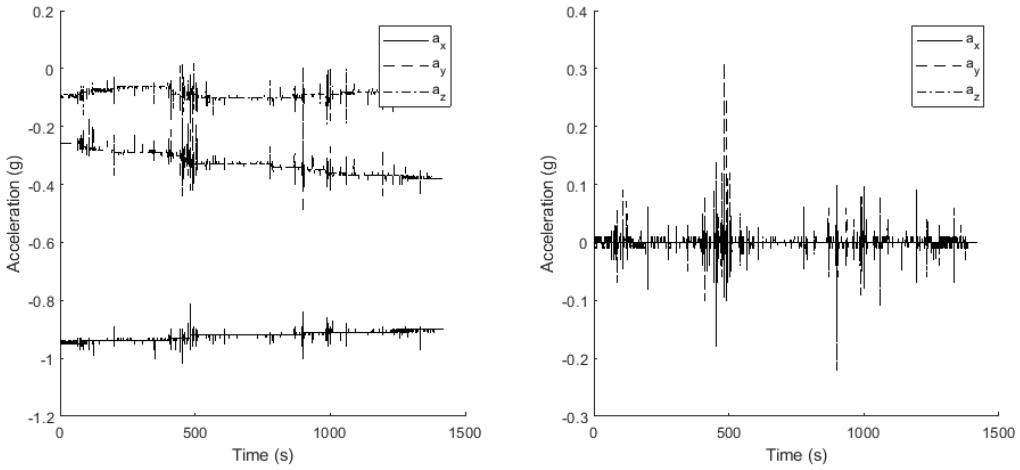

Figure 6.7: Left: data with gravitational acceleration. Right: data without acceleration due to gravity.

6.9.2. Linear impact velocity

To compute the linear velocity for each axis, the acceleration without the gravitational acceleration (a) is integrated. The integration is done for the total duration of the movement, consisting of n measurements. For the integration the midpoint rule is used, Equation 6.7. It is assumed that the linear velocity is zero before and after each event.

The sensor measures with a sample rate of around 100 Hz. When the measured data is stored to the main storage of the sensor, the sample frequency is temporarily lowered to around 2 Hz (Caldera, 2019). When this is the case, the time interval Δt does not correctly represent the time for the measured acceleration. To reduce the error when integrating between two measurements with a large Δt. A threshold value of Δt = 0.02 seconds is used. When the threshold is exceeded, a time step of Δt = 0.01 seconds (100 Hz) is used for integration of that time step.

The linear velocity per event is found by integrating the acceleration for each axis separately. The resultant velocity is found by taking the modulus of the velocity vector, see Equation 6.9. The impact velocity is determined by taking the maximum of the resultant angular velocity $max(v_{res,i})$.

$$v_i = \sum_{i=1}^{n} \frac{a(i+1) + a(i)}{2 * \Delta t(i)} \tag{6.7}$$

$$v_{res,i} = \sqrt{v_{x,i}^2 + v_{y,i}^2 + v_{z,i}^2} \tag{6.8}$$

$$v_{i,linear} = max(v_{res,i}) \tag{6.9}$$

where

v_i	linear velocity at point i
$a(i)$	acceleration at point i (m/s^2)
$\Delta t(i)$	$t(i+1) - t(i)$, with $t(i)$ = time at point i
$v_{res,i}$	resultant linear velocity at point i
n	number of data points in the event
$v_{i,linear}$	linear impact velocity during the movement (m/s).

Error due to rotation within an event

During an event the sensor is rotating between almost zero up to 25 degrees, as shown in figure 8.6. As discussed above the gravitational acceleration during an event is assumed to be constant. However, due to rotations the gravitational acceleration is not constant during an event. The error due to a constant rotation can be estimated by assuming a rotation angle and calculating the gravitational component due to this rotation. By assuming a typical time step Δt = 0.01s and a duration until the impact the component of the gravitational acceleration can be integrated to estimate the error in linear velocity, see Equation 6.10. This is the error for each axis individually, the total error per time step is estimated by taking the modulus of the error vector, Equation 6.11. The cumulative error for multiple time steps can be estimated using Equation 6.12. By assuming a linear rotation, a time steps of 0.01s and a variable duration until impact the cumulative error can be found depending on the angle of rotation, the result is shown in Figure 6.8. The resulting errors for the largest rotation and longest time before the impact results in a maximum error of 0.09 m/s. For this worst case scenario the error is maximum 10% of the extreme values for the linear impact velocity.

$$E_i = tan(\alpha(i)) * g * \Delta t(i) \tag{6.10}$$

$$E_t = \sqrt{E_{x,i}^2 + E_{y,i}^2 + E_{z,i}^2} \tag{6.11}$$

$$E_T = \sum_{t=1}^{n} E_t \tag{6.12}$$

Where

E_i Error due to a rotation within an event (m/s) for one axis
E_t Total error per time step
E_T Cumulative error
α Rotation angle (deg)
g Gravitational acceleration (m/s^2)
n number of samples until impact

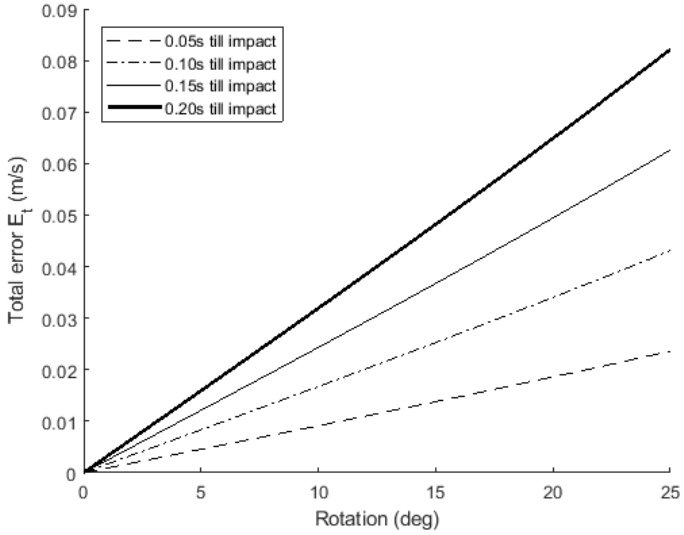

Figure 6.8: Estimated error in linear velocity (m/s) due to a rotation within an event for $\Delta t = 0.01s$

6.10. Distribution impact velocity

The empirical probability density function of the impact velocity, as shown in Figure 6.9, is used to assess which distribution function can be used to describe the impact velocity data. The data appears to have a bimodal distribution, which is most apparent in the large tail. It is found that it is not possible to describe the data with a unimodal distribution function. This is true for both the linear as well as the angular impact velocity.

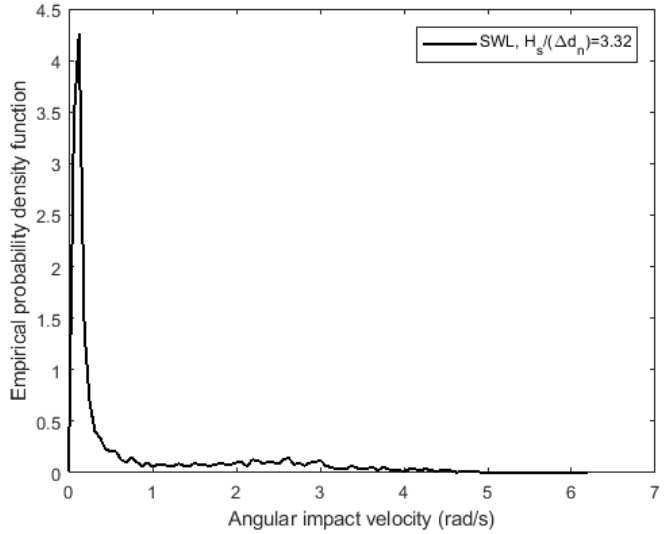

Figure 6.9: Empirical probability density function for the angular impact velocity at SWL.

Another possibility is to describe the data by looking at the probability of exceedance curve, as shown in Figure 6.10. The exceedance probability has been plotted on a logarithmic scale to give more emphasis on the extreme values. Several distribution functions were tried and it was found that the tail of the extreme values distribution can be described most accurately using the generalized Pareto distribution (GPD). This distribution type is often used to model the tails of another distribution. For engineering purposes, often the 2% or 1% exceedance probability values are used. For this reason the location parameter, determining where the tail starts, was set arbitrarily at the 5% exceedance probability, as shown in Figure 6.10. Because of this reason, the GPD is only valid for values with an exceedance probability of 5% or less. It was found that both the linear as well as the angular impact velocity can be described using the GPD distribution function. The exceedance curve for each location and wave condition can be found in Appendix G.

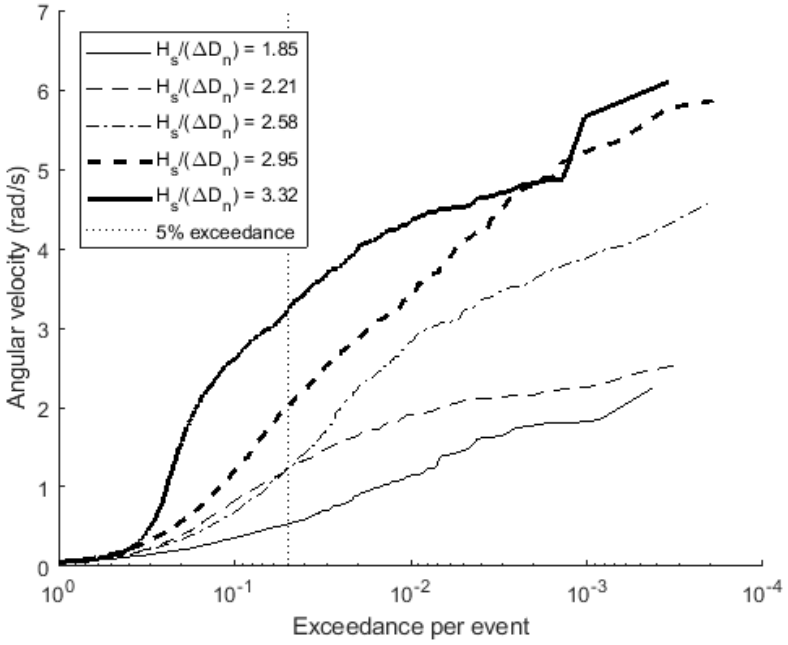

Figure 6.10: Empirical cumulative density for the angular impact velocity at SWL.

The cumulative density function for the generalized Pareto distribution (GPD) is given by Equation 6.13. The three parameters (k, θ, σ) have been estimated for both the linear and the angular impact velocity, using the Matlab distribution fitter application and can be found in Appendix F, Table F.1 and F.2. An example of the empirical exceedance curve can be found in Figure 6.11.

$$F(v_i) = \left(1 - \left(1 + k\frac{v_i - \theta}{\sigma}\right)^{-1/k}\right) * 0.05 + 0.95 \qquad \text{for } F(x) \geq 0.95 \tag{6.13}$$

where

$F(v_i)$	cumulative density of the impact velocity
k	index parameter
v_i	impact velocity in radians per second or meters per second
θ	location parameter
σ	scale parameter

The GPD can be rewritten to find the impact velocity $v_{i,p\%}$ for a given exceedance probability p in percentage, Equation 6.14. This equation is only valid for an exceedance probability p of 5% or less. The parameters for the equation can be found in Table F.1 and F.2. If the table for the angular velocity is used, the answer is in radians per second else the answer is in meters per second. For each combination of wave condition and location on the slope the exceedance curve, GPD fit and 95% confidence bound are shown in Appendix F.

$$v_{i,p\%} = \left(\left(\frac{1}{1 - \frac{1-p/100-0.95}{0.05}} \right)^{k} - 1 \right) \frac{\sigma}{k} + \theta \qquad \text{for } p \leq 5\%. \tag{6.14}$$

where

$v_{i,p\%}$	impact velocity with a given probability of exceedance p in rad/s or m/s
p	exceedance probability in percentage ($p \leq 5\%$)
k	index parameter
θ	location parameter
σ	scale parameter

6.10.1. Angular impact velocity in m/s

The exceedance probability for the angular impact velocity can be calculated for different wave conditions using Equation 6.13 and the values from Table F.1. With these values the angular impact velocity can be found in radians per second. The angular impact velocity in meters per second is estimated using Equation 6.15.

$$v_{i,angular} \approx \omega * h \tag{6.15}$$

where

$v_{i,angular}$	angular impact velocity in meters per second
ω	angular velocity in radians per second
h	nominal diameter of the Xbloc used in the scale model (h = 0.056 m)

6.10.2. 95% confidence boundary

The 95% confidence boundary for the empirical cumulative density is calculated using the ecdf() function in Matlab. This function applies Greenwoods method to determine the lower and upper 95% confidence boundary of the empirical cumulative density function. This method can be used as a variance estimation of an empirical cumulative density function (Lawless, 2003). An example of an exceedance curve, the 95% confidence bound and the GPD fit is shown in Figure 6.11. The 95% confidence boundaries for each exceedance curve of the impact velocity are shown in Appendix F. The confidence boundary for the velocity exceeded by 2% of the waves is estimated from these graphs and is shown in Table G.1 and Table G.2.

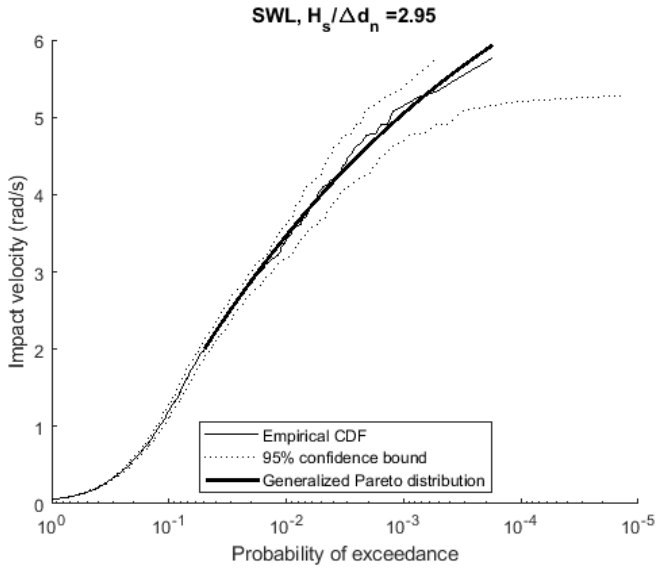

Figure 6.11: Empirical exceedance curve, fit using the GPD function and the 95% confidence bound for the angular impact velocity at SWL and for a stability number of 2.95.

6.11. Differential rotation

Each event may result in a change in differential rotation. The differential rotation is defined as the difference in orientation between just before and just after an event. To determine this change in orientation, the data from the accelerometer is used to calculate the angle between the gravitational acceleration vector before and after the event using Equation 6.16. The results from the differential rotation calculations are shown in Appendix E. The vectors a and b contain the three components of the accelerometer data before and after the event. The value of these vectors is determined by taking the mean of 20 data points before and after the event, to reduce the error due to noise in the accelerometer. If there are less than 20 data points between two events, the mean is taken of all the data points between these events. In Figure 6.12, the accelerometer data of two events is given. On the right side, an event without a change in orientation and on the left side, an event with a change in orientation can be observed by looking at the three components of the accelerometer before and after the events.

$$cos(\theta) = \frac{\mathrm{a} * \mathrm{b}}{|\mathrm{a}| * |\mathrm{b}|} \tag{6.16}$$

where

θ = differential rotation angle

$$\mathrm{a} = \begin{bmatrix} \mathrm{a}_x \\ \mathrm{a}_y \\ \mathrm{a}_z \end{bmatrix}, \mathrm{b} = \begin{bmatrix} \mathrm{a}_x \\ \mathrm{a}_y \\ \mathrm{a}_z \end{bmatrix}$$

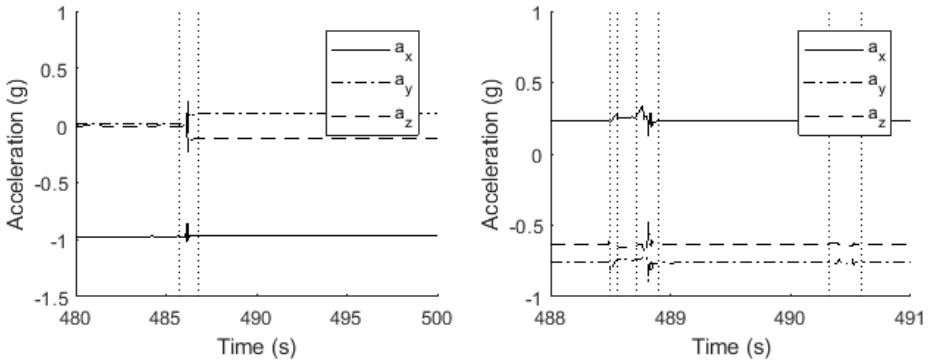

Figure 6.12: Event with a change in orientation (left) and an event without a change in orientation (right).

6.12. Rotation during event

The rotation during an event can be found by integrating the angular velocity. The maximum rotation during a movement equals the movement space of the armour unit. This rotation is more closely related to the visual observations. The angular velocity data is integrated over the duration of an event, consisting of n points, using the midpoint rule, Equation 6.17. The total rotation with respect to the starting position can be found by taking the modulus of the rotation vector for each step of the movement separately, see Equation 6.18. The maximum rotation during the movement is found by taking the maximum of the total rotation max($r_{tot,i}$).

$$r_i = \sum_{i=1}^{n} \frac{\omega(i+1) + \omega(i)}{2 * \Delta t(i)} \tag{6.17}$$

$$r_{tot,i} = \sqrt{r_{x,i}^2 + r_{z,i}^2 + r_{y,i}^2} \tag{6.18}$$

$$r = max(r_{tot,i}) \tag{6.19}$$

where

r_i	rotation at point i (deg)
$r_{tot,i}$	total rotation at point i (deg)
$\omega(i)$	angular velocity at data point i (deg/s)
$\Delta t(i)$	$t(i+1)$-$t(i)$
r	rotation angle during an event (deg)

6.13. Wave characteristics

Three wave gauges were used to measure the wave conditions, the gauges were placed half way the wave flume at 10 m from the scale model. The waves have been analysed using the method of Zelt and Skjelbreia (1992). The script to analyze the data was provided by the TU Delft. An example of the wave spectrum is shown in Figure 6.13. The wave conditions for each test run are shown in Appendix A.

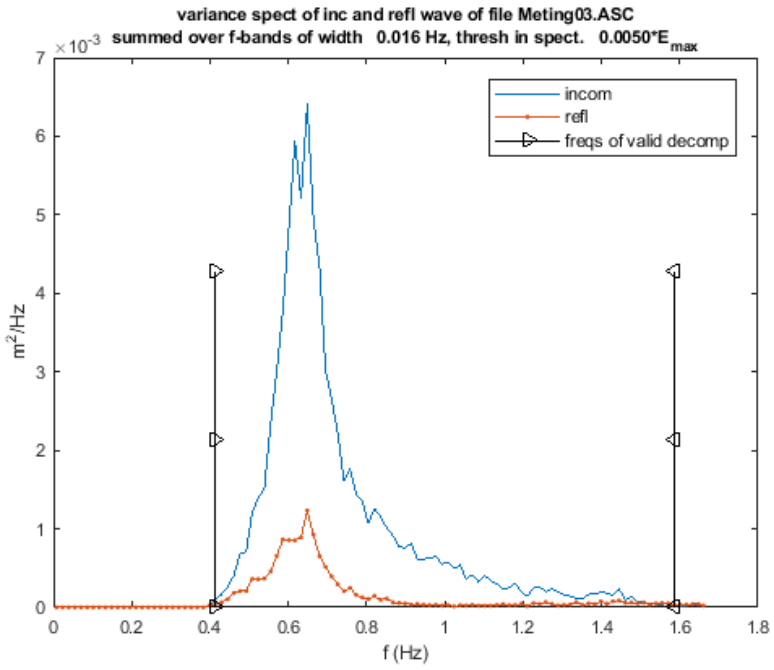

Figure 6.13: Example of a wave spectrum for the third test run.

7 Results

In this section the main results are presented. Scale model tests have been carried out to gather rocking data with smart Xbloc armour units. Measurements were executed for increasing stability numbers and at three depths: still water level (SWL), still water level + $2d_n$ (SWL+$2d_n$) and still water level - $2d_n$ (SWL-$2d_n$), where d_n is the nominal diameter of the armour unit.

7.1. Number of impacts

The number of impacts is assumed to be equal to the number of events. The number of events has been calculated and for each event one impact velocity has been determined, see Section 6.2 for the definition of an event. The number of events per 1000 waves has been determined for three locations on the slope and 5 different stability numbers. The results are presented with an exceedance curve, as shown in Figure 7.1. The parameters for the log normal distribution fit and the empirical 95% confidence boundary are shown in Appendix H.

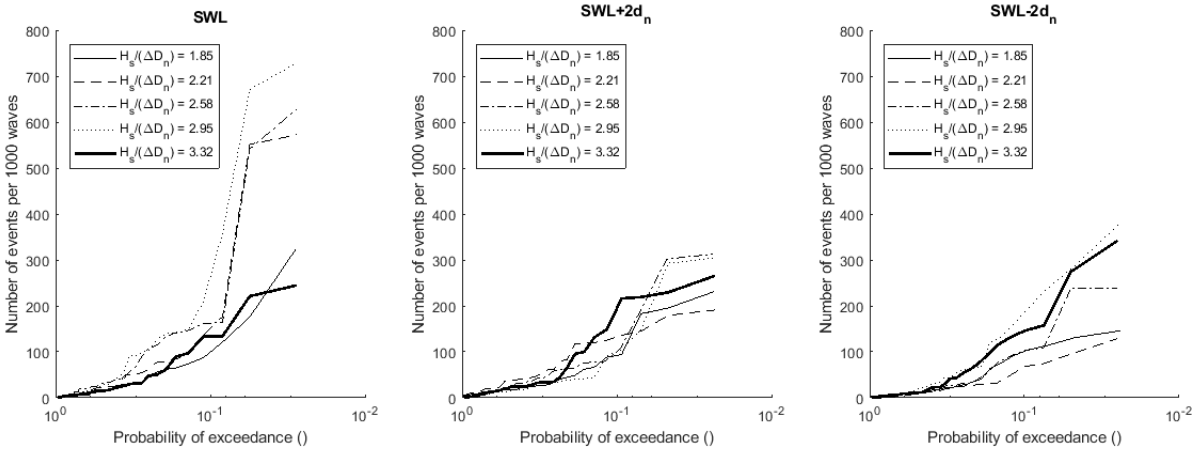

Figure 7.1: Probability of exceedance for the number of events per 1000 waves for 3 different locations on the slope.

7.2. Impact velocity

The impact velocity per event has been determined with two methods, as discussed in Section 6.8 and Section 6.9. The exceedance curve for the angular and linear velocity are shown in Figure 7.2 and 7.3. The determined parameters for the generalized Pareto distribution can be found in Appendix F. The exceedance curve including the fit with the GPD and the 95% confidence bound are also shown in Appendix F. The 95% confidence boundary for the impact velocities with a 2% probability of exceedance are shown in Appendix G.

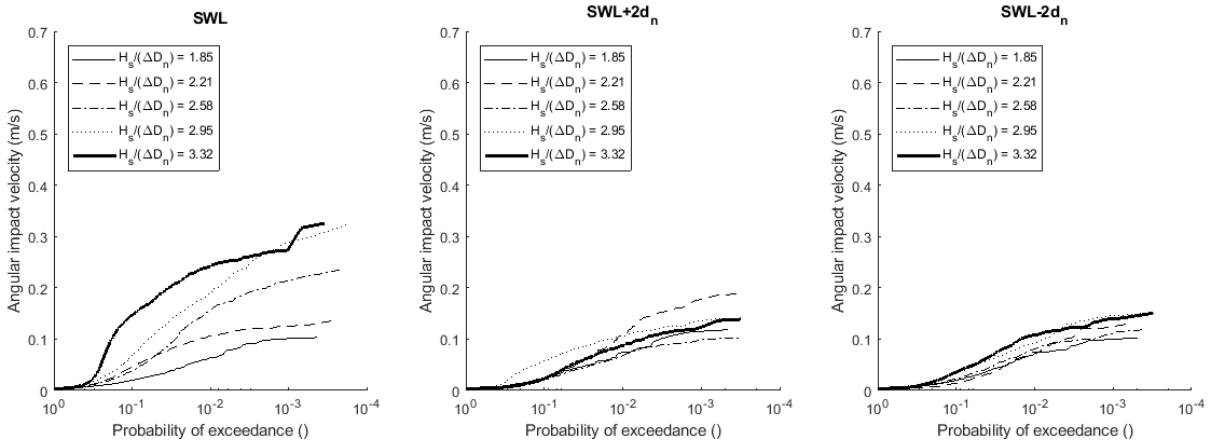

Figure 7.2: Exceedance curve for the angular impact velocity in meters per second.

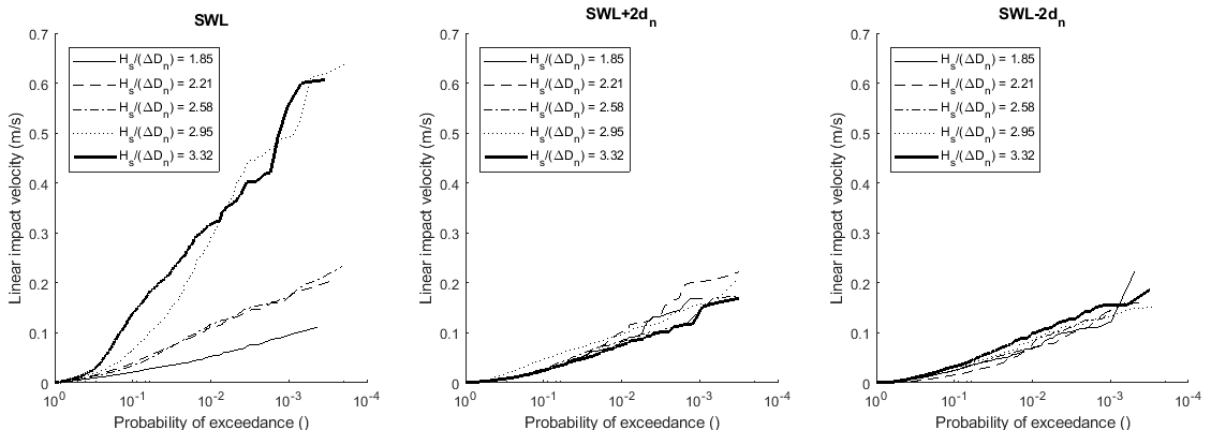

Figure 7.3: Exceedance curve for the linear impact velocity in meters per second.

7.3. Differential rotation

The differential rotation for each event has been calculated as discussed in Section 6.11. The results are presented in Figure 7.4. In this scatter plot the differential rotation and the angular impact velocity per event are plotted.

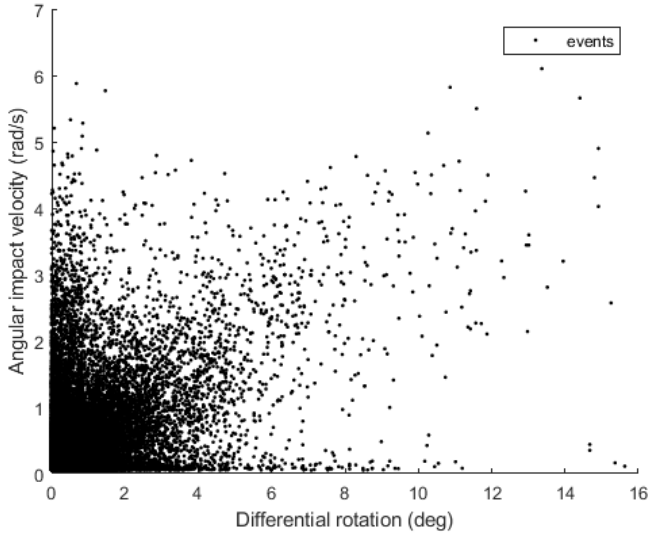

Figure 7.4: The maximum angular velocity and differential rotation angle per event.

7.4. Rotation during event

The rotation during an event has been calculated as discussed in Section 6.12. The results are presented in Figure 7.5, in this scatter plot the rotation during the event and the impact velocity of the event are plotted.

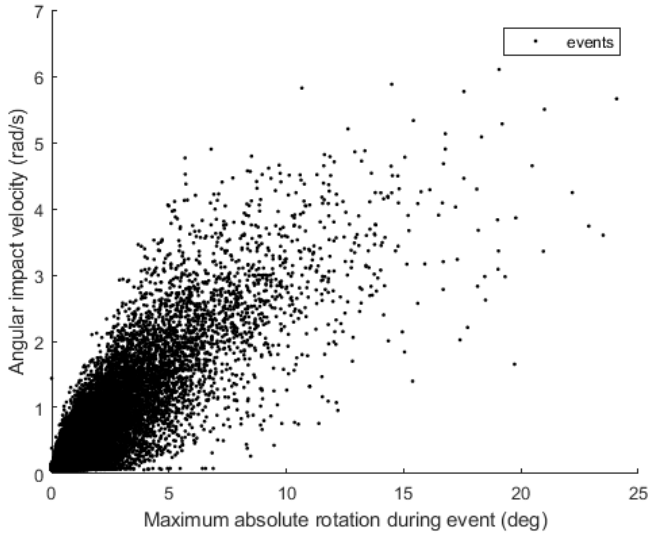

Figure 7.5: The maximum absolute rotation (deg) within each event and the angular impact velocity in (rad/s).

7.5. Wave conditions

Each test series consists of 5 test runs with an increasing wave height. The incoming significant wave height has been measured with wave gauges and analyzed using the method of Zelt and Skjelbreia (1992). The average incoming significant wave height $H_{m0,i}$ of the test series is shown in Table 7.1. The measured wave conditions for each test run are shown in Appendix A. Each test run consists of around 1200 waves.

Table 7.1: Average measured wave conditions for each test run, one test run consisted of around 1200 waves

Test run	Significant wave height $H_{m0,i}$ (m)	Stability number N_s	Wave steepness s_{op}	Peak period T_p (s)
1	0,10	1,85	0,04	1,28
2	0,12	2,21	0,04	1,41
3	0,14	2,58	0,04	1,54
4	0,16	2,92	0,03	1,75
5	0,18	3,32	0,03	1,90

8

Analysis

In this chapter the results are analyzed more in-depth. First the variation of the number of events and the impact velocities are discussed. Second the relation between the rotation and impact velocities are assessed. Finally, the visual observations are compared to the rotation angle and the expected impact velocity.

8.1. Number of moving armour units

During each test tun at least some movements were measured with the smart Xbloc. In previous studies there was always a certain number of non moving armour units. Because the smart Xbloc provides more detailed information, at least some movements were detected for each armour unit during each test run. The number of moving armour units was found to be 100%. The distribution of the number of impacts provides more information about the variation between the number of impacts.

8.2. Number of impacts

The number of impacts is assumed to be equal to the number of events. The definition of an event is: a number of consecutive gyroscope measurements for which the total rotation (ω) is larger than 0.011 rad/s and at least once exceeding the value of 0.051 rad/s, see also Section 6.6. The distribution of the number of events varies, depending the stability number and the location on the slope. The variation of the number of events can be described by the log-normal distribution using: Equation 8.1 and the values from Table 8.1. The equation has been normalized for 1000 waves, thus giving the probability for a number of events per 1000 waves. The spatial variation of the number of impacts ranges between 10 up to almost 1000 impacts per 1000 waves.

$$f(N_E) = \frac{1}{\sigma N_E \sqrt{2\pi}} e^{-\frac{(ln(N_E)-\mu)^2}{2\sigma^2}} \tag{8.1}$$

where

N_E	number of events per 1000 waves
$f(N_E)$	probability of N_E
σ	standard deviation of $Ln(N_E)$, see table 8.1
μ	mean of $Ln(N_E)$, see table 8.1

Table 8.1: Mean (μ) and standard deviation (σ) of the natural-logarithm of the number of events per 1000 waves.

Stability number	1,85		2,21		2,58		2,92		3,32	
	μ	σ	μ	σ	μ	σ	μ	σ	μ	σ
SWL+$2d_n$	3,10	1,03	3,54	1,07	3,02	1,55	2,78	1,46	3,00	1,54
SWL	3,05	1,30	3,22	1,52	3,53	1,55	3,46	1,77	2,93	1,49
SWL−$2d_n$	2,82	1,18	2,34	1,38	2,50	1,66	2,96	1,65	2,65	1,84

Over 45,000 individual events with a rotational velocity were found in 1,560,000 potential events. On average 2.9% of the waves induced a rocking motion, assuming that there are two events per rocking motion and one rocking motion per wave. The spatial and temporal variation of the number of events per 1000 waves is further analyzed by looking at the mean values as well as the distribution and the extreme values.

8.2.1. Mean number of events

The mean number of events per 1000 waves, for each wave condition and location on the slope, is shown in Figure 8.1. This graph is used to analyze the spatial and temporal variation of the number of impacts. The outcomes of the analysis are presented by the following points:

- The average number of events per 1000 waves at SWL increases with increasing wave height for the first 4 wave conditions, which is around 4800 waves. Afther the fourth wave condition the number drops significantly to a level similar as the other locations.
- $2d_n$ above and below SWL, the average number of events per 1000 waves does not vary much for an increasing stability number. Also, the mean number of impacts at these locations are in the same order of magnitude.

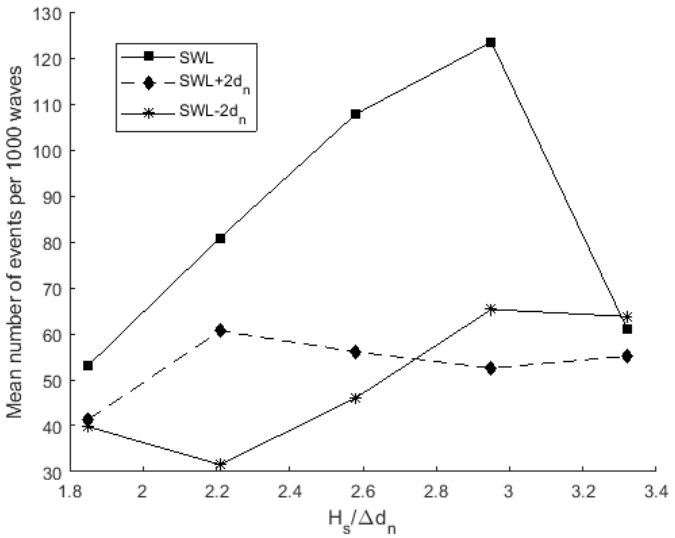

Figure 8.1: Mean number of events per 1000 waves for different stability numbers and locations on the slope

8.2.2. Spatial variation number of events

The empirical cumulative density plot can be used to assess the spatial variation of rocking and explore the full of range of number of impacts. The empirical cumulative density for the 5 wave conditions and 3 locations have been plotted in Figure 8.2. From this figure the following observations can be made:

- All the empirical CDF's have a similar shape. A general formula to describe this shape is the log-normal distribution, which depends on the location and stability number. This was also found in Section 6.7.

- For a row of armour units at a certain depth, the spatial variation ranges between 1 or 2 events up to 400 to 1000 events per 1000 waves. The rocking motion is usually described as an back and forth motion, this is measured as two separate events. So per 1000 waves there are 2000 potential events.

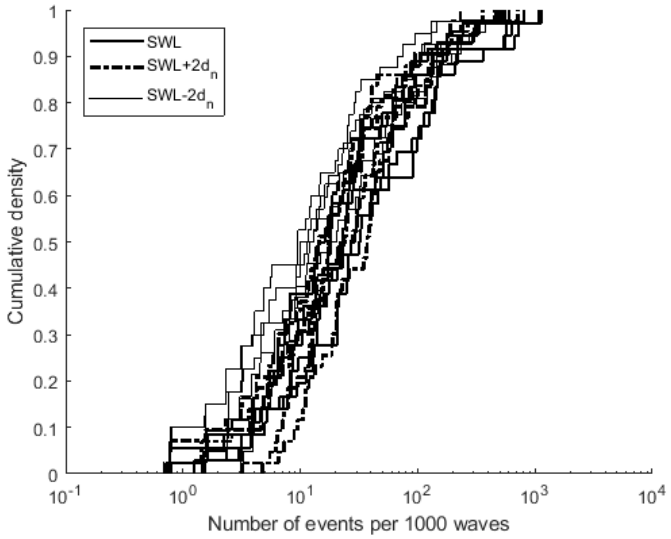

Figure 8.2: Empirical cumulative density function of the number of events per 1000 waves for 5 stability numbers and 3 locations on the slope

8.2.3. Extreme values number of events

The spatial variation of the extreme values of the number of events per 1000 waves is analyzed. This is done by looking at the probability of exceedance for different stability numbers and locations, as shown in Figure 7.1. The analysis of the spatial and temporal variation of the extreme values are presented by the following points:

- After the first wave series, the extreme number of events increases around SWL with a factor 2. After the fourth wave condition the number of impacts reduces significantly to roughly the same level as for the first wave condition.

- $2d_n$ above SWL, the extreme values for the number of impacts is lower than at SWL and does not seem to be influenced strongly by the stability number.

- $2d_n$ below SWL, the extreme number of impacts seems to increase for higher stability numbers. However, this relationship is not very strong as the second wave condition shows lower extreme values than the first one. The number of impacts is lower than at SWL.

8.3. Impact velocity

The smart Xbloc gathers data with an accelerometer and a gyroscope. Data from both sensors has been used to determine the impact velocity per event. With the accelerometer data the linear velocity has been determined, the gyroscope measures angular velocity directly. The distribution for the impact velocities, as discussed in Section 6.10, is bimodal and can not be modelled with a standard unimodal distribution function. The extreme values, with a probability of exceedance of $p \leq 5\%$, can be described using the generalized Pareto distribution, Equation F.1. The distribution depends on the stability number and location on the slope, the location and scale parameters can be found in Appendix F, Table F.1 and F.2.

$$v_{i,p\%} = \left(\left(\frac{1}{1 - \frac{1-p/100-0.95}{0.05}} \right)^{k} - 1 \right) \frac{\sigma}{k} + \theta \qquad \text{for } p \leq 5\%. \tag{8.2}$$

where

$v_{i,p\%}$	Impact velocity with a given probability of exceedance p in rad/s or m/s
p	exceedance probability in percentage ($p \leq 5\%$)
k	index parameter
θ	location parameter
σ	scale parameter

The variation of impact velocities is further analyzed by comparing the extreme values, for different locations and stability numbers. The two methods for determining the impact velocity are also compared.

8.3.1. Extreme values

The extreme values with a probability of exceedance $p \leq 5\%$, can be described with the generalized Pareto distribution (GPD), as discussed in section 6.10. The GPD has been used to calculate the impact velocity with a certain probability of exceedance p. In Figure 8.3 the impact velocity ($v_{i,2\%}$) in meter per second with $p = 2\%$ is plotted for both the angular and linear impact velocity. Based on this figure the variation in extreme values is analysed.

- The $v_{i,2\%}$ at SWL increases for an increasing stability number. The drop in number of events after the 4th wave condition, as discussed in the previous section, did not result in a decrease of the impact velocity.
- $2d_n$ above and below SWL the impact velocities $v_{i,2\%}$ do not seem to depend on the stability number. The values are in the same order of magnitude and seem to be constant around v_i = 0.05 m/s. This is also observed in the exceedance curves as shown in Figure 7.2 and Figure 7.3.
- The magnitude of the extreme impact velocities ($v_{i,2\%}$) are similar for the angular velocity and for the rotational velocity.

8.3.2. Angular versus Linear impact velocity

The angular and linear impact velocity are compared by looking at the exceedance curves shown in Figure 7.2 and Figure 7.3. The outcomes of the analysis are presented by the following points:

- $2d_n$ above and below SWL the exceedance curves for the linear and angular velocity have a similar shape and have similar values. The difference between the exceedance curve for different wave conditions is small.
- At SWL the exceedance curve of the linear and angular velocity, for the first three wave conditions have a similar shape and similar values. For the two largest wave conditions there is a large difference between the impact velocities. The exceedance curve for the linear velocity goes up to values almost twice as large as the angular velocity.

A scatter plot is made to further assess the difference between the linear and angular impact velocity. For each event the angular impact velocity is plotted against the rotational impact velocity, see Figure 8.4. This plot has been created for all the data with a wave steepness of 4%. The following observations can be made from Figure 8.4:

- Most of the events are of similar magnitude for both the linear and the angular impact velocity.
- The extreme values in angular impact velocity do not exceed 0.35 m/s while the linear impact velocity has some values between 0.35 and 0.9 m/s.

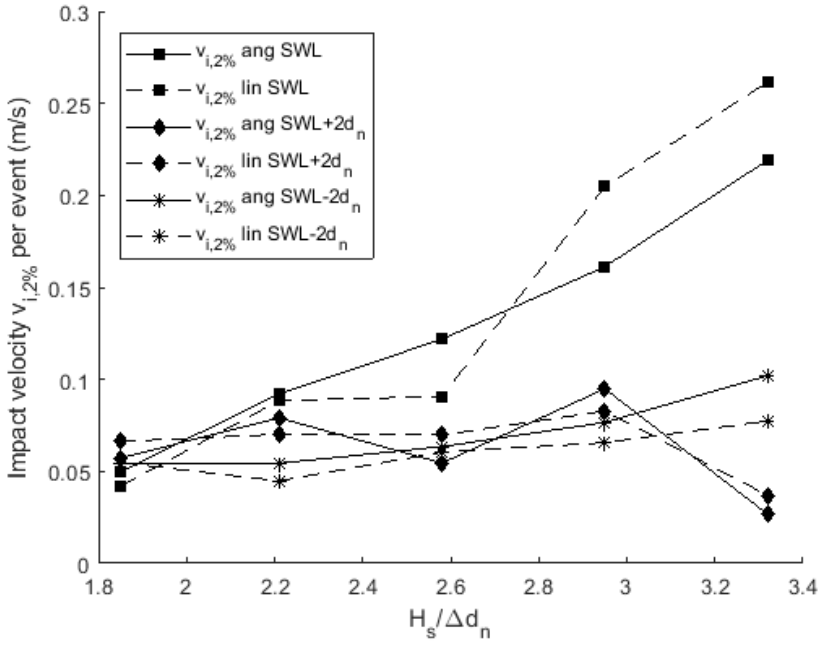

Figure 8.3: Overview of the impact velocity in meter per second with a 2% probability of exceedance per event.

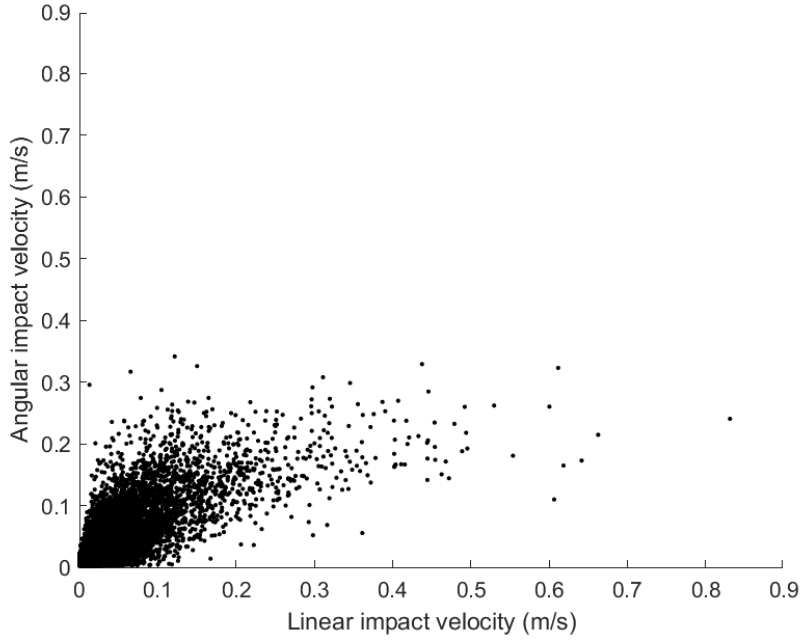

Figure 8.4: Maximum angular and linear impact velocity per event.

8.4. Rotation during an event

Rocking in model tests is usually observed by visual observation of the number of rocking armour units. The rotation during a rocking movement can be compared to the visual observations. Therefore, the maximum absolute rotation compared to the starting position of the block for each event has been calculated. This is called the rotation during an event (r_{tot}), see Section 6.12. The rotation during an event is analysed in the this section.

8.4.1. Visual observations

During each test visual observations were made using the observations form, as shown in Appendix I. This made it possible to combine the sensor data with my own visual observations. It should be noted that these visual observations do not provide information on individual events, nor does it give information on the exact wave for which the armour unit had been observed to be rocking. It only provides information for which sensor visual observations were done during the test series. For the analysis the impact velocity data is divided in two groups:

- Group 1: all events from test series where rocking was observed visually.
- Group 2: all events for which no visual observations of rocking were done during the test series.

For both groups the impact velocity and rotation have been plotted in Figure 8.5. Of the total number of events, 57.5% came from group 1. From the figure the following can be observed:

- From the two plots it can be seen that there are almost no rotations larger than 5 degrees for the sensor data without any visual observations. Some events have a larger rotation than 5 degrees but this only 0.03% of the total number of events. The visual observations were done by one person with the naked eye and it seems that rotations smaller than around 5 degrees were not visually observable.
- For group 1 the percentage of rotations larger than 5 degrees is 5.3%. For group 2 the percentage is 0.03%.

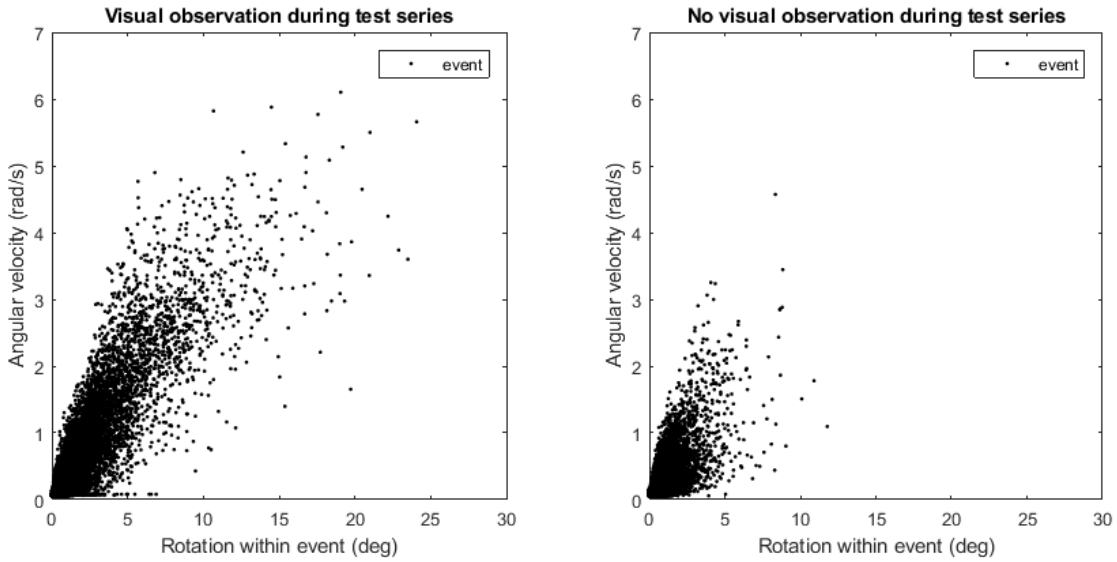

Figure 8.5: Angular impact velocity and rotation of all events during a test series. On the left results from test series for which rocking was observed visually are plotted, on the right the test series are plotted for which no visual movements were observed.

8.5. Visual observable rotations

As shown in Figure 8.5 the threshold for visual observable movements lies around 5 degrees. This was also found by analyzing rocking videos (Zwanenburg, 2012). The smart Xbloc provides much more detailed information than visual observations. Therefore, it is interesting to compare the impact velocities and number of impacts for the visual and the non-visual observable rotations. To do this the threshold for a visible rotation of 5 degrees is used, the events are divided into two groups:

- Group 1: all events with a rotation smaller than 5 degrees.
- Group 2: all events with a rotation larger than 5 degrees.

The percentage of events with a rotation larger than 5 degrees are shown in Table 8.2. From this table it can be found that at SWL both the largest number of events are found (41.5 % of the total number of events). As well as the largest percentage of events with a rotation larger than 5 degrees (4.8 % of the movements at SWL).

Table 8.2: First column gives the depth, the second column gives the percentage of the total events for each depth. The third column gives the percentage of the number of events at a certain depth with a rotation larger than 5 degrees.

Location	Percentage of total number of events (%)	Percentage of events with a rotation >5 degrees (%)
SWL	41.5	4,8
SWL +2d_n	31.3	1,0
SWL -2d_n	27.2	0,7

Kinetic energy

The kinetic energy due to the combined impacts of all the events have been calculated and are shown in Table 8.3. From this table the following observations can be made:

- The total energy for group 1 and group 2 are very close to each other, this means that around half of the impact energy is missed by looking purely at the rotations larger than 5 degrees. However, it should be noted that only 3% of the total events have a rotation larger than 5 degrees. This means that the impact energy for the group larger than 5 degrees is much larger per individual event.
- At SWL the total kinetic energy due to impacts is much larger than $2d_n$ above and below SWL. Especially for the group within the visually observable rotations.

Table 8.3: Kinetic energy of all the events together at a certain depth and for a rotation smaller or larger than 5 degrees.

Location	Kinetic energy (J) rotation <5 (deg)	Kinetic energy (J) rotation >5 (deg)
SWL	0,95	1,64
SWL+2d_n	0,37	0,09
SWL-2d_n	0,32	0,06
Total	1,64	1,79

8.5.1. Rotation and impact velocity

Visual observations is an often used method of measuring rocking in a scale model. However, this method does not provide information on the magnitude of the impact. Because of this, it is interesting to look at the impact velocities and the rotation during each event, as shown in Figure 8.6. The following points can be made by analyzing this figure:

- There is a correlation between the angular impact velocity and the rotation within an event. A larger rotation coincides with a larger impact velocity.
- A rotation of 5 degrees is considered visually observable. It has been found that 97% of the events have a smaller rotation than 5 degrees. These events cannot be detected by visual observations.
- The impact velocities for events with a rotation larger than 5 degrees are around 1.7 times as large as the highest values found for a rotation smaller than 5 degrees. So generally it could be said that a larger rotation has a larger impact and a higher probability of breakage due to rocking. However, the impact for a rotation smaller than 5 degrees can be significant and might also lead to breakage due to rocking.

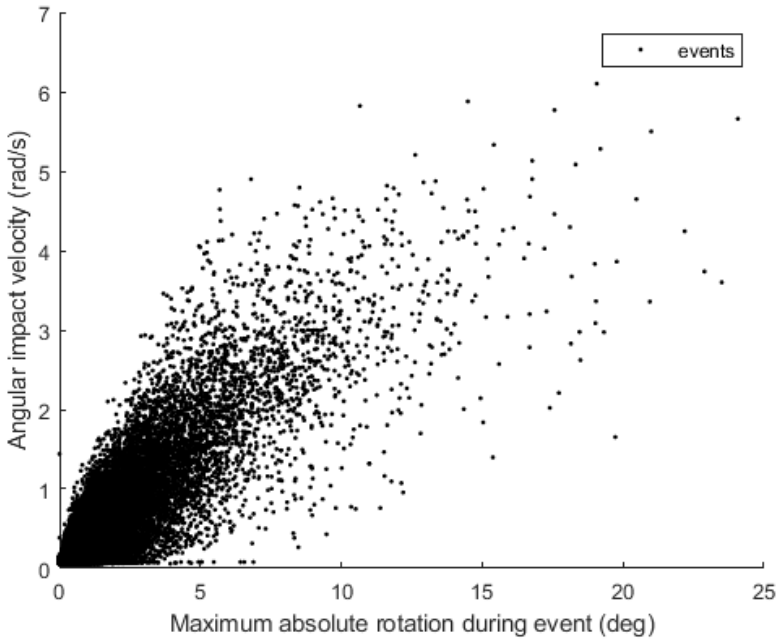

Figure 8.6: The maximum absolute rotation (deg) within each event and the angular impact velocity in (rad/s).

9

Discussion

9.1. Number of impacts

The results of the number of impacts per 1000 waves were analyzed in Section 8.2. It was observed that there is a large variation between armour units located at the same row. Also, the number of events at still water level (SWL) drops significantly after the 4th wave condition. Possible explanations for these observations are discussed in the following points:

- The variation in number of events per 1000 waves between armour units subjected to the same wave conditions and located on the same row is very large. The variation ranges between 1 or 2 events up to 400 to a 1000 events per 1000 waves. This could be explained because there is a large variation between individual parameters of the armour unit, like the movement space. An armour unit that is effectively interlocked between the surrounding armour units has little to no movement space. When this armour unit is subjected to a wave force, it will not start rocking. Another armour unit that is not effectively interlocked and has some movement space it is more likely to start rocking under the same wave condition.
- At SWL the number of events drops significantly after the 4th test run. This could be related to the settlement of the armour layer. When the armour layer is settling the packing density changes, around SWL the packing density increases. With a higher packing density there is less space between the armour units. The movement space of the armour units reduces, reducing also the number of impacts. A similar behaviour has also been observed in the field. In the past several breakwaters failed during the first storm, even though it was a storm below the design condition. While older breakwaters survived storms with more intense wave conditions. The armour layer of a breakwater seems to increase after a certain number of waves.

9.2. Impact velocity

The impact velocity is analyzed in Section 8.3. It was observed that the largest impact velocities are found at SWL and increase for an increasing wave height. Above and below SWL the extreme values of the impact velocity are of a similar magnitude. Also, the angular and linear velocity are of a similar order of magnitude except for the extreme values. Possible explanations for these observations are discussed in the following points:

- At SWL the extreme values increased for an increasing stability number. This was not observed at the other depths, where the $v_{i,2\%}$ did not seem to depend on the stability number. At SWL the increasing impact velocity for larger stability numbers can be explained because at this location the run up velocity is larger than at the other locations.
- $2d_n$ above and below SWL similar impact velocities were found for different stability numbers. The impact velocity did not seem to depend on the stability number. This is an unexpected find because waves did reach these areas. A possible explanation could be that the run up velocities are limited at these locations.

- $2d_n$ above and below the SWL the extreme values for the number of events are more or less similar. The difference compared to SWL can be explained because the armour units at SWL are subjected to largest wave forces during run up and run down.

9.2.1. Angular versus linear impact velocity

The results of the angular and linear impact velocity have been compared in Section 8.3.2. It was observed that $2d_n$ above and below SWL the exceedance curve for the linear and angular impact velocity are very similar. However, at SWL there is large difference in the last two test runs with the highest stability numbers. The exceedance curve for the linear impact velocity reaches values almost twice as large as the angular impact velocity. Possible explanations for this behaviour are discussed in the following point:

- Above and below SWL similar impact velocities are found. This could be explained by the way the sensor works. The accelerometer and gyroscope are located at the centre of the Xbloc. If during rocking the rotation point of the armour unit is located on one of the legs a small rotation will also result in a small translation of the centre of the unit. Therefore, the angular and linear velocity of this small rotation is measured by both the accelerometer and gyroscope.

The difference in angular and linear impact velocity is only found at SWL for the two largest stability numbers. There are multiple possible explanations for this observation:

- The first possible explanation is that there is an error in the linear velocity. This could be because the gravity component is not removed from the accelerometer data correctly. However, it was calculated in Section 6.9.2 that this error in extreme cases could be around 10% of the impact velocity which is not enough to explain the difference. Also, because the large difference in extreme values is only found at still water level and only for certain wave conditions it is not likely that there is a systematic error in determining the linear velocity.

- Another explanation could be that at SWL very large wave forces or settlements can lead to translations of the armour unit. These translations could reach larger impact velocities if there is enough space available for the translation. Due to the design of the Xbloc larger rotations are unlikely because the interlocking between the armour units limits the movement space.

- Experiments performed by Caldera (2019) also resulted in larger linear impact velocities compared to the angular velocity from the gyroscope. The difference was explained due to several uncertainties of the integration method of the accelerometer.

9.3. Visual observations and the Smart Xbloc

Visual observations is the main method of measuring rocking in scale models. The angle of rotation has been calculated and compared to the visual observations. It has been found that the threshold for a visually observable rotation lies around 5 degrees, this threshold was also found by Zwanenburg (2012). The percentage of events in the visually observable range is 3% of the total number of events that were measured. The data was analyzed by comparing the visually observable events with a rotation larger than 5 degrees and smaller than 5 degrees. The observations are discussed in the following points:

- The smart Xbloc provides much more detailed information than can be measured by visual observations. From the comparison of the two methods is has been found that at still water level 95% of the events cannot be observed visually. This is not necessarily a problem as larger rotations coincide with larger impacts and are therefore more likely to cause damage to the armour unit.

- The kinetic energy due to the impacts has been determined and it was found that at still water level 63% of the impact energy comes from rotations that are visually observable. The largest number of movements, around 95%, occur below the visual level and these movements do also result in significant impact velocities that might lead to breakage of armour units. It is therefore recommended to use the results of this thesis as input for the model as proposed by Goud (2020) to assess if the events with a rotation of less than 5 degrees can lead to significant breakage of armour units.

9.4. Number of events versus number of impacts

The technical definition used for an event is: a number of consecutive gyroscope measurements for which the total rotation rate (ω) is larger than 0.011 rad/s and at least once exceeds the value of 0.051 rad/s. This definition has been applied because it is a robust method, capable of extracting events in the wide variety of movements found in the measurement data. The number of impacts is assumed to be 1 impact per event. Most events contain only one impact, as can be observed in an example from the data as shown in Figure 9.1. In this figure the duration of four times T_p is shown. In the figure the impact velocity per event are marked. When looking at the distance between events, it is clear that the definition used for events includes both the upward rocking motion during wave run up and the downward rocking motion during run down of the wave. However, some cases were found where the up and down motion are coupled and detected as one event. This is expected to happen for waves with a small period. Therefore, the number of events for wave conditions with lower wave height and shorter periods might be underestimated. The second observation is that sometimes small movements in between events are seen as separate impacts, as can be observed in Figure 9.1. Therefore, the number of events with a low impact velocity might be overestimated.

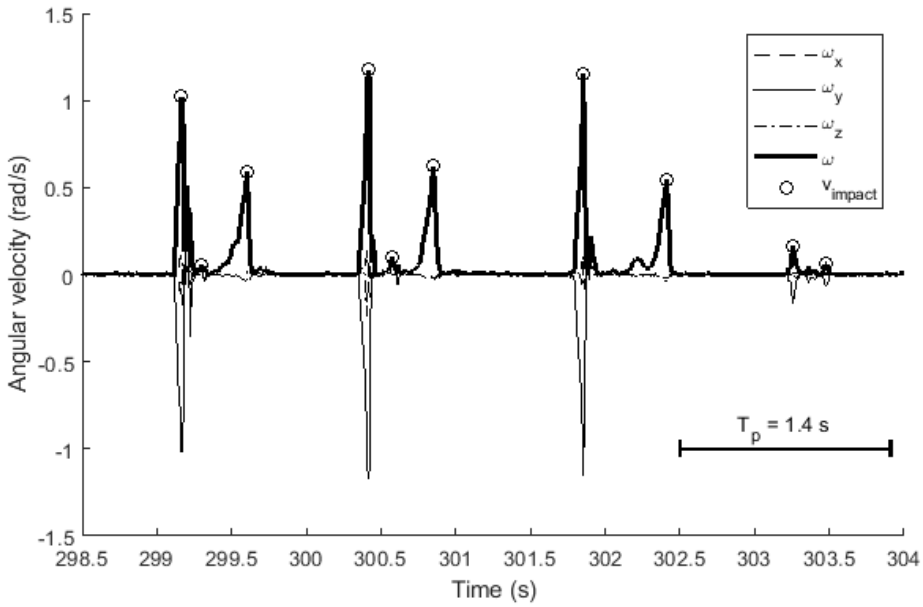

Figure 9.1: Example from the data, showing the total rotation ω and the detected impacts.

9.5. Confidence level number of events

The 95% confidence level has been calculated using Greenwood's formula as described by Lawless, (2003). An example of the 95% confidence bound of the cumulative density function for the number of Events per 1000 waves is shown in Figure 9.2. The results for each wave condition and location on the slope are shown in Appendix H. During each test run 9 smart Xbloc sensors were used and 5 repetitions were done at each location. This resulted in 42 measurements, 3 measurements failed due to a malfunction of the sensor. Because of this relatively low number of measurements for the number of events the 95% confidence level is rather low. Resulting in a relatively large confidence bound, as can also be observed in figure 9.2.

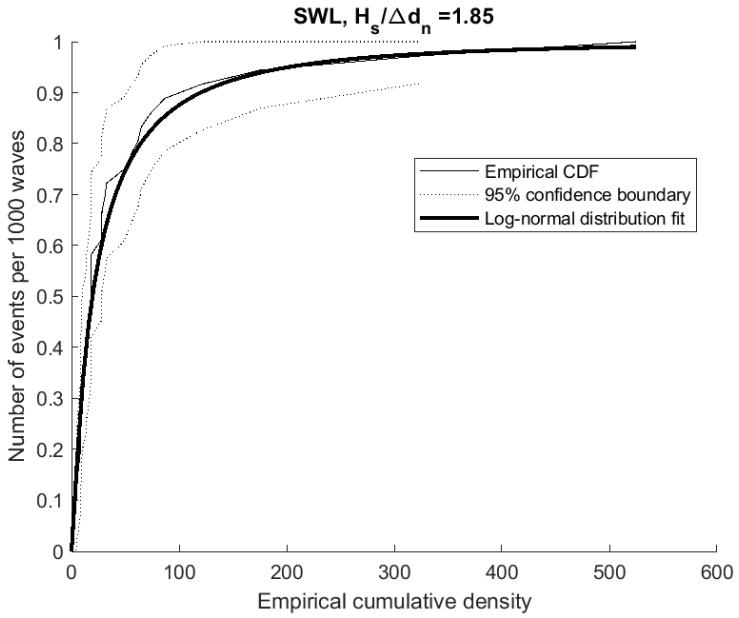

Figure 9.2: The empirical cumulative density for the number of events (N_E) at SWL, the fit using the log-normal distribution and the 95% confidence boundary.

9.6. Confidence level impact velocity

The 95% confidence level has been calculated using Greenwood's formula as described by Lawless (2003). An example of the 95% confidence bound of the exceedance curve for the impact velocity in radians per second is shown in Figure 9.3. The exceedance curves and 95% confidence boundaries for each wave condition and location on the slope are shown in Appendix F. The 95% confidence boundary has also been determined for the impact velocity exceeded by 2% of the waves. The results can be found in Appendix G, Table G.1 and G.2. For the 2% exceeded impact velocity the 95% confidence bound is on average ±10% of the impact velocity.

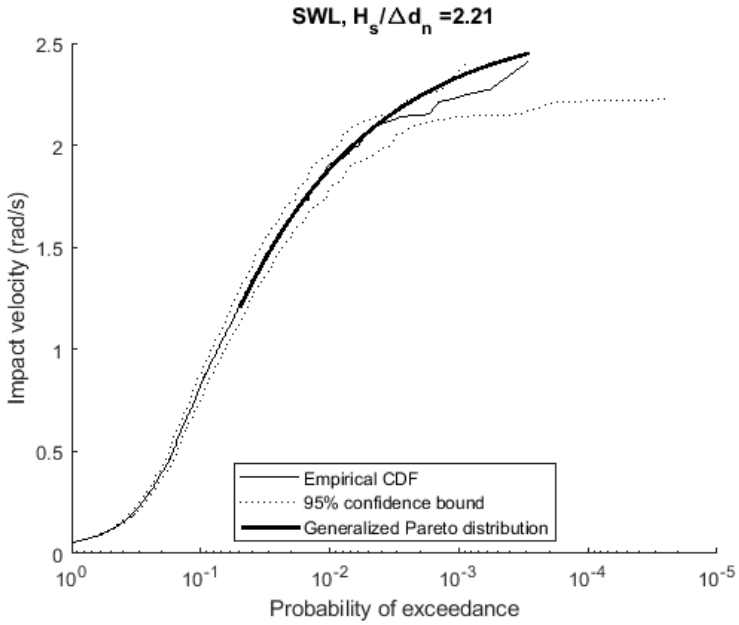

Figure 9.3: The empirical exceedance curve, generalized Pareto distribution fit and the 95% confidence boundary for the impact velocity at SWL and a stability number of 2.21.

9.7. Spatial and temporal distribution

Measurements with a single unit provides the temporal distribution of the number of events and the impact velocity. To find the spatial variation between these temporal distributions measurements were done with 10 smart Xbloc units. The spatial and temporal distribution have been measured as one and the data has been analyzed as one group, which provides the temporal spatial distribution.

9.8. Literature

In this section the results and analysis are compared to previous studies about rocking and the differences in results are discussed.

9.8.1. Number of impacts

CUR-70

The research by the CUR C70 work-group concluded that most of the rocking will be concentrated around SWL and the distribution of the impacts will be more or less uniform from SWL to the toe (Van der Meer and Heydra, 1991). In this research it was also found that the highest number of impacts can be found around SWL but the number of impacts is not uniformly distributed but reduces both above and below the waterline. The CUR C70 report did not provide a spatial distribution of the number of impacts at a certain level. This was not possible because of the limited number of samples.

Rocking revisited III

It was concluded by Caldera (2019) that several factors affect the number of events and it does not rely on the stability number only. The order of magnitude for the number of events per 1000 waves that were measured by Caldera (2019) are of a similar order of magnitude as was found in this thesis. Also, the number of events does indeed not only depend on the stability number. It is found that there is a large spatial variation for the same location on the slope and stability number, ranging from less than 10 up to almost 100 events per 1000 waves.

Rocking revisited IV

The model as proposed by Goud (2020) does not specify the number of impacts as a variable. The number of impacts is implicitly assumed to be equal to 50% of the waves. This simplification is not justified as the number of impacts varies both in space and time and can be described with a log-normal distribution. These distributions could be used to expand the model and increase its accuracy.

9.8.2. Impact velocity

CUR C70

In the CUR C70 research as described by Van der Meer and Heydra (1991) the impact velocities were determined for cubes and tetrapods. The values for the impact velocity are in the same order of magnitude as the velocities found in this research, except for the extreme values. The highest impact velocity for cubes goes up to 0.2 m/s which is lower than was measured for the Xbloc armour unit. This could be due to the fact that cubes and Tetrapods respond different than Xbloc armour units but also due to a difference in measurement technique and the number of sensors and the number of repetitions during testing.

Rocking Revisited III

The impact velocities exceeded by 2% of the events as found by Caldera (2019) can be found in Figure 9.4. The values and the direction of the graph is compared to the results found in this thesis as shown in Figure 9.5. The impact velocities are in the same order of magnitude, starting around 0.04 m/s, for a stability number below 2.5. However, Caldera found that the highest impact velocities occur for a stability number of 2.5 and decrease for higher stability numbers. In this research, it has been found that the impact velocity at SWL keep increasing with increasing wave height. This difference could be because of the use of only 2 sensors by Caldera (2019) and a small number of repetitions in the model tests.

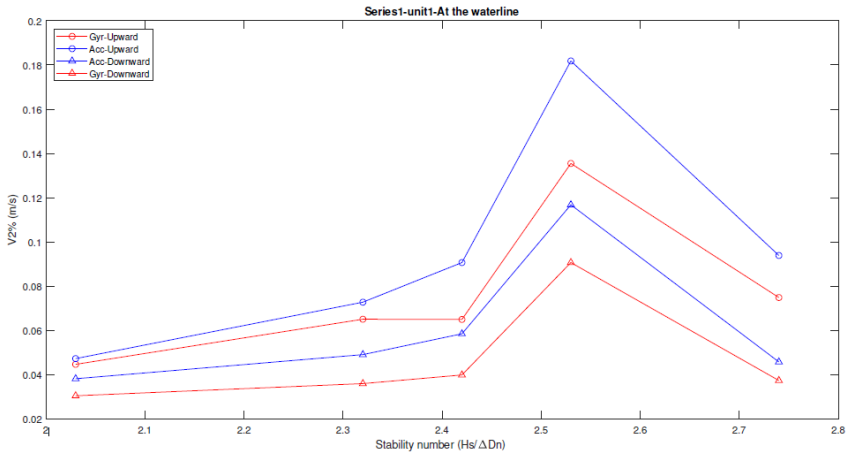

Figure 9.4: Characteristic impact velocity $v_{i,2\%}$ at SWL, (Caldera, 2019)

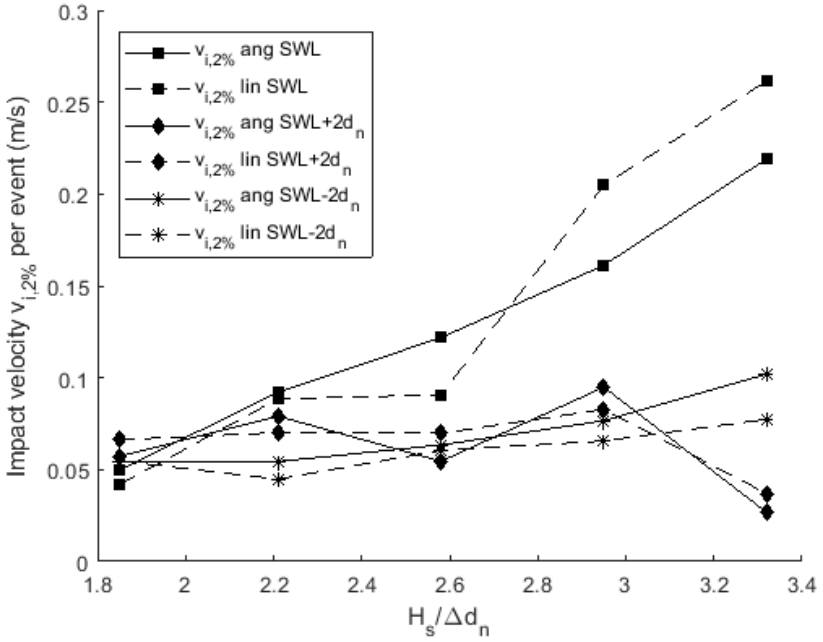

Figure 9.5: Linear (lin) and angular (ang) impact velocity $v_{i,2\%}$ with an exceedance probability of 2%

Rocking revisited IV

In the model proposed by Goud (2020), the impact velocity formula has been derived based on the rotation of an armour unit due to a wave induced drag force. The resulting impact velocity distribution is shown in Figure 9.6, for H_s=11.5 cm and the same Xbloc size (h=0.056 m) as used in this thesis. The values can therefore be compared to the empirical exceedance curve of the angular impact velocity with a stability number of 2.21, see Figure 9.7. The model for the impact velocity overestimates the measured impact velocities. Moreover, the shape of the probability of exceedance plot does not match the measurements. The difference can be explained because assumptions had to be made for the impact velocity formula, some of these assumptions could be validated by the results of the model tests.

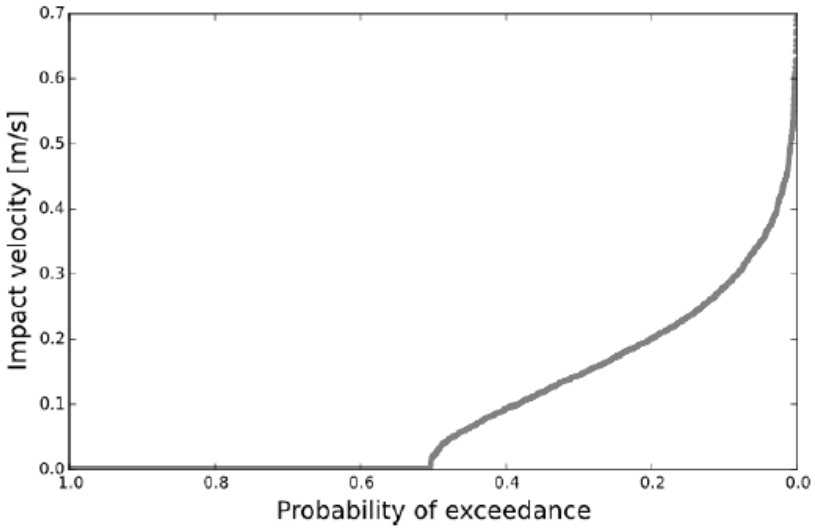

Figure 9.6: Probability of exceedance impact velocity for H_s = 11.5 cm and d_n = 3.91 cm as used by Goud (2020)

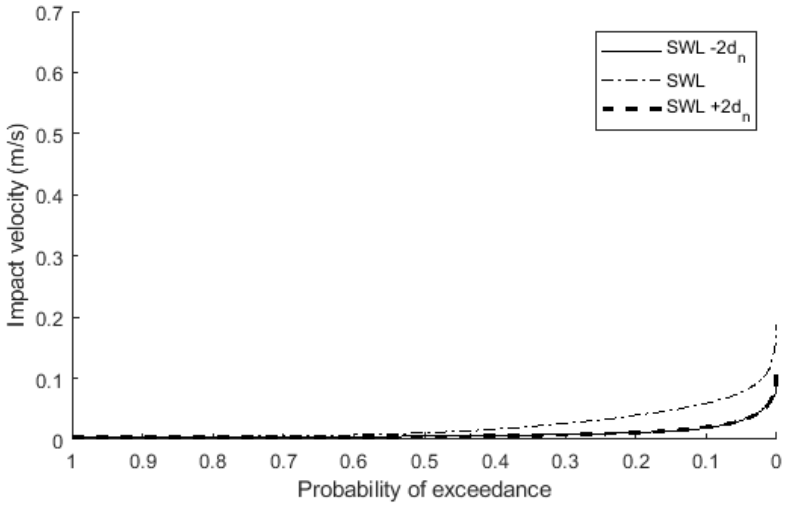

Figure 9.7: Empirical probability of exceedance impact velocity for H_s = 12 cm and d_n = 3.91 cm of the measured impact velocity

10

Conclusion

The rocking of single layer concrete armour units is a difficult, highly variable and not well understood phenomenon. The gained knowledge on the spatial and temporal variation of this phenomenon can help in better understanding and modelling of rocking.

The development of the smart Xbloc armour unit makes it possible to measure accelerations and rotations of a single armour unit, with a sampling frequency around 100 Hz. Data from a smart Xbloc provides the temporal variation of a single rocking armour unit under wave attack. This new technology has been implemented successfully in a scale model. By applying 10 smart Xbloc units per model test and multiple repetitions a large amount of data has been collected. The results provide the combined temporal and spatial variation of rocking armour units.

Number of impacts and number of moving armour units
The number of moving armour units is much higher than was found in previous studies. This is mainly because the smart Xbloc provides much more detailed information than previously used measuring techniques. The number of impacts has been determined, analyzed and discussed to answer how many impacts a single armour unit experiences and how the number of impacts varies in space and time depending on the location and stability number. The following conclusions are drawn about the number of impacts per 1000 waves:

- The distribution of the number of impacts can be described with the lognormal distribution and depends on the location on the slope and stability number.
- There is a large variation between armour units located at the same depth and subjected to the same wave condition. The number of impacts depends not only on the wave conditions but is dominated by individual parameters of the armour unit, like the movement space. Most impacts per 1000 waves were found at still water level.
- At still water level the number of impacts increased for an increasing stability number during the first four test runs, consisting of around 4800 waves in total. During the fifth test run the number of impacts reduced significantly, even though the wave height was increased. This reduction can most likely be attributed to a change in packing density due to settlements. An increase in the packing density reduces the movement space of individual armour units, and therefore also the number of impacts is reduced.

Impact velocity
For each impact an impact velocity has been determined, to find how large the impact velocities are and how the impact velocity varies for different locations and stability numbers. The impact velocity did not follow an uni-modal distribution. The extreme values can be described using the generalized Pareto distribution and the derived parameters. The following conclusions were drawn from the analysis of the impact velocity:

- At still water level the impact velocity increased for an increasing stability number. The decrease in number of events after 4 wave conditions did not have an effect on the impact velocity.
- At still water level the largest impact velocities were found. The impact velocity at the other locations was lower but significant.
- $2d_n$ above and below still water level the impact velocity did not seem to dependent on the stability number. A more or less constant exceedance curve of the impact velocity was found at these depths.

Two methods have been used to determine the impact velocity. The angular impact velocity is found by measuring the angular velocity directly, using a gyroscope. The linear velocity is found by integration of the accelerometer data. The two methods have been compared and the following conclusions were drawn:

- Both the angular and linear velocity result in similar impact velocities per event. At still water level, for the largest two wave conditions it was found that the extreme values of the linear impact velocity are around 2 times as large compared to the angular velocity. This might be due to translations induced by settlements instead of the rotational movements due to rocking, but further investigation is necessary.
- Gyroscope data is less prone to errors as no integration is needed. Therefore, it is recommended to determine the impact velocity using the gyroscope.

Visual observations and the smart Xbloc
Besides measuring rocking with the smart Xbloc, also visual observations have been done. The smart Xbloc measures rotations and this makes it possible to calculate the rotation angle and impact velocity of each movement. These values were compared to the visual observations and the following conclusions were drawn:

- From the combination of visual observations and measured rotations it is concluded that the limit for visual observable rotations with the human eye lies around 5 degrees. Most movements with a visually observable rotation occur at still water level. The smart Xbloc measurements have shown that only 5% of the events had a rotation within the visual observable range. 95% of the events happen outside of the visual observable range and cannot be observed with visual measuring techniques.
- Generally speaking a larger rotation angle also resulted in a larger impact velocity. However, the scatter was quiet large and small rotations can still result in significant impact velocities.

The collected data, results, analysis and discussion provide a unique look into the behaviour of single layer concrete armour units under wave attack. The main variables for rocking, the number of impacts and the impact velocity, can now be described in a statistical way. These results can be used to improve modelling of rocking armour units.

The rocking of single layer armour units is still a difficult phenomenon. However, with the gained knowledge it is now possible to understand the spatial and temporal variation of rocking from the perspective of a single armour unit.

11

Recommendations

11.1. Settlement analysis

Before and after each test run a photograph has been taken. These photographs can be used to determine the settlement after each test run. It is possible to determine the settlement rates and changes in packing density of the armour layer. These results could help to explain why the number of impacts reduced after the fourth wave condition. And could provide the information to conclude if there is a relation between the packing density, settlements, movement space and the number of impacts.

11.2. Angular and linear velocity

The differences between angular and linear impact velocities around still water level cannot be explained definitely. The extreme values of the linear impact velocities are almost twice as large and could therefore be normative in case of breakage of armour units due to rocking. There are different theories: it could be related to errors in the integration method but the larger linear impact velocities could also be explained because of translations. it is recommended to validate the linear velocity in a controlled environment. If extreme impacts due to translations are larger than rotations, than this could be an even more important mechanism than rocking for the breakage of armour units.

11.3. Rocking revisited IV

The empirical density function can be combined with the model as proposed by Goud (2020). The model can be validated and extended. This will provide a tool that can be used to estimate breakage due to rocking. The current model does not take the spatial distribution of the number of impacts into account, also the impact velocity is overestimated. Therefore, it is recommended to expand the model and use the distributions of the number of events to improve the representation of the number of impact in reality. Also, the formula that is used to describe the impact velocity should be adapted to better fit the probability of exceedance as was found in this thesis.

11.4. Smart Xbloc

For further use of the smart Xbloc it is recommended to use the auto-calibration technique as described in section 5.1. Also, the number of samples before writing the data to the main storage could be reconsidered. With the current settings this happens often during a movement, which results in loss of sample frequency during rocking.

Bibliography

[1] S.S. Arefin. Measurement on rocking of cubes in a double layer on a breakwater. MSc Thesis. Delft: Deft University of Technology, 2017.

[2] H.P.G.M. Caldera. Rocking of single layer armour units: Rocking revisited 3. MSc Thesis. Delft: Deft University of Technology, 2019.

[3] CUR. Golfbrekers. sterkte betonnen afdekelementen. samenvatting onderzoek. *Verslag werkgroep 1. Civiel Centrum Uitvoering Research en Regelgeving. in Dutch.*, 1990.

[4] DMC. Xbloc armour unit development. *Technical report, 210006-r-03 rev. 0*, 2003.

[5] DMC. Guidelines for xbloc concept design. *Technical Report*, 2018.

[6] DMC. Xbloc.com. 2019. URL `https://www.xbloc.com/en/construction/placement`.

[7] I Frosio, F Pedersini, and N.A. Borghese. Autocalibration of mems accelerometers. *IEEE TRANSACTION ON INSTRUMENTATIONAND MEASUREMENT, VOL. 58, NO.6*, 2009.

[8] N. Garcia, S. Richardson, and T. Rigden. Physical model testing of the hydraulic stability of single-layer armour units. *ICE Edinburg*, 2013.

[9] T. Goud. Rrocking revisited 4: Analysis of rocking-induced stresses for concrete breakwater armour units. MSc Thesis. Delft: Deft University of Technology, 2020.

[10] B. Hofland and M.R.A. van Gent. Automatic settlement analysis of single-layer armour layers. *Coastlab16*, 2016.

[11] B Hofland, S.S. Arefin, C. van der Lem, and M.R.A. van Gent. Smart rocking armour units. *Coastlab18*, 2018.

[12] J. Kirkegaard, G. Wolters, J. Sutherland, R. Soulsby, L. Frostick, S. McLelland, T. Mercer, and H. Gerritsen. *Users Guide to Physical Modelling and Experimentation: Experience of the HYDRALAB network*. Taylor & Francis Group, LLC, 2011.

[13] J.F. Lawless. *Statistical Models and Methods for Lifetime Data. 2nd ed.* Jown Wiley Sons, INC., 2003.

[14] T.N. Le. Rocking of a single cube on a breakwater slope. MSc Thesis. Delft: Deft University of Technology, 2016.

[15] J. P. van den Bos and J. P. Verhagen. *Breakwater Design*. Lecture Notes. TU Delft, 2018. ISBN 06923510029.

[16] J. W. Van der Meer and G. Heydra. Rocking armour units: Number, location and impact velocity. *Breakwaters. Coastal Engineering*, 1991.

[17] J. Zelt and J. E. Skjelbreia. Estimating incident and reflected wave fields using an arbitrary number of wave gauges. *Coastal Engineering Proceedings, 1(23)*, 1992.

[18] S.A.A. Zwanenburg. The influence of the wave height distribution on the stability of single layer concrete armour units. *Student Thesis TU Delft*, 2012.

A

Measured wave conditions per test series

During each test series the waves were measured using three wave gauges. The data has been analyzed using the method of Zelt and Skjelbreia (1992), the results are shown in the following table.

Table A.1: Measured wave conditions for each test run

Test	Test run 1		Test run 2		Test run 3		Test run 4		Test run 5	
	$H_{m0,i}$ (m)	T_p (s)	$H_{m0,i}$ (m)	T_p (s)	$H_{m0,i}$ (m)	T_p (s)	$H_{m0,i}$ (m)	T_p (s)	$H_{m0,i}$ (m)	T_p (s)
T4	0.10	1.26	0.12	1.41	0.14	1.54	0.16	1.71	0.18	1.91
T5	0.10	1.30	0.12	1.41	0.14	1.54	0.16	1.71	0.18	1.91
T6	0.10	1.26	0.12	1.41	0.14	1.54	0.16	1.75	0.18	1.90
T7	0.10	1.30	0.12	1.41	0.14	1.53	0.16	1.76	0.18	1.89
T8	0.10	1.29	0.12	1.41	0.14	1.53	0.16	1.77	0.18	1.91
T9	0.10	1.27	0.12	1.42	0.14	1.53	0.16	1.77	0.18	1.89
T10	0.10	1.32	0.12	1.42	0.14	1.54	0.16	1.77	0.18	1.91
T11	0.10	1.27	0.12	1.41	0.14	1.53	0.16	1.77	0.18	1.91
T12	0.10	1.27	0.12	1.42	0.14	1.53	0.16	1.77	0.18	1.91
T13	0.10	1.29	0.12	1.41	0.14	1.53	0.16	1.76	0.18	1.91
T14	0.10	1.27	0.12	1.41	0.14	1.58	0.16	1.77	0.18	1.91
T15	0.10	1.26	0.12	1.41	0.14	1.55	0.16	1.71	0.18	1.91
T16	0.10	1.27	0.12	1.41	0.14	1.53	0.16	1.76	0.18	1.91
T17	0.09	1.27	0.12	1.42	0.14	1.57	0.16	1.74	0.18	1.91
T18	0.10	1.27	0.12	1.40	0.14	1.55	0.16	1.75	0.16	1.74
T19	0.10	1.27	0.12	1.41	0.14	1.57	0.16	1.74	0.18	1.91
T20	0.10	1.27	0.12	1.41	0.14	1.53	0.16	1.76	0.18	1.92
T21	0.09	1.27	0.12	1.33	0.13	1.53	0.15	1.76	0.17	1.91
T22	0.10	1.27	0.12	1.41	0.14	1.55	0.16	1.74	0.18	1.91
T23	0.10	2.21	0.12	2.64	0.15	3.06	-	-	-	-
T24	0.10	2.21	0.13	2.64	0.15	3.03	-	-	-	-

B

Measurement overview

Table B.1: Overview of tests series, sensor location, water depth and wave steepness.

Test series	Date	Sensor location	Water depth h (m)	Wave steepness S_{0p}
T4	17-1-2020	SWL	0.6	0.04
T5	20-1-2020	SWL	0.6	0.04
T6	21-1-2020	SWL	0.6	0.04
T7	22-1-2020	SWL	0.6	0.04
T8	23-1-2020	SWL	0.6	0.04
T9	24-1-2020	SWL	0.6	0.04
T10	27-1-2020	$SWL - 1d_n$	0.6	0.04
T11	28-1-2020	$SWL - 1d_n$	0.6	0.04
T12	29-1-2020	$SWL + 2d_n$	0.6	0.04
T13	30-1-2020	$SWL + 2d_n$	0.6	0.04
T14	31-1-2020	$SWL + 2d_n$	0.6	0.04
T15	03-2-2020	$SWL + 3d_n$	0.6	0.04
T16	04-2-2020	$SWL + 2d_n$	0.6	0.04
T17	05-2-2020	$SWL - 2d_n$	0.6	0.04
T18	06-2-2020	$SWL + 2d_n$	0.6	0.04
T19	07-2-2020	$SWL - 2d_n$	0.6	0.04
T20	10-2-2020	$SWL - 2d_n$	0.6	0.04
T21	11-2-2020	$SWL - 2d_n$	0.6	0.04
T22	12-2-2020	$SWL - 2d_n$	0.6	0.04
T23	13-2-2020	$SWL + 2d_n$	0.6	0.02
T24	14-2-2020	$SWL + 2d_n$	0.6	0.02

C

Calibration values accelerometer

C.0.1. Results calibration

Table C.1: Calibration values, calibration measurement 1

Sensor	Bias parameters			Main-axis Scale factor			Cross-axis Scale factor		
	Ox	Oy	Oz	Sxx	Syy	Szz	Sxy	Sxz	Syz
S2	0,019	0,015	-0,009	1,003	0,999	0,991	9,99E-08	9,91E-08	9,94E-08
S3	0,012	0,009	-0,027	1,003	0,995	1,003	9,96E-08	1,00E-07	9,97E-08
S4	0,024	0,005	0,009	1,004	0,999	0,996	9,86E-08	9,84E-08	9,98E-08
S5	0,018	-0,010	0,000	1,002	0,999	0,991	9,88E-08	9,88E-08	9,93E-08
S6	-0,002	-0,013	-0,014	1,000	0,998	1,007	1,00E-07	1,00E-07	1,01E-07
S7	0,009	0,021	0,026	1,003	1,000	0,994	9,99E-08	9,91E-08	9,97E-08
S8	0,018	0,006	-0,016	1,004	1,002	0,996	1,01E-07	1,03E-07	9,98E-08
S10	0,020	0,008	0,025	0,998	0,999	0,993	9,98E-08	9,94E-08	9,94E-08
S11	0,017	0,014	0,001	0,974	1,021	0,992	9,91E-08	9,84E-08	1,00E-07

Table C.2: Calibration values, calibration measurement 2

Sensor	Bias parameters			Main-axis Scale factor			Cross-axis Scale factor		
	Ox	Oy	Oz	Sxx	Syy	Szz	Sxy	Sxz	Syz
S1	0,010	0,010	-0,025	0,996	1,006	0,993	9,99E-08	9,94E-08	9,95E-08
S2	0,023	0,008	-0,017	0,999	1,002	0,994	1,00E-07	9,96E-08	9,95E-08
S3	0,023	0,005	-0,032	1,004	1,002	1,000	1,00E-07	1,00E-07	1,00E-07
S5	0,033	-0,011	-0,002	1,001	1,002	0,991	1,00E-07	9,94E-08	9,93E-08
S6	0,000	-0,017	-0,014	1,001	0,999	1,005	1,00E-07	1,00E-07	1,00E-07
S7	0,020	0,013	0,038	1,002	0,999	0,997	1,00E-07	9,94E-08	9,97E-08
S8	0,017	0,013	-0,018	1,005	1,005	0,995	1,01E-07	9,93E-08	9,92E-08
S9	0,030	-0,002	-0,023	1,003	1,005	1,000	1,01E-07	1,01E-07	1,00E-07
S10	0,017	0,013	0,025	0,993	1,009	0,993	9,97E-08	9,93E-08	9,94E-08

D

Exceedance curves angular impact velocity

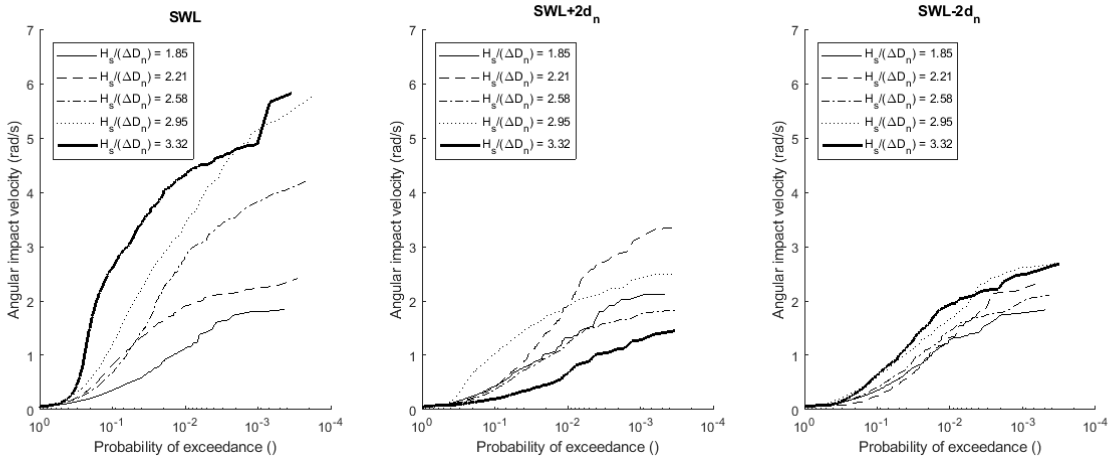

Figure D.1: Exceedance curve for the angular impact velocity in radial per second

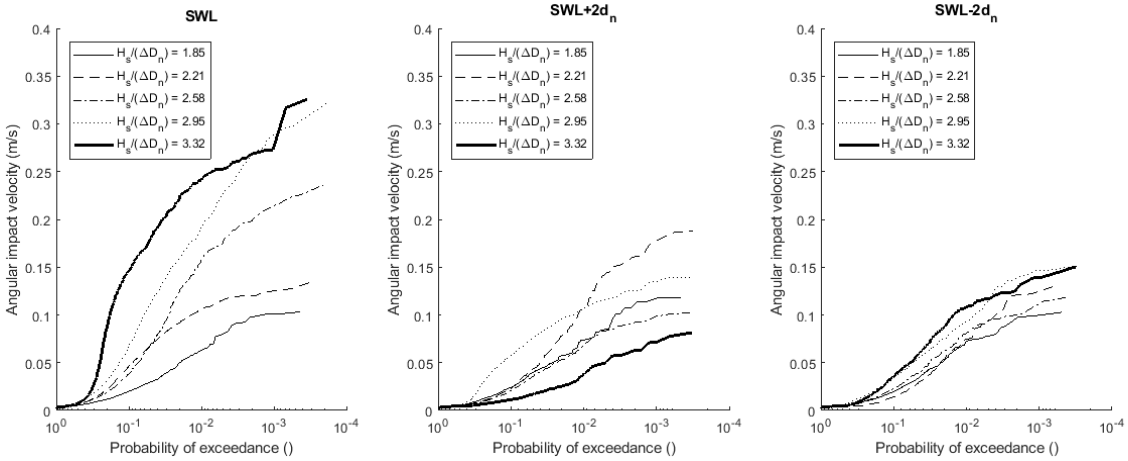

Figure D.2: Exceedance curve for the estimated angular impact velocity in meter per second

E

Differential rotation results

The rotation of the gravitational acceleration between the moment just before and after each event (the differential rotation) and the maximum angular velocity during each event are plotted in Figure E.1.

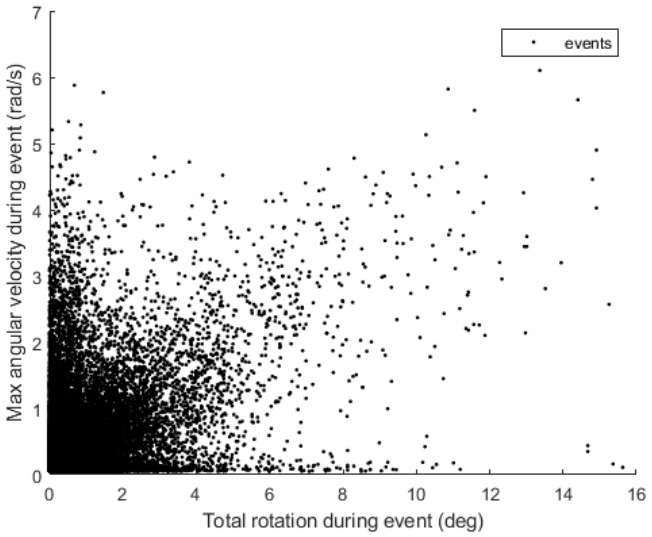

Figure E.1: The maximum angular velocity and rotation angle per event

F

Extreme value distribution impact velocity

F.1. Angular impact velocity in radians per second

The extreme values of the angular impact velocity in radians per second can be estimated using the following equation and the parameters from the table F.1.

$$v_{i,p\%} = \left(\left(\frac{1}{1 - \frac{1-p/100-0.95}{0.05}} \right)^{k} - 1 \right) \frac{\sigma}{k} + \theta \qquad \text{for } p \leq 5\%. \tag{F.1}$$

where

$v_{i,p\%}$	Impact velocity with a given probability of exceedance p in rad/s or m/s
p	exceedance probability in percentage ($p \leq 5\%$)
k	index parameter
θ	location parameter
σ	scale parameter

Table F.1: Parameters for the GPD for the angular impact velocity in radians per second

SWL					
$H_s/\Delta dn$	1,85	2,21	2,58	2,95	3,32
k	-0,139	-0,407	-0,329	-0,148	-0,246
sigma	0,455	0,580	1,234	1,026	0,870
theta	0,50	1,20	1,20	2,00	3,20
SWL+2dn					
$H_s/\Delta dn$	1,85	2,21	2,58	2,95	3,32
k	0,038	-0,059	-0,141	-0,214	0,244
sigma	0,346	0,721	0,399	0,427	0,172
theta	0,70	0,77	0,63	1,34	0,30
SWL-2dn					
$H_s/\Delta dn$	1,85	2,21	2,58	2,95	3,32
k	-0,210	-0,089	-0,281	-0,052	-0,380
sigma	0,473	0,570	0,561	0,478	0,750
theta	0,58	0,47	0,68	0,94	1,00

F.2. Linear impact velocity

The exceedance probability for the linear impact velocity in meter per second can be calculated using the GPD, equation 6.13 and the three estimated parameters from table F.2.

Table F.2: Parameters for the GPD for the linear impact velocity in meter per second

SWL					
$H_s/\Delta dn$	1,85	2,21	2,58	2,95	3,32
k	0,172	-0,032	-0,120	0,054	0,098
sigma	0,012	0,032	0,041	0,101	0,072
theta	0,03	0,06	0,06	0,11	0,19
SWL+2dn					
$H_s/\Delta dn$	1,85	2,21	2,58	2,95	3,32
k	0,09	-0,12	-0,08	0,09	0,14
sigma	0,028	0,031	0,028	0,021	0,012
theta	0,040	0,043	0,045	0,063	0,025
SWL-2dn					
$H_s/\Delta dn$	1,85	2,21	2,58	2,95	3,32
k	0,274	0,398	0,083	0,006	-0,062
sigma	0,016	0,016	0,023	0,025	0,031
theta	0,04	0,03	0,04	0,04	0,05

F.3. Angular velocity exceedance curves SWL

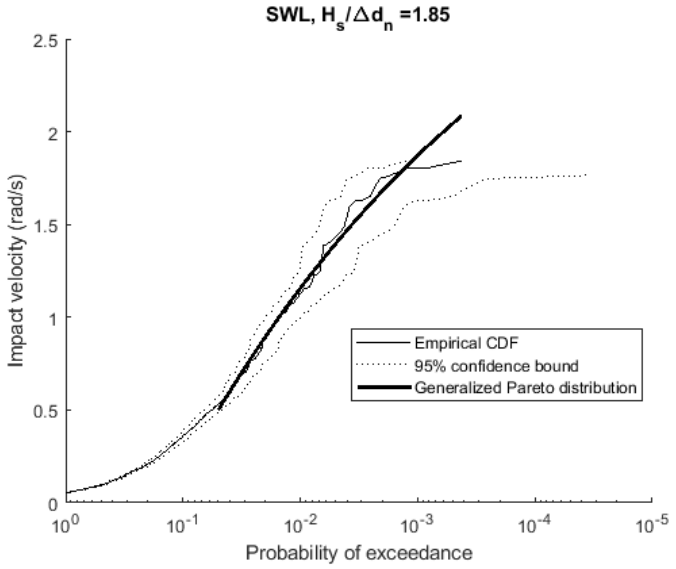

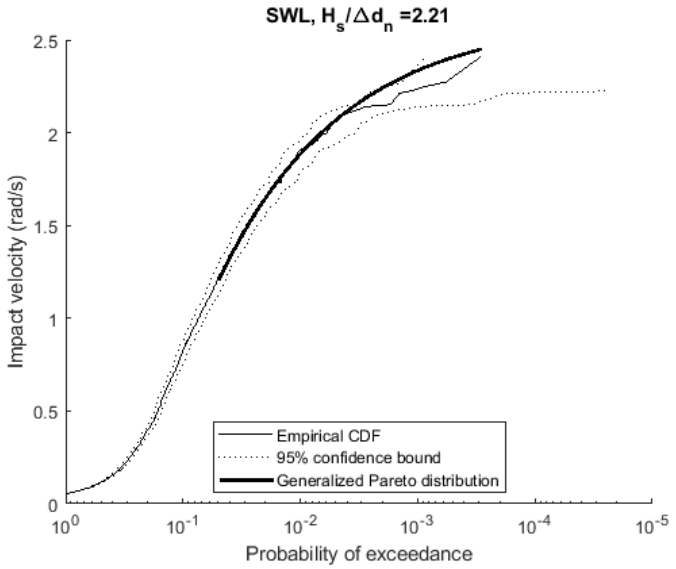

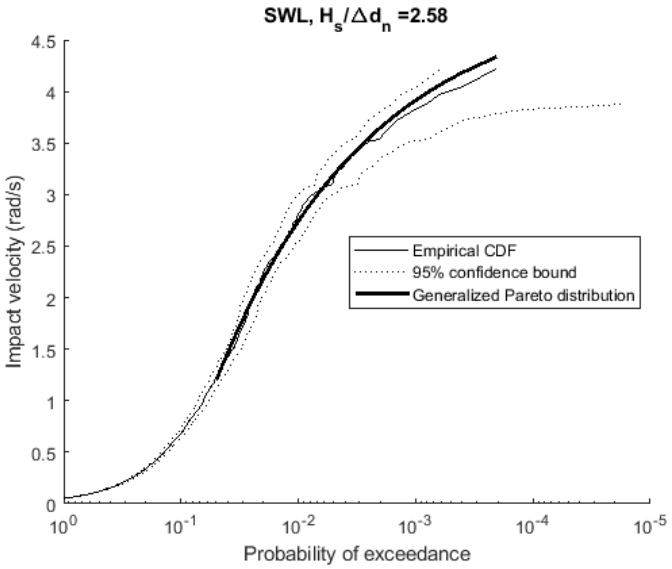
SWL, $H_s/\Delta d_n$ =2.58
Impact velocity (rad/s)
Probability of exceedance
Empirical CDF
95% confidence bound
Generalized Pareto distribution

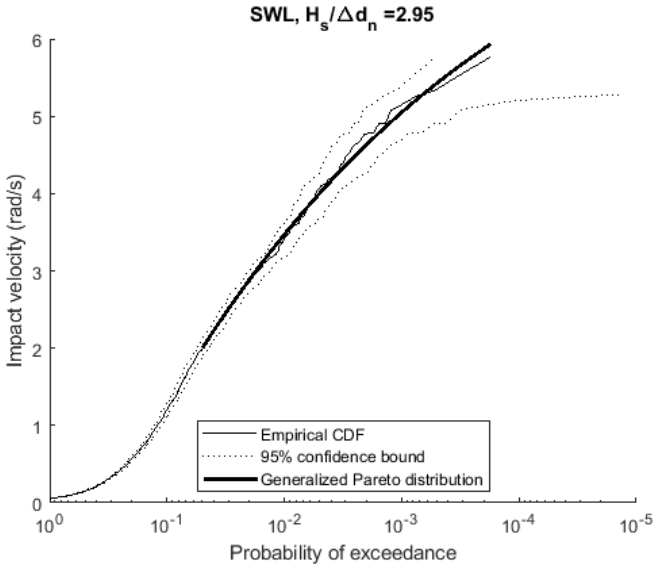
SWL, $H_s/\Delta d_n$ =2.95
Impact velocity (rad/s)
Probability of exceedance
Empirical CDF
95% confidence bound
Generalized Pareto distribution

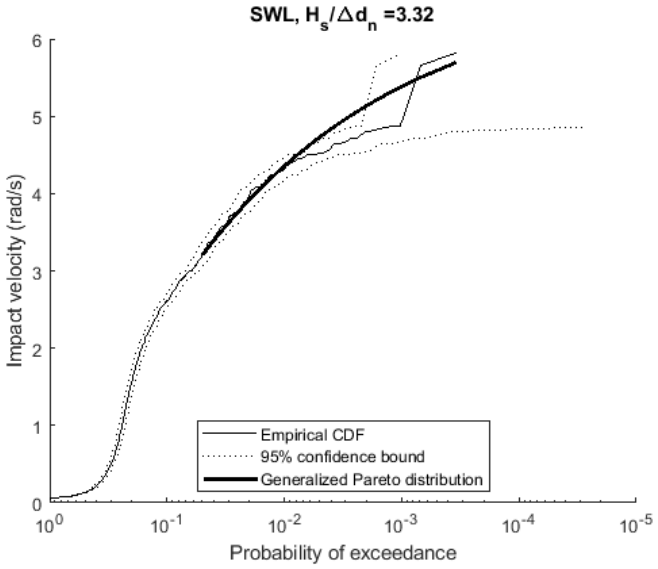
SWL, $H_s/\Delta d_n$ =3.32
Impact velocity (rad/s)
Probability of exceedance
Empirical CDF
95% confidence bound
Generalized Pareto distribution

F.4. Angular velocity exceedance curves SWL+2dn

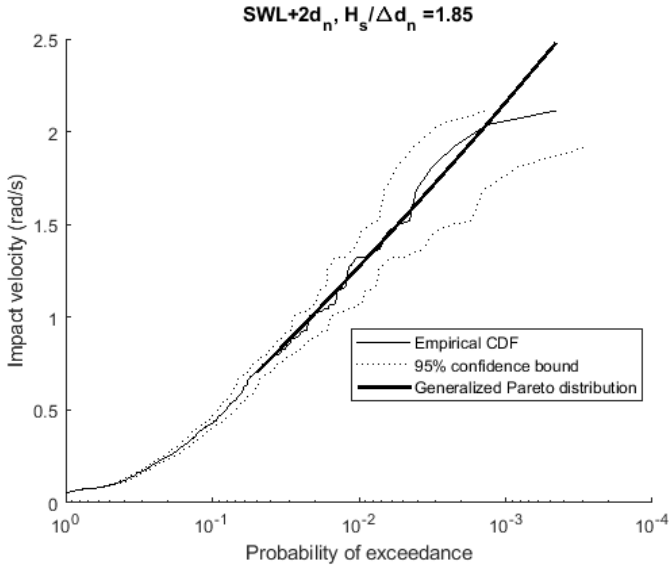

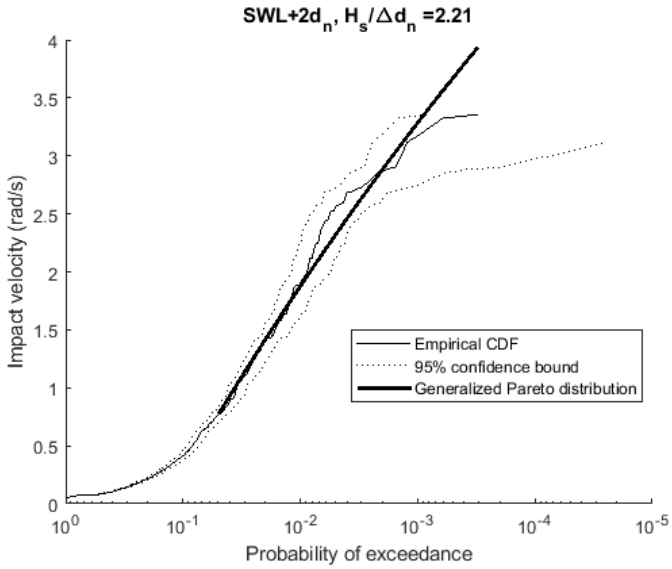

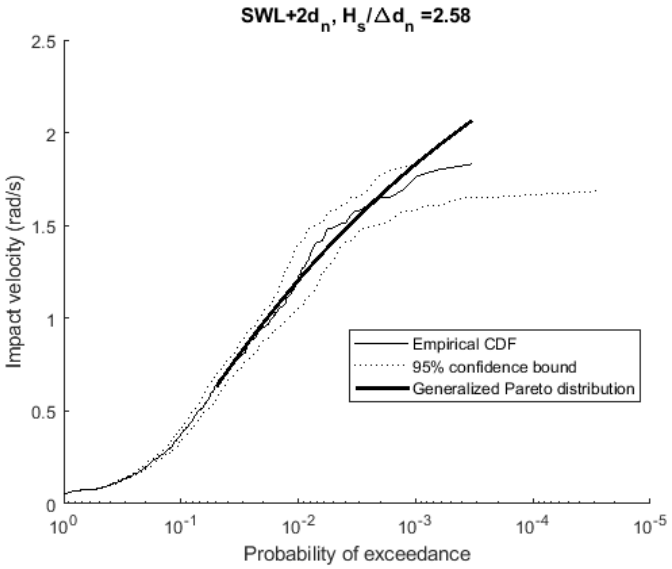
SWL+2d$_n$, H$_s$/Δd$_n$ =2.58
Impact velocity (rad/s)
Probability of exceedance
Empirical CDF
95% confidence bound
Generalized Pareto distribution

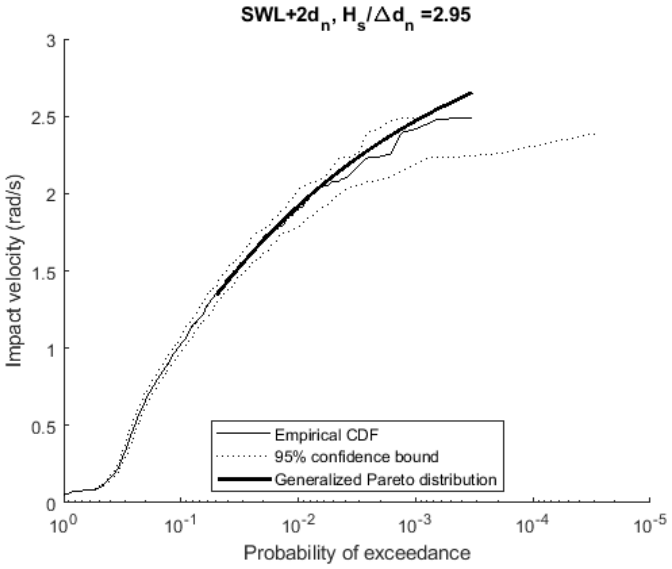
SWL+2d$_n$, H$_s$/Δd$_n$ =2.95
Impact velocity (rad/s)
Probability of exceedance
Empirical CDF
95% confidence bound
Generalized Pareto distribution

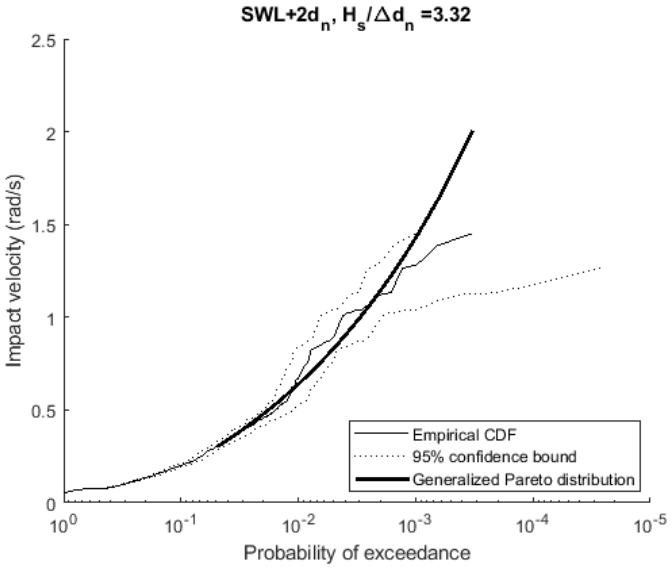
SWL+2d$_n$, H$_s$/Δd$_n$ =3.32
Impact velocity (rad/s)
Probability of exceedance
Empirical CDF
95% confidence bound
Generalized Pareto distribution

F.5. Angular velocity exceedance curves SWL-2dn

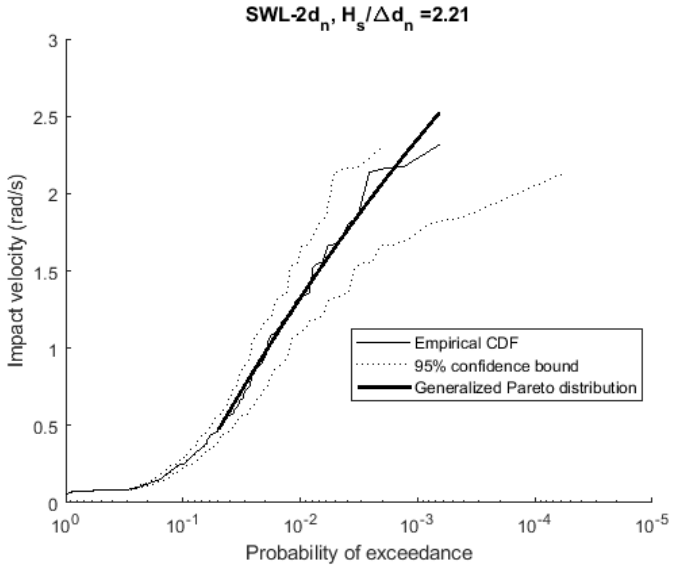

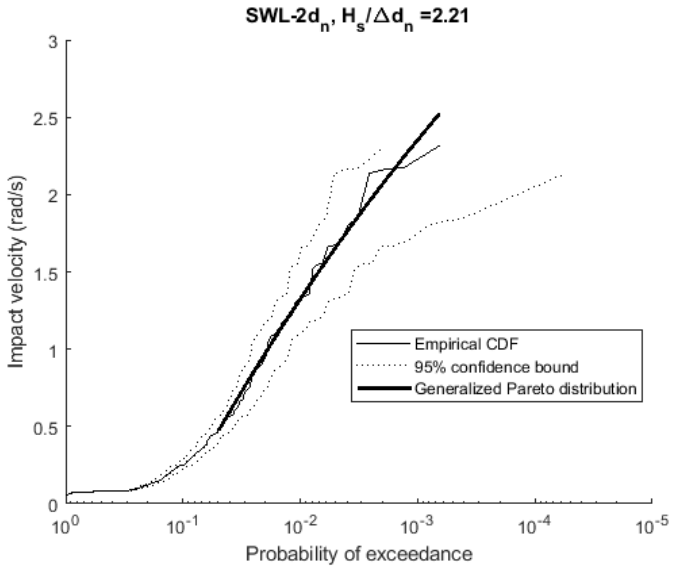

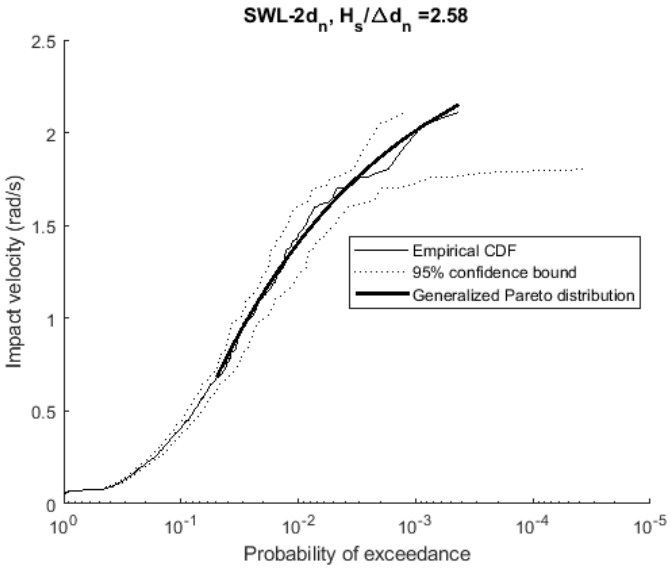
SWL-2d$_n$, H$_s$/Δd$_n$ =2.58
Impact velocity (rad/s)
Probability of exceedance
Empirical CDF
95% confidence bound
Generalized Pareto distribution

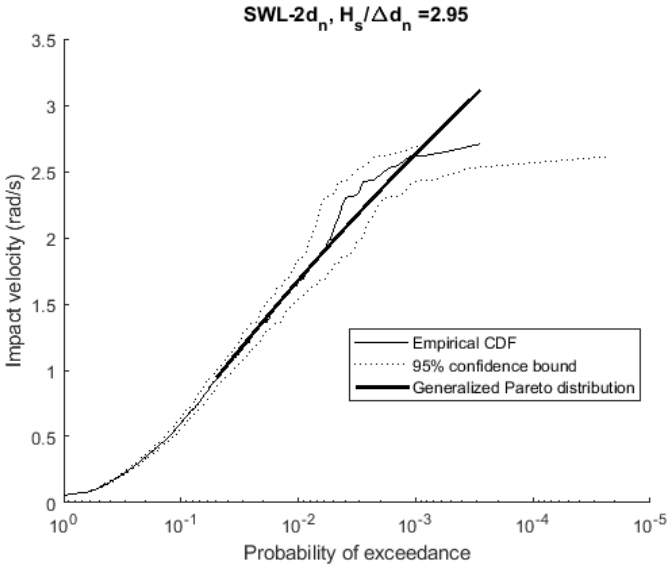
SWL-2d$_n$, H$_s$/Δd$_n$ =2.95
Impact velocity (rad/s)
Probability of exceedance
Empirical CDF
95% confidence bound
Generalized Pareto distribution

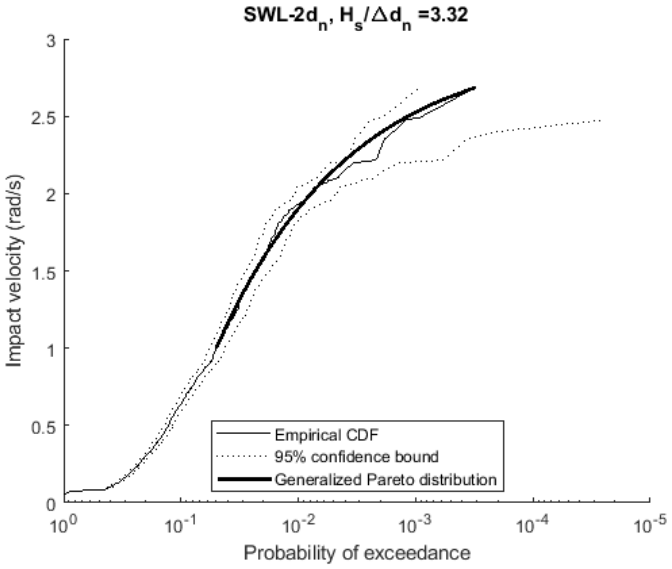
SWL-2d$_n$, H$_s$/Δd$_n$ =3.32
Impact velocity (rad/s)
Probability of exceedance
Empirical CDF
95% confidence bound
Generalized Pareto distribution

F.6. Linear velocity exceedance curves SWL

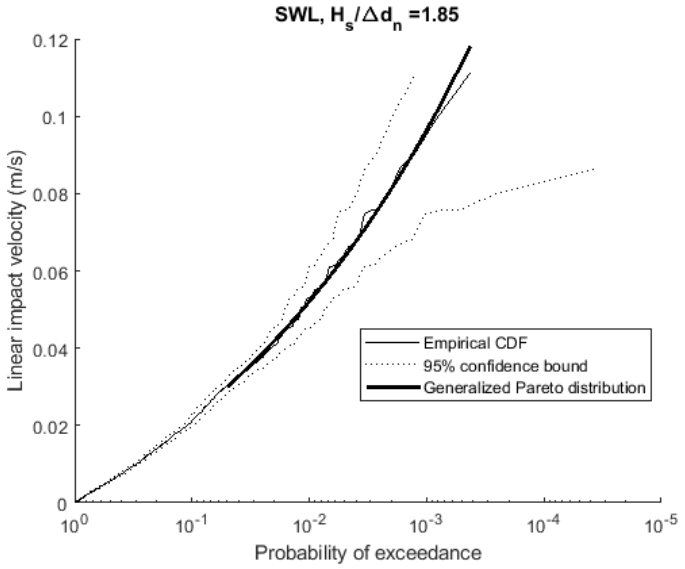

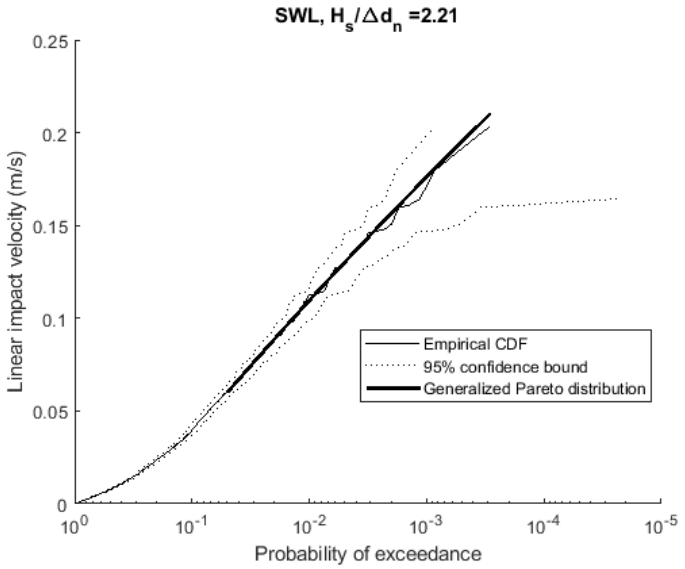

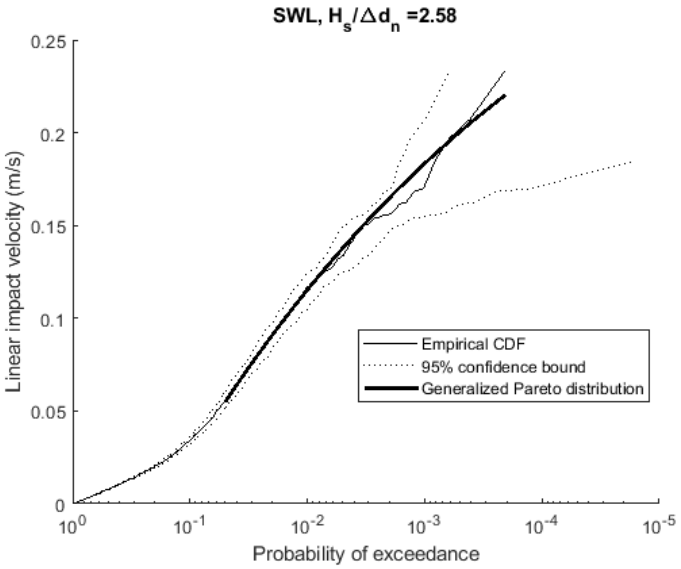
SWL, $H_s/\Delta d_n$ =2.58
Linear impact velocity (m/s)
0.25
0.2
0.15
0.1
0.05
0
10^0
10^{-1}
10^{-2}
10^{-3}
10^{-4}
10^{-5}
Probability of exceedance
Empirical CDF
95% confidence bound
Generalized Pareto distribution

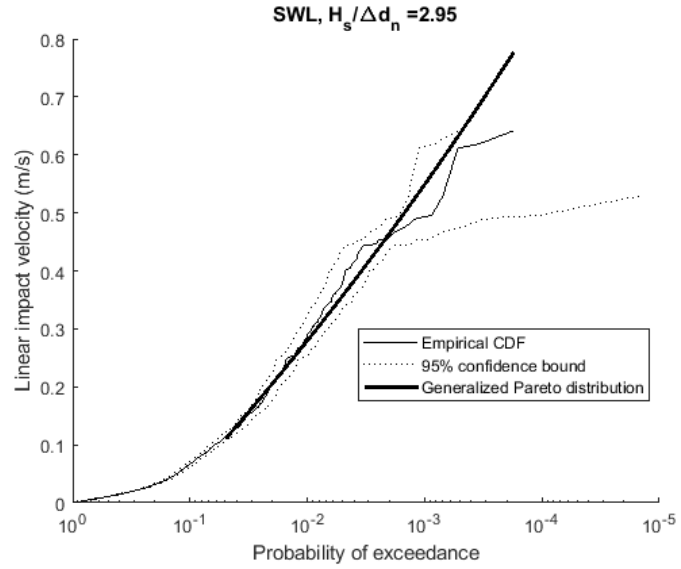
SWL, $H_s/\Delta d_n$ =2.95
Linear impact velocity (m/s)
0.8
0.7
0.6
0.5
0.4
0.3
0.2
0.1
0
10^0
10^{-1}
10^{-2}
10^{-3}
10^{-4}
10^{-5}
Probability of exceedance
Empirical CDF
95% confidence bound
Generalized Pareto distribution

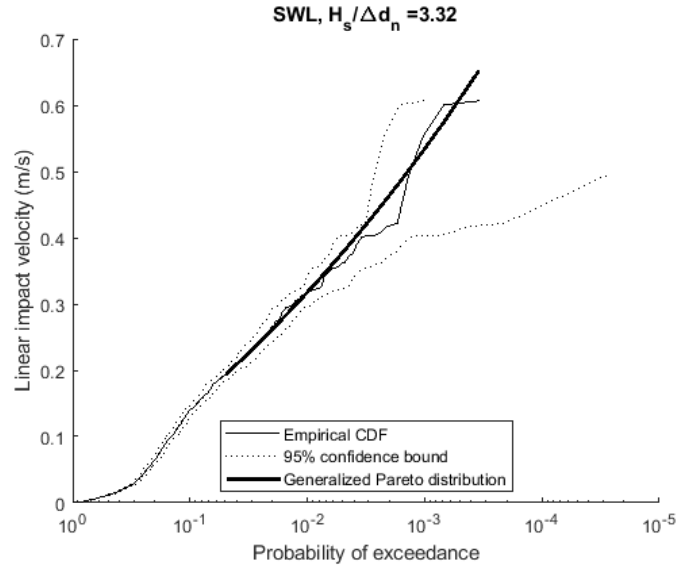
SWL, $H_s/\Delta d_n$ =3.32
Linear impact velocity (m/s)
0.7
0.6
0.5
0.4
0.3
0.2
0.1
0
10^0
10^{-1}
10^{-2}
10^{-3}
10^{-4}
10^{-5}
Probability of exceedance
Empirical CDF
95% confidence bound
Generalized Pareto distribution

F.7. Linear velocity exceedance curves SWL+2dn

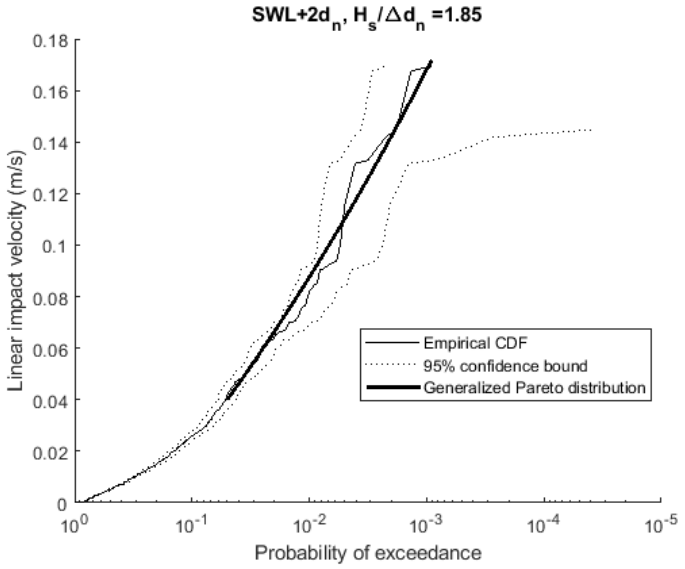

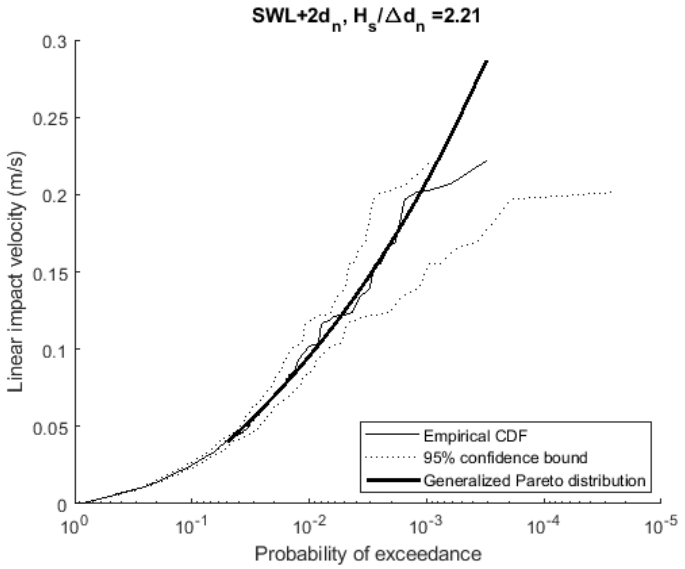

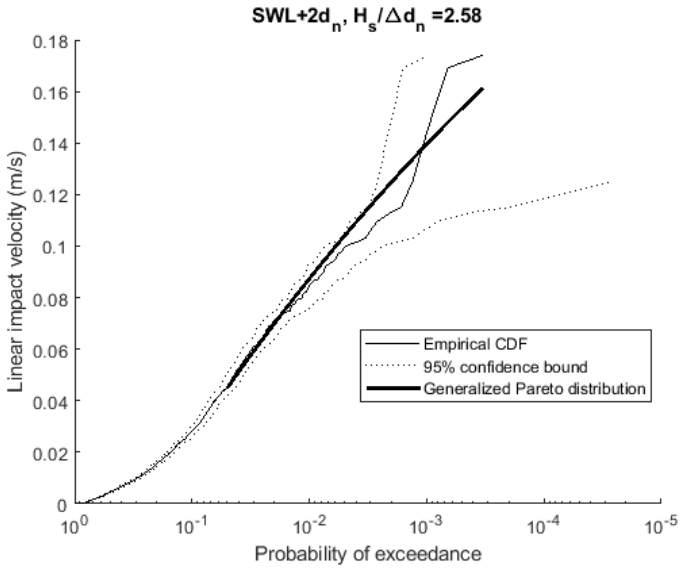
SWL+2d$_n$, H$_s$/Δd$_n$ =2.58
Linear impact velocity (m/s)
0.18
0.16
0.14
0.12
0.1
0.08
0.06
0.04
0.02
0
Empirical CDF
95% confidence bound
Generalized Pareto distribution
10^0
10^{-1}
10^{-2}
10^{-3}
10^{-4}
10^{-5}
Probability of exceedance

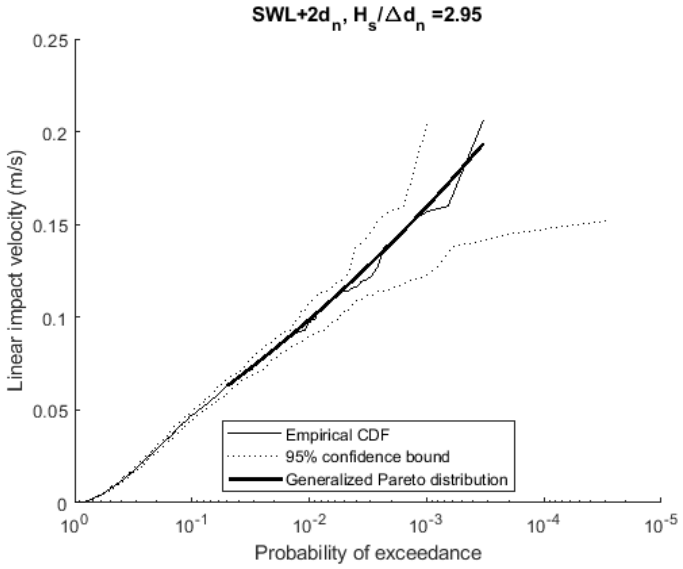
SWL+2d$_n$, H$_s$/Δd$_n$ =2.95
Linear impact velocity (m/s)
0.25
0.2
0.15
0.1
0.05
0
Empirical CDF
95% confidence bound
Generalized Pareto distribution
10^0
10^{-1}
10^{-2}
10^{-3}
10^{-4}
10^{-5}
Probability of exceedance

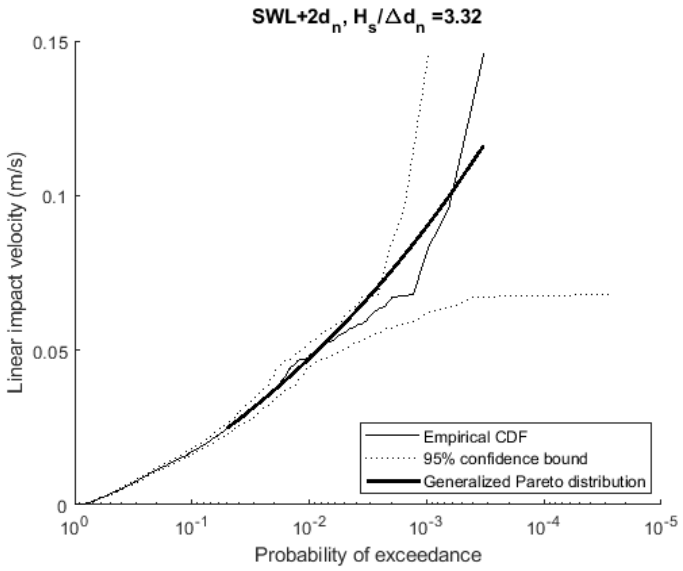
SWL+2d$_n$, H$_s$/Δd$_n$ =3.32
Linear impact velocity (m/s)
0.15
0.1
0.05
0
Empirical CDF
95% confidence bound
Generalized Pareto distribution
10^0
10^{-1}
10^{-2}
10^{-3}
10^{-4}
10^{-5}
Probability of exceedance

F.8. Linear velocity exceedance curves SWL-2dn

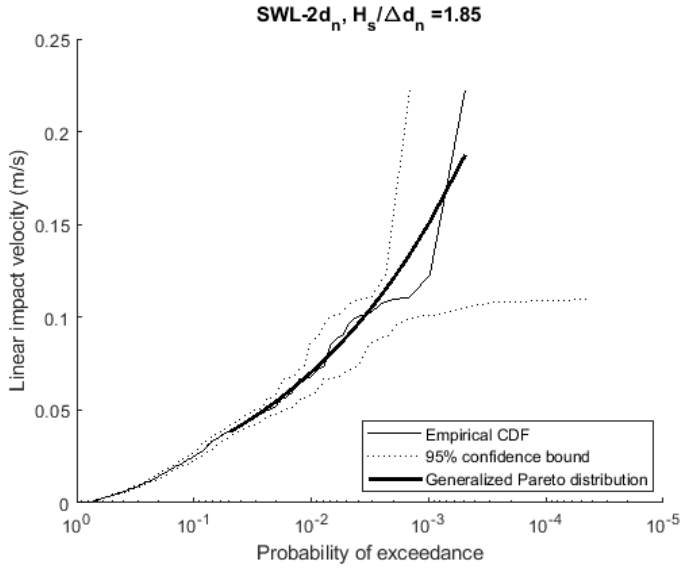

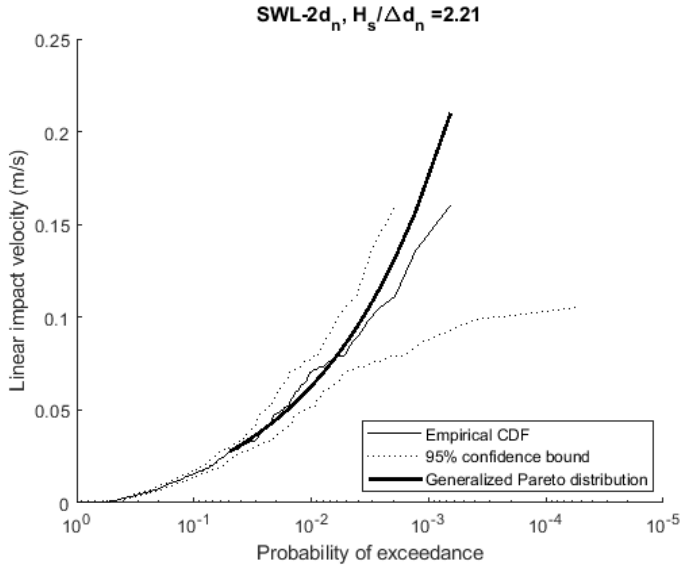

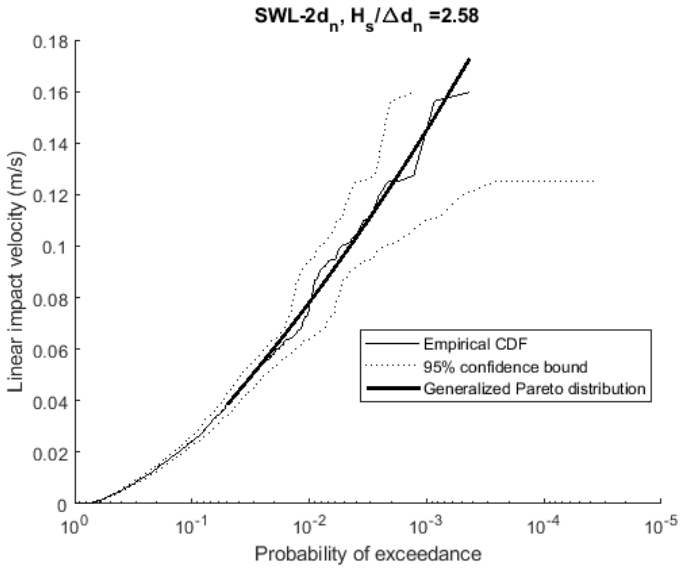
SWL-2d$_n$, H$_s$/Δd$_n$ =2.58
Linear impact velocity (m/s)
Probability of exceedance
Empirical CDF
95% confidence bound
Generalized Pareto distribution

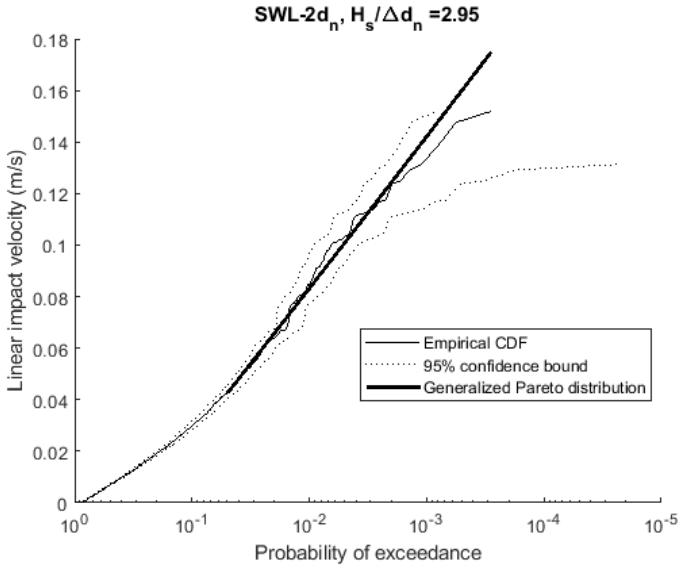
SWL-2d$_n$, H$_s$/Δd$_n$ =2.95
Linear impact velocity (m/s)
Probability of exceedance
Empirical CDF
95% confidence bound
Generalized Pareto distribution

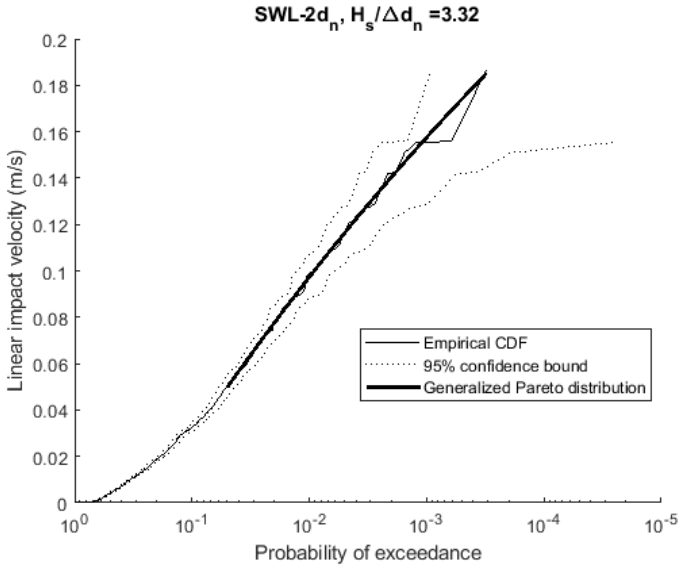
SWL-2d$_n$, H$_s$/Δd$_n$ =3.32
Linear impact velocity (m/s)
Probability of exceedance
Empirical CDF
95% confidence bound
Generalized Pareto distribution

G

Impact velocity confidence boundary

The 95% confidence boundary of the impact velocity exceeded by 2% of the impacts ($v_{i,2\%}$) has been determined by calculating the confidence bound for the empirical cumulative density function using Greenwood's method. The results for the 2% impact velocity can be found in table G.1 and G.2.

Table G.1: Empirical impact velocity with a 2% probability of exceedance ($v_{i,2\%}$) and the upper and lower 95% confidence boundary for the angular impact velocity

SWL					
Stability number	1,85	2,21	2,58	2,95	3,32
Upper 95% confidence bound (rad/s)	1,00	1,72	2,38	3,01	4,12
Empirical $v_{i,2\%}$ (rad/s)	0,89	1,65	2,24	2,85	3,97
Lower 95% confidence bound (rad/s)	0,76	1,56	2,01	2,73	3,76
SWL+2dn					
Stability number	1,85	2,21	2,58	2,95	3,32
Upper 95% confidence bound (rad/s)	1,07	1,55	1,03	1,77	0,50
Empirical $v_{i,2\%}$ (rad/s)	1,03	1,40	0,95	1,72	0,46
Lower 95% confidence bound (rad/s)	0,89	1,23	0,88	1,61	0,41
SWL-2dn					
Stability number	1,85	2,21	2,58	2,95	3,32
Upper 95% confidence bound (rad/s)	1,12	1,18	1,24	1,48	1,75
Empirical $v_{i,2\%}$ (rad/s)	0,96	0,97	1,12	1,36	1,57
Lower 95% confidence bound (rad/s)	0,82	0,74	1,00	1,28	1,45

Table G.2: Empirical impact velocity with a 2% probability of exceedance ($v_{i,2\%}$) and the upper and lower 95% confidence boundary for the linear impact velocity

SWL					
Stability number	1,85	2,21	2,58	2,95	3,32
Upper 95% confidence bound (m/s)	0,045	0,096	0,097	0,224	0,294
Empirical $v_{i,2\%}$ (m/s)	0,041	0,088	0,092	0,205	0,266
Lower 95% confidence bound (m/s)	0,037	0,080	0,084	0,176	0,241
SWL+2dn					
Stability number	1,85	2,21	2,58	2,95	3,32
Upper 95% confidence bound (m/s)	0,070	0,081	0,075	0,088	0,042
Empirical $v_{i,2\%}$ (m/s)	0,064	0,069	0,071	0,083	0,037
Lower 95% confidence bound (m/s)	0,057	0,063	0,064	0,078	0,034
SWL-2dn					
Stability number	1,85	2,21	2,58	2,95	3,32
Upper 95% confidence bound (m/s)	0,059	0,060	0,064	0,067	0,085
Empirical $v_{i,2\%}$ (m/s)	0,052	0,048	0,059	0,064	0,077
Lower 95% confidence bound (m/s)	0,048	0,037	0,053	0,059	0,070

H

Distributions number of events

The number of events per 1000 waves can be described using the log-normal distribution. The equation and the parameters are given in this appendix. For each combination of wave condition and location on the slope the plot showing both the empirical CDF and the calculated CDF using the determined parameters are also given.

$$f(N_E) = \frac{1}{\sigma N_E \sqrt{2\pi}} e^{-\frac{(ln(N_E)-\mu)^2}{2\sigma^2}} \quad \text{(H.1)}$$

where

N_E	number of events per 1000 waves
$f(N_E)$	probability of N_E
σ	standard deviation of $Ln(N_E)$
μ	mean of $Ln(N_E)$

Table H.1: Mean (μ) and standard deviation (σ) for the natural-logarithm of the number of events per 1000 waves.

$H_s/\Delta d_n$	1.85		2.21		2.58		2.92		3.32	
	μ	σ	μ	σ	μ	σ	μ	σ	μ	σ
SWL+$2d_n$	3,10	1,03	3,54	1,07	3,02	1,55	2,78	1,46	3,00	1,54
SWL	3,05	1,30	3,22	1,52	3,53	1,55	3,46	1,77	2,93	1,49
SWL−$2d_n$	2,82	1,18	2,34	1,38	2,50	1,66	2,96	1,65	2,65	1,84

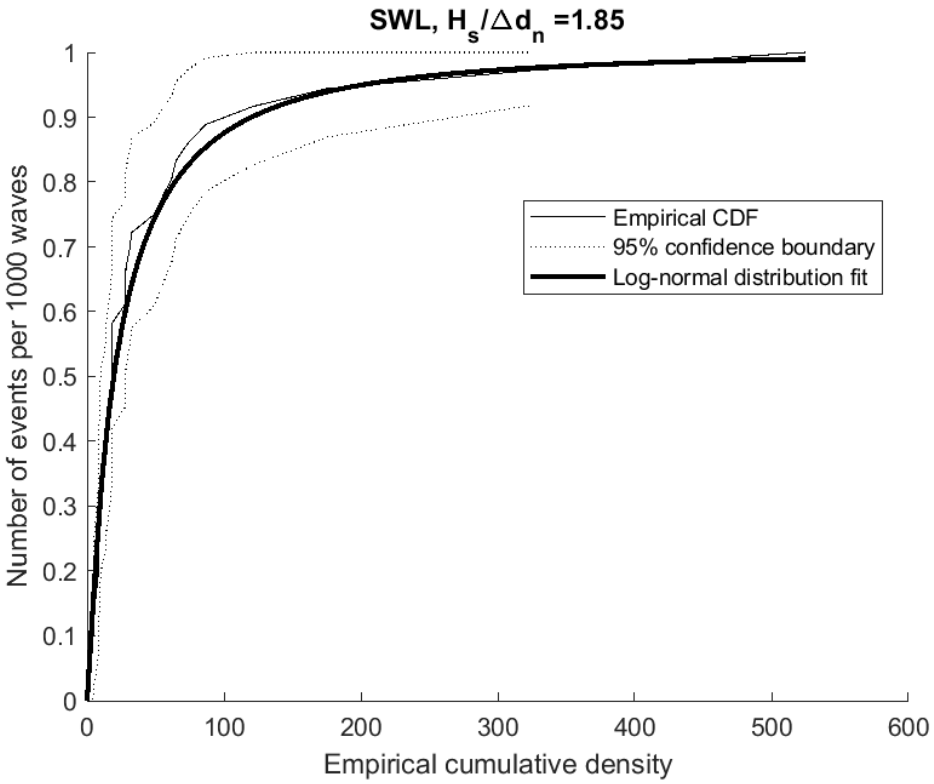

Figure H.1: The empirical and calculated cumulative density for the number of events (N_E) at SWL

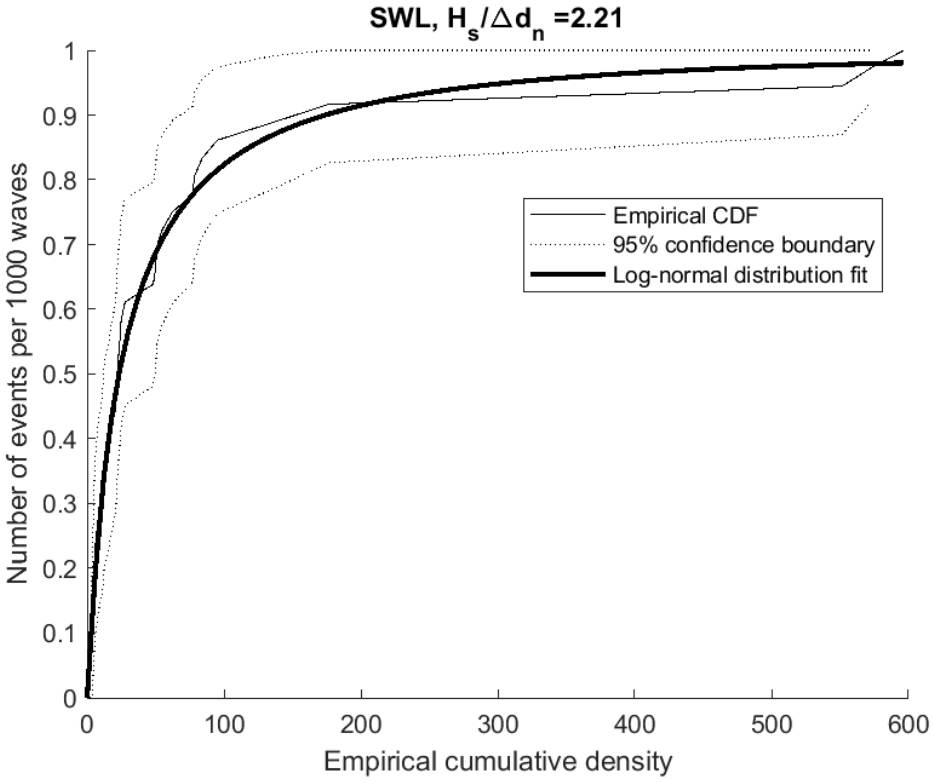

Figure H.2: The empirical and calculated cumulative density for the number of events (N_E) at SWL

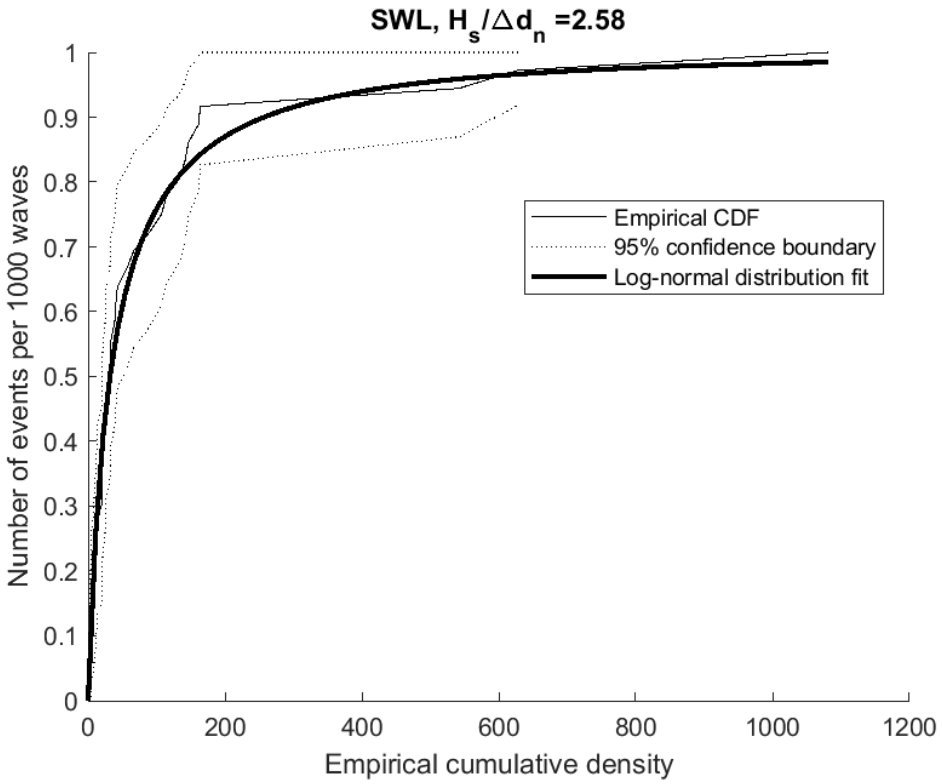

Figure H.3: The empirical and calculated cumulative density for the number of events (N_E) at SWL

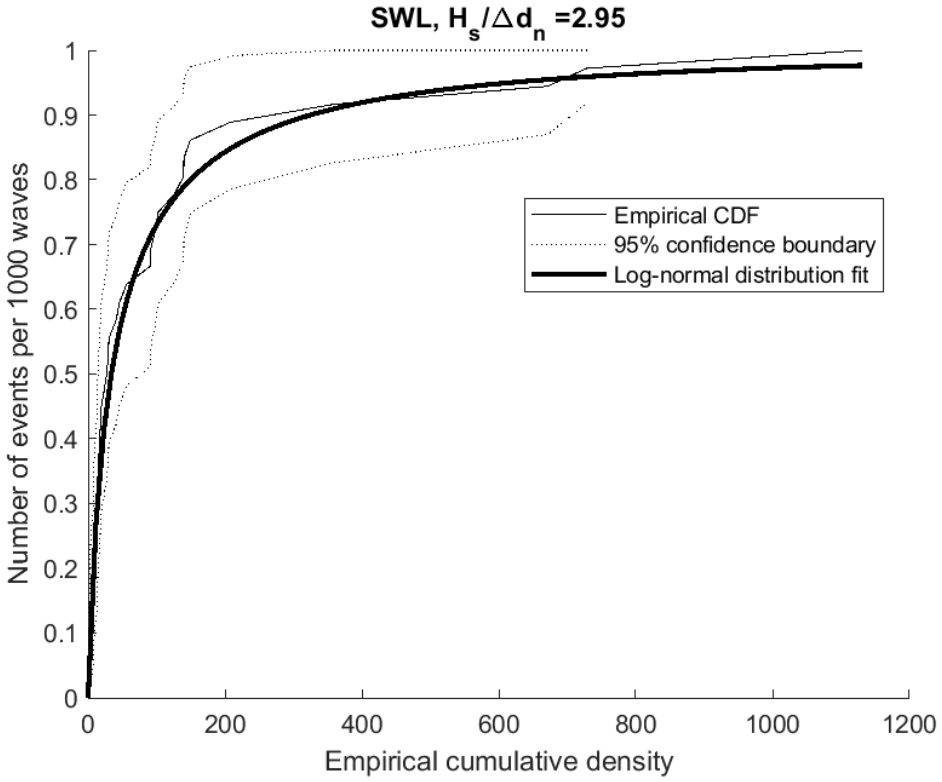

Figure H.4: The empirical and calculated cumulative density for the number of events (N_E) at SWL

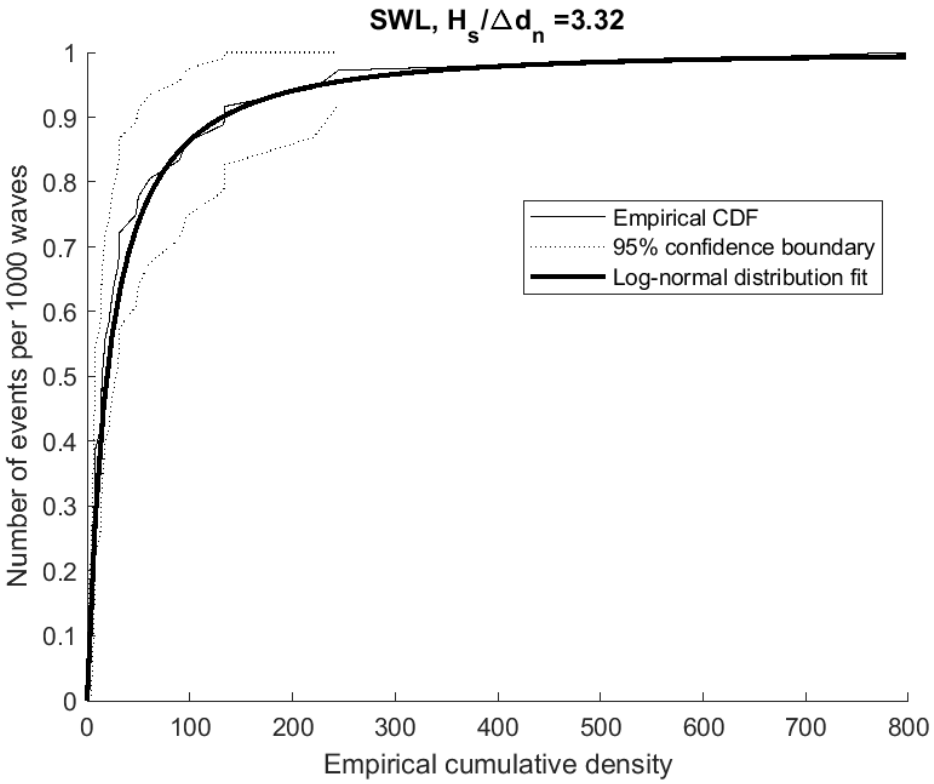

Figure H.5: The empirical and calculated cumulative density for the number of events (N_E) at SWL

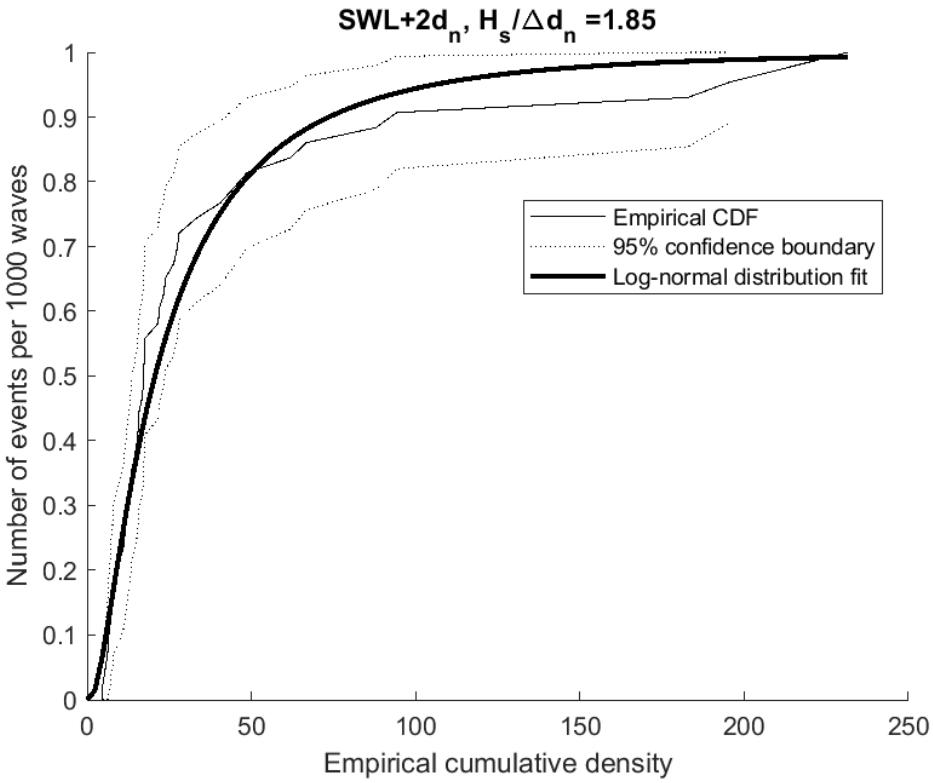

Figure H.6: The empirical and calculated cumulative density for the number of events (N_E) at SWL

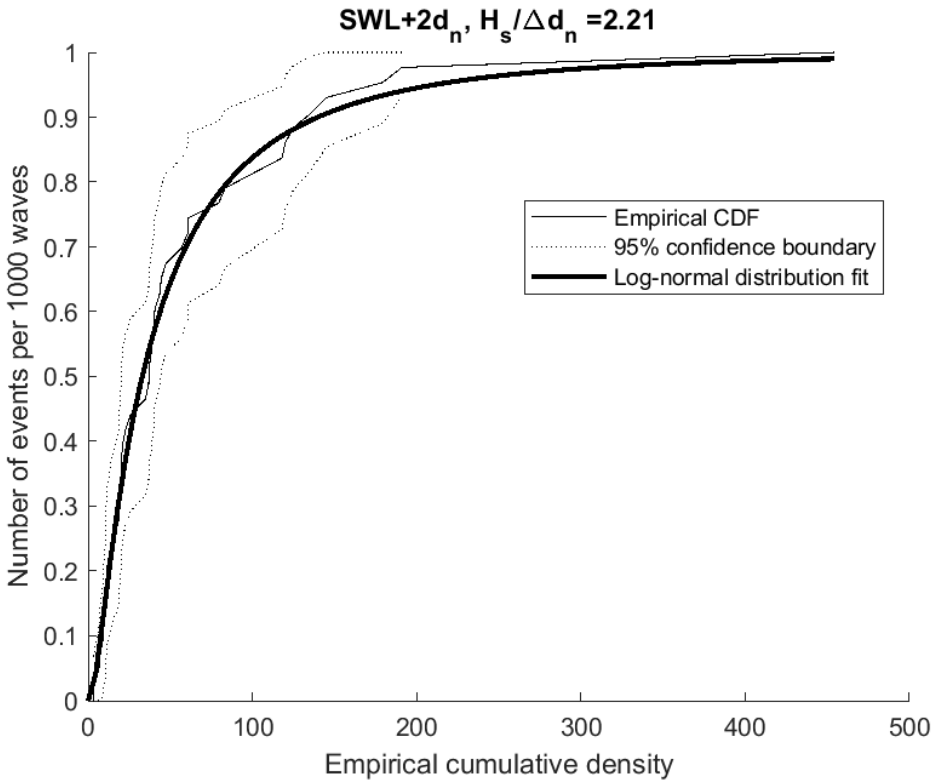

Figure H.7: The empirical and calculated cumulative density for the number of events (N_E) at SWL

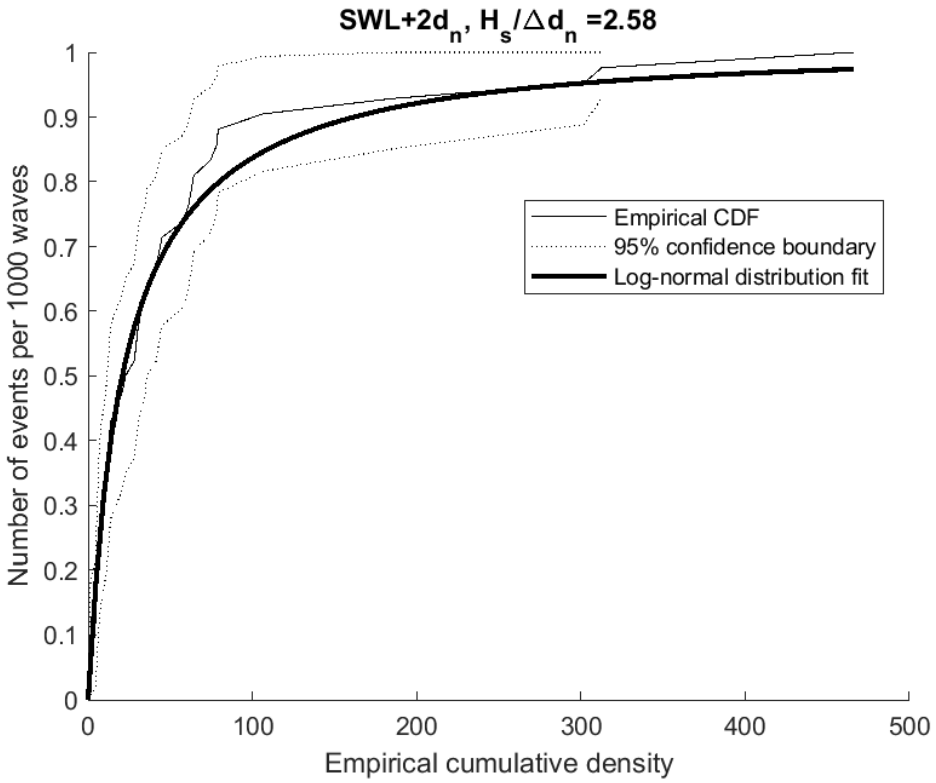

Figure H.8: The empirical and calculated cumulative density for the number of events (N_E) at SWL

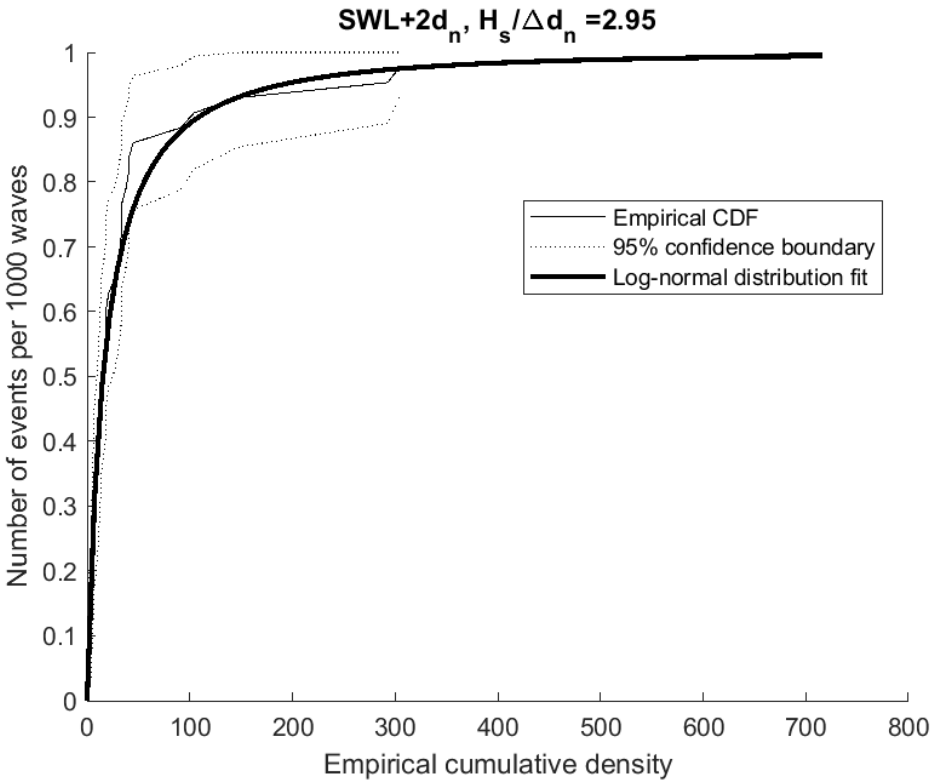

Figure H.9: The empirical and calculated cumulative density for the number of events (N_E) at SWL

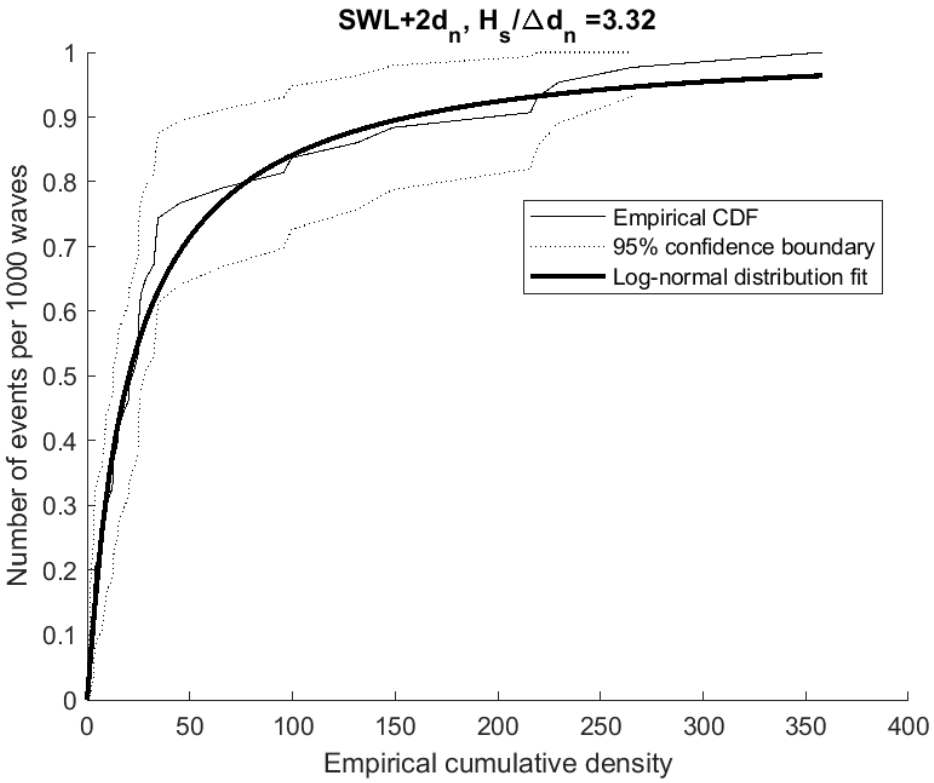

Figure H.10: The empirical and calculated cumulative density for the number of events (N_E) at SWL

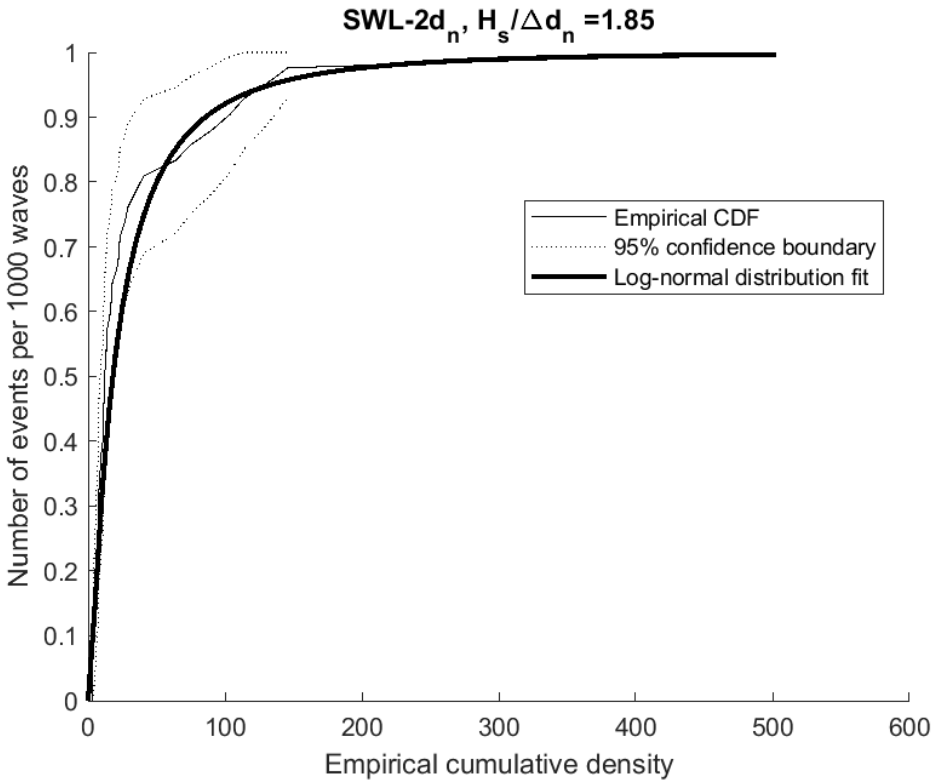

Figure H.11: The empirical and calculated cumulative density for the number of events (N_E) at SWL

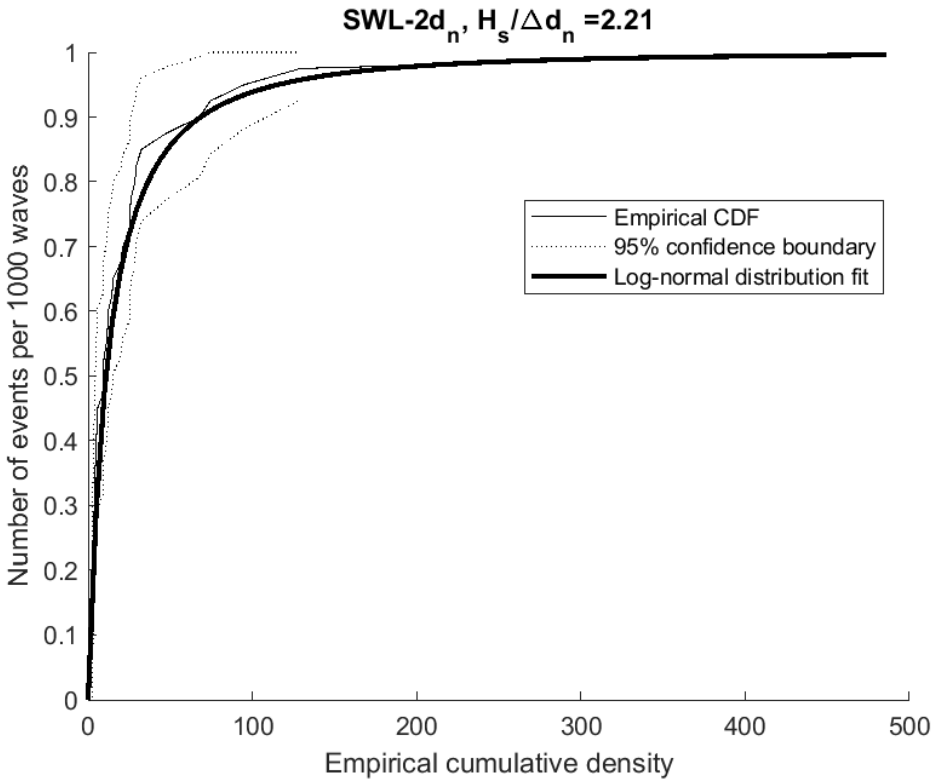

Figure H.12: The empirical and calculated cumulative density for the number of events (N_E) at SWL

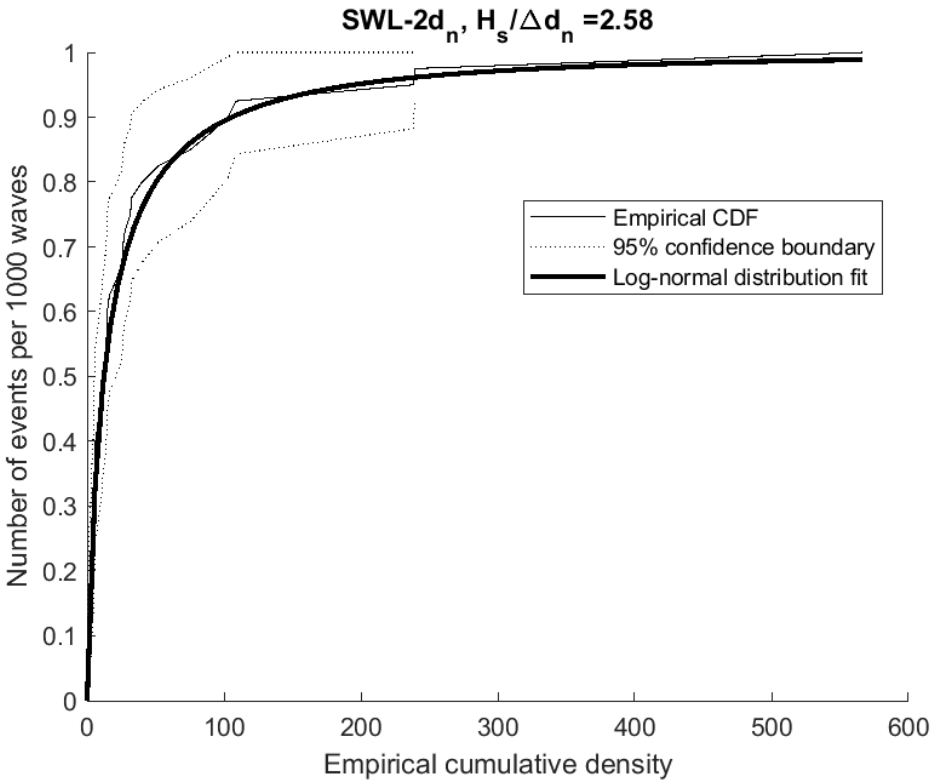

Figure H.13: The empirical and calculated cumulative density for the number of events (N_E) at SWL

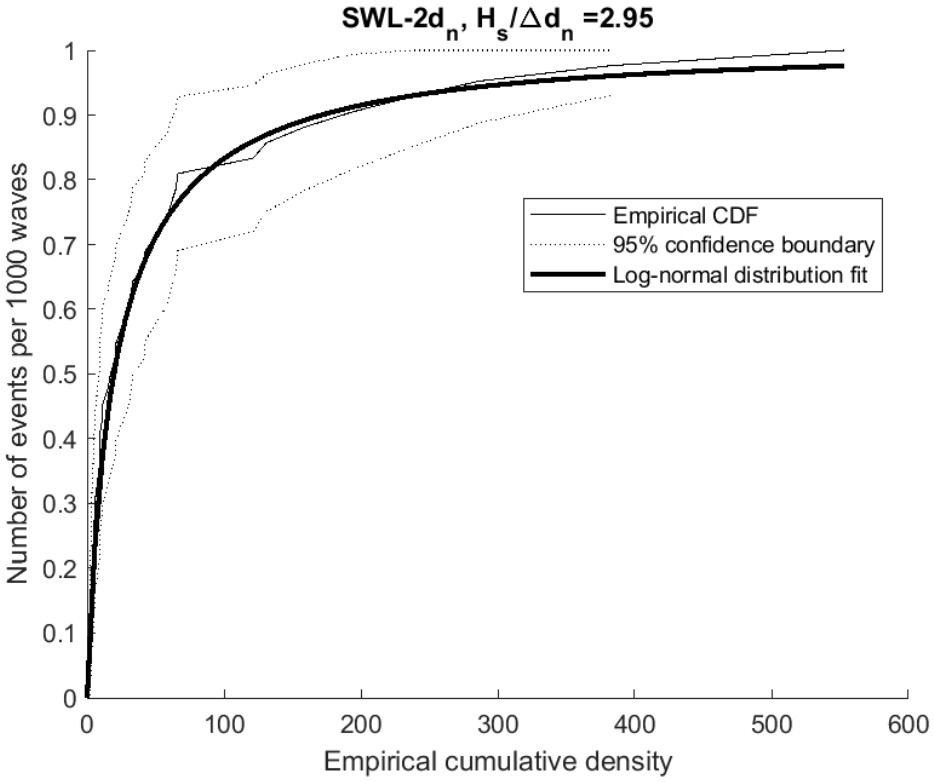

Figure H.14: The empirical and calculated cumulative density for the number of events (N_E) at SWL

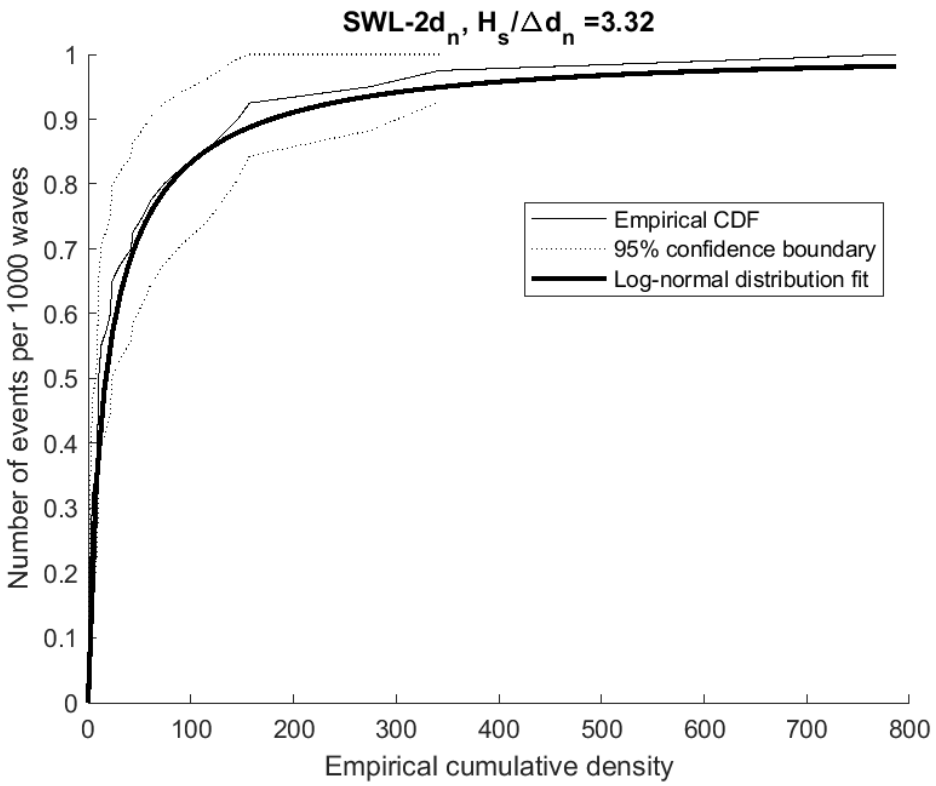

Figure H.15: The empirical and calculated cumulative density for the number of events (N_E) at SWL

Observations forms

The form was used in the following way. On the bottom of the form there is a grid representing the Xbloc units in the armour layer. When a certain unit is rocking a number is given to this unit in the grid, this number corresponds with the numbers in the table. The rocking magnitude (1), the wave height for which rocking occurs (2) and the duration the unit is rocking (3) are written down. Symbols were used to describe this and an overview of the symbols used can be found in table I.1. The filled in observation forms for test 4 till 24 can be found in appendix I.

Symbol	Meaning
(1)	Rocking magnitude
S	Small movements (barely visible)
M	Medium movements (clearly visible)
L	Large movements (clearly visible)
(2)	Wave height
L	Low wave height (Unit rocks for almost every wave)
M	Medium wave height (Unit rocks only for medium and large waves)
H	High wave height (Unit rocks only for larger waves)
(3)	Duration
S	Short duration (Unit rocks for a short time)
M	Medium duration (Unit rocks for medium time)
L	Long duration (Unit rocks for almost the entire test duration)

Table I.1: Explanation symbols as used in the observation form

Date	
Test	
Water depth	
Depth sensors	
ARC on	

TU Delft

	Photo time		Photo time		Photo time		Photo time		Photo time		Photo time
	Sensors on		Sensors on		Sensors on		Sensors on		Sensors on		
	Wave file name + on		Wave file name + on		Wave file name + on		Wave file name + on		Wave file name + on		
	Start time		Start time		Start time		Start time		Start time		
	Stop time		Stop time		Stop time		Stop time		Stop time		
	Wave series 1		**Wave series 2**		**Wave series 3**		**Wave series 4**		**Wave series 5**		
1											
2											
3											
4											
5											
6											
7											
8											
9											
10											
General observations											

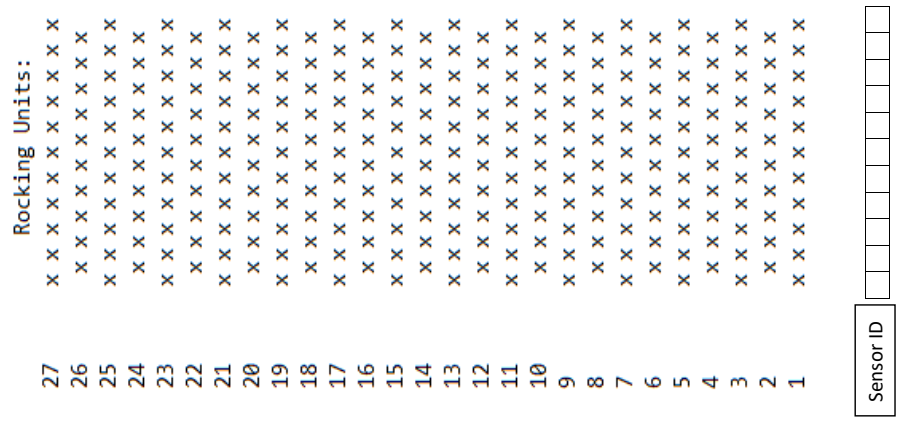

Figure I.1: Observation form

Date	17-01-2020
Test	Test 4
Water depth	0,6
Depth sensors	0,6

ARC ON 8

	Photo time	12:31		Photo time	13:13		Photo time	13:48		Photo time	14:41		Photo time	15:19		Photo time:	
	Sensors on	R:41		Sensors on	2x		Sensors on	3x | 8		Sensors on	4x | 8		Sensors on	5 | 8		16:22	
	Wave file name + on	0001 12:41	8	Wave file name + on	0002	8	Wave file name + on	0003	8	Wave file name + on	0004	8	Wave file name + on	0005	8		
	Start time	12:42		Start time	13:17		Start time	~~13:57~~ 14:00		Start time	14:41		Start time	15:33			
	Stop time	13:09		Stop time	13:~~09~~ 42		Stop time	14:28		Stop time	15:13		Stop time	16:11			
	Wave series 1			**Wave series 2**			**Wave series 3**			**Wave series 4**			**Wave series 5**				
1																	
2													Small movements				
3																	
4																	
5																	
6																	
7																	
8																	
9																	
10																	
General observations	H_s = 0,1 m T_p: 1,26 1) Small waves. Some waves 2) movement for some waves I) During entire series II) Stopped after few minutes			11) Some movements 3) Rocking for every wave 4) very tiny movements			11) Clear rocking 5) Started rocking 6) Larger waves rocking 5) Stopped rocking after 1min.			6) ~~moving~~ 9 medium, largest 7 small, largest 8 Both started moving large for medium waves (medium, ~~large~~ Largest some) 10) ~~Small~~, medium Large			6) moving: Li often 10) Small, some waves 11) M/L; R 12) M; L: Soms 10) M; M: Very often 13) M; L; sometime				

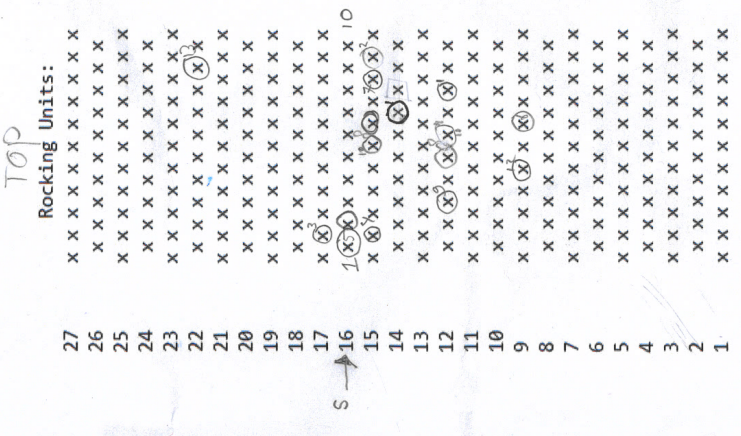

Date	20-01-2020
Test	
Water depth	0.6m
Depth sensors	0.6m 0.458
ARC on	YES

	Photo time	Sensors on	Wave file name + on	Start time	Stop time	Wave series 1 0.10	Photo time	Sensors on	Wave file name + on	Start time	Stop time	Wave series 2 0.12	Photo time	Sensors on	Wave file name + on	Start time	Stop time	Wave series 3 0.14	Photo time	Sensors on	Wave file name + on	Start time	Stop time	Wave series 4 .16	Photo time	Sensors on	Wave file name + on	Start time	Stop time	Wave series 5 .18	Photo time:
	13:28	IX / 8	01 / 8	13:47	14:09		14:17	24 / 8	02 / 8	14:18	14:46		14:49	2 / 8	03 / 8	14:52	15:17		15:24	111 / 8	04 / 8	15:35	16:05		16:15	1 / 8	05 / 8	16:15	16:42		16:56
1	S	L	S																												
2	M	L/M	S																												
3	M	L	S																												
4				L	all	S																								
5				S	all	S																								
6				S	H	S							L	M/H	S				ML	L				8L	M	L				
7													M	H	S															
8													L	H	S															
9													M	H	S				DAMAGE											
10													M	H	S				M	L										
11																			M	L	M									
12																			M	L	M			12	L	L	12			
13																			S	L	L/S									
14																			L	L	L									
15																			M	L	L									
16																			S	L	L/S									
General observations																			14 Removed from slope											

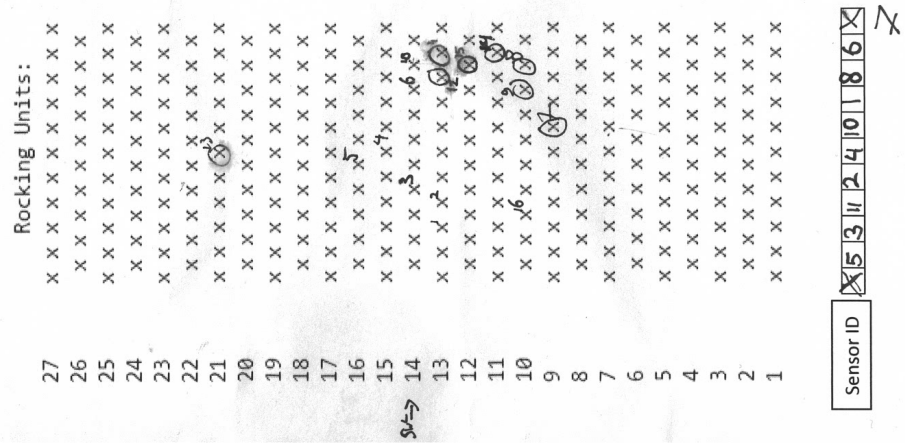

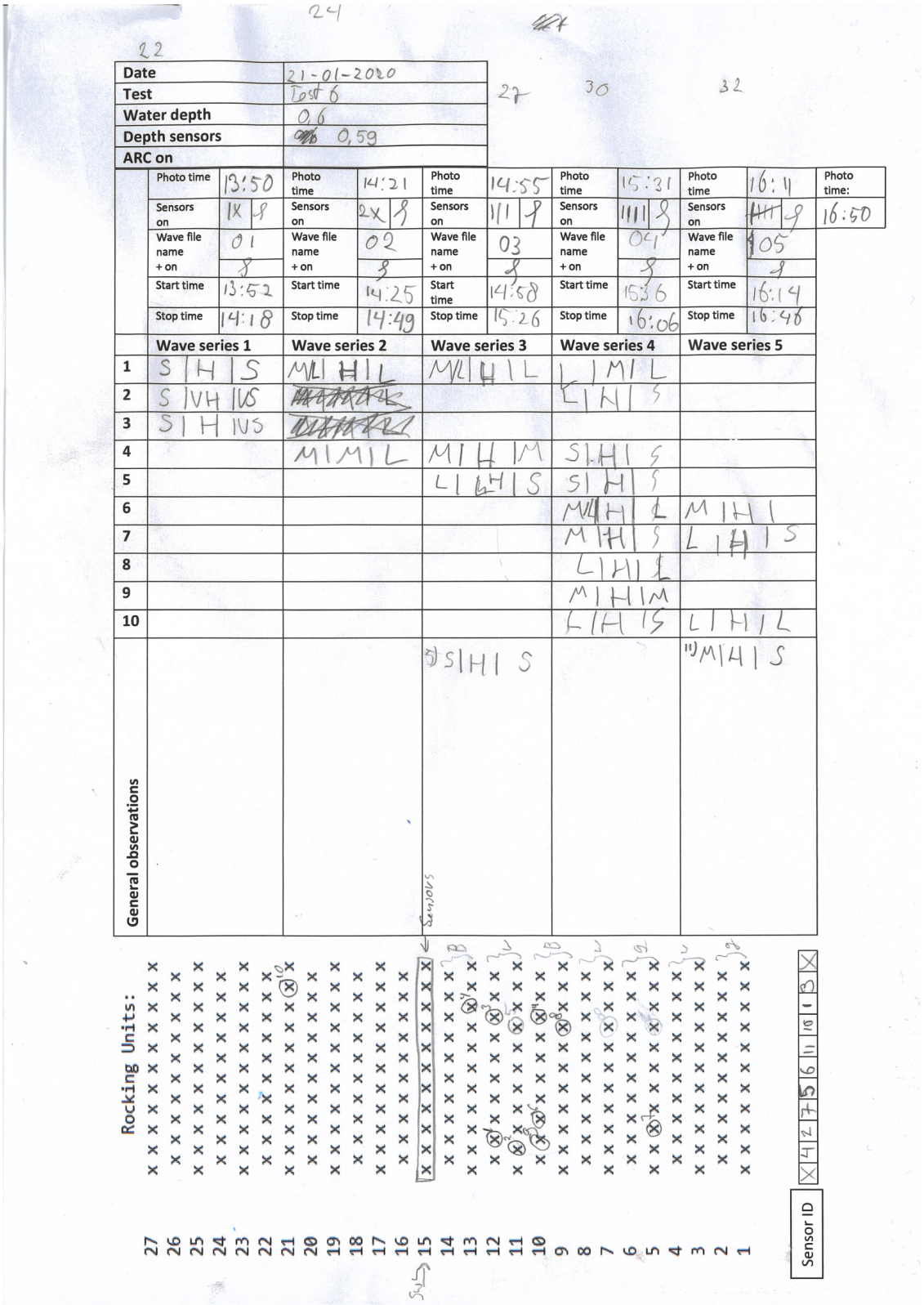

Date	21-01-2020
Test	Test 6
Water depth	0,6
Depth sensors	~~0,6~~ 0,59
ARC on	

	Wave series 1	Wave series 2	Wave series 3	Wave series 4	Wave series 5
Photo time	13:50	14:21	14:55	15:31	16:11
Sensors on	1X 8	2X 8	1/1 8	1111 8	~~HH~~ 8
Wave file name + on	01 8	02 8	03 8	04 8	05 8
Start time	13:52	14:25	14:58	15:36	16:14
Stop time	14:18	14:49	15:26	16:06	16:48
1	S H S	M L H L	M L H L	L M L	
2	S VH VS	~~M L H L~~		L H S	
3	S H VS	~~M L H L~~			
4		M M L	M H M	S H S	
5			L H S	S H S	
6				M H L	M H L
7				M H S	L H S
8				L H L	
9				M H M	
10				L H S	L H L
General observations			9) S H S		11) M H S

Photo time: 16:50

Rocking Units:

Sensors

Sensor ID

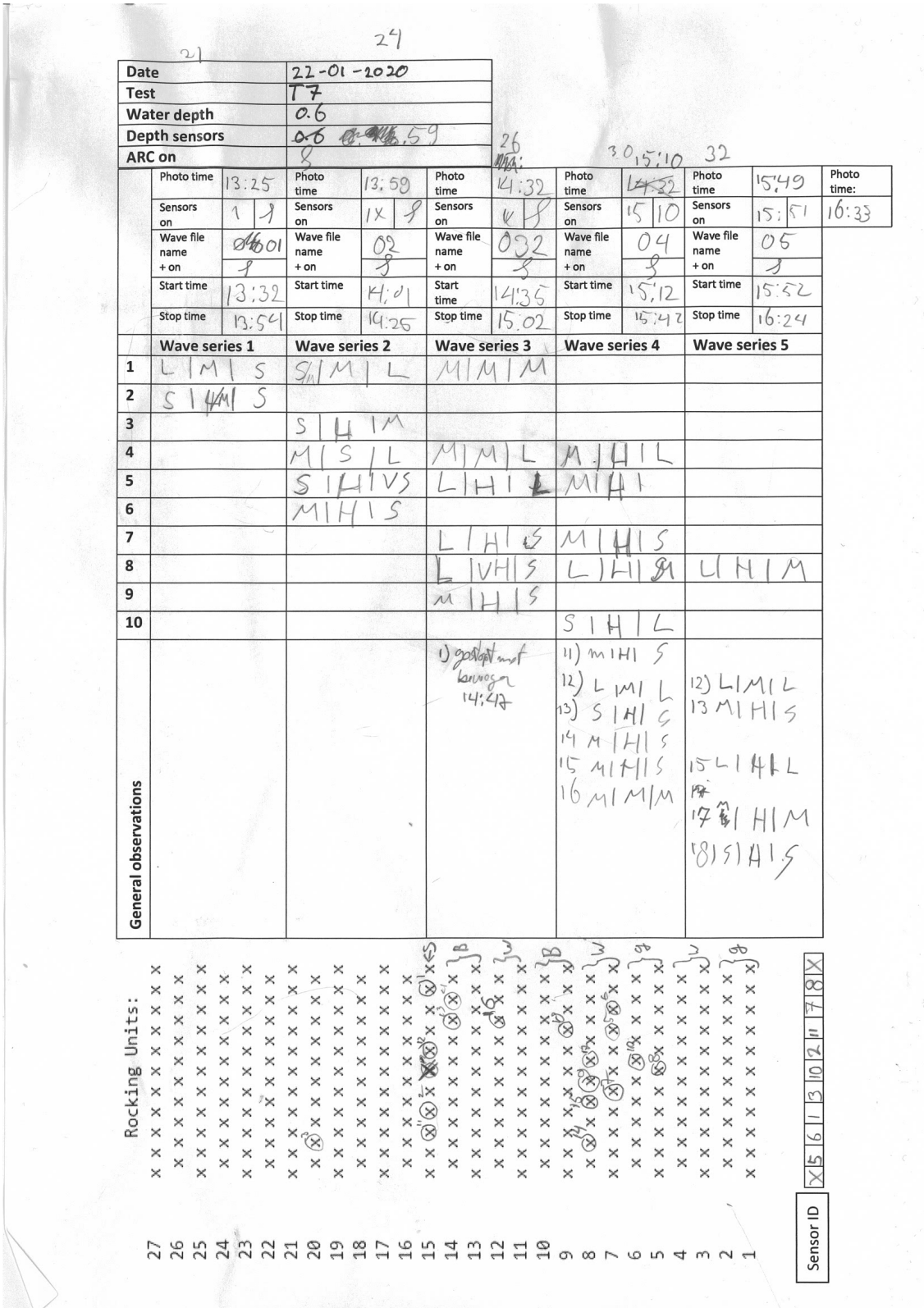

Date	22-01-2020
Test	T7
Water depth	0.6
Depth sensors	0.6 0.59
ARC on	8

	Wave series 1	Wave series 2	Wave series 3	Wave series 4	Wave series 5
Photo time	13:25	13:59	14:32	15:10	15:49
Sensors on	1 | 9	1X | 9	4 | 9	15 | 10	15:51
Wave file name + on	0001 / 9	02 / 9	032 / 9	04 / 9	05 / 9
Start time	13:32	14:01	14:35	15:12	15:52
Stop time	13:54	14:25	15:02	15:47	16:24
Photo time:					16:33
1	L | M | S	S | M | L	M | M | M		
2	S | M | S				
3		S | H | M			
4		M | S | L	M | M | L	M | H | L	
5		S | H | VS	L | H | L	M | H	
6		M | H | S			
7			L | H | S	M | H | S	
8			L | VH | S	L | H | S	L | H | M
9			M | H | S		
10				S | H | L	
General observations			1) geplaatst met kraanwagen 14:47	11) M | H | S 12) L | M | L 13) S | H | S 14 M | H | S 15 M | H | S 16 M | M | M	12) L | M | L 13 M | H | S 15 L | H | L 17 M | H | M 18 S | H | S

Rocking Units:

Sensor ID: X 5 6 11 13 10 12 11 7 8 X

Date	23-01-2020
Test	T18
Water depth	0,6
Depth sensors	~~0,59~~ 0,60
ARC on	S

	Photo time	13:30		Photo time	13:56		Photo time	14:27		Photo time	15:03		Photo time	15:43		Photo time:	16:26			
	Sensors on	13	31	Sensors on	13	57	Sensors on	14	29	Sensors on	15	04	Sensors on	15	44					
	Wave file name + on	01	S	Wave file name + on	02	S	Wave file name + on	03	S	Wave file name + on	04	S	Wave file name + on	05	S					
	Start time	13:31		Start time	13:59		Start time	1430		Start time	1505		Start time	15:46						
	Stop time	13:53		Stop time	14:22		Stop time	14:56		Stop time	15:35		Stop time	16:18						
	Wave series 1 21			**Wave series 2** 24			**Wave series 3** 26			**Wave series 4** 30			**Wave series 5** 32							
1	S	M	S	S	M	S	S	H	L	S	H									
2	S	M	S																	
3	S	H	S	S	H	L	M	M	M											
4	L	H	L	L	H	L	L	M	L											
5				S	H	S	L	M	L											
6							M	H	M											
7							M	M	M	L	H	L	L	H	L					
8							M	H	S											
9										S	H	S								
10										S	H	S								
General observations							5) Removed from slope!			11) S H S 12 S H S			11) M H M 12) S M M							

Rocking Units:

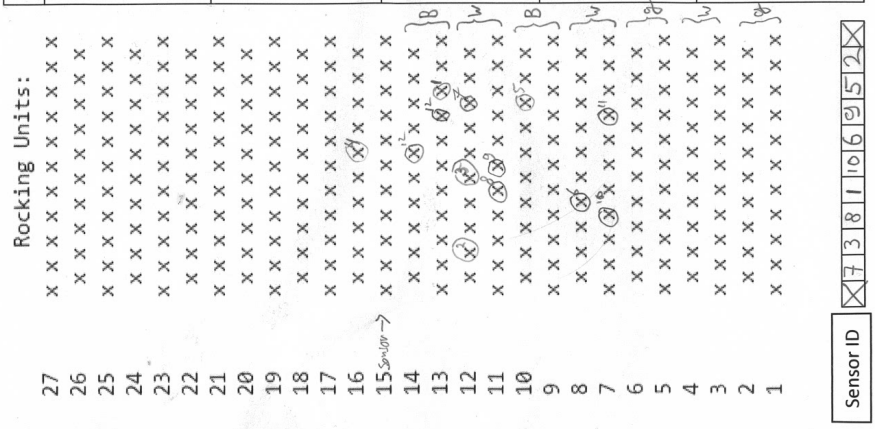

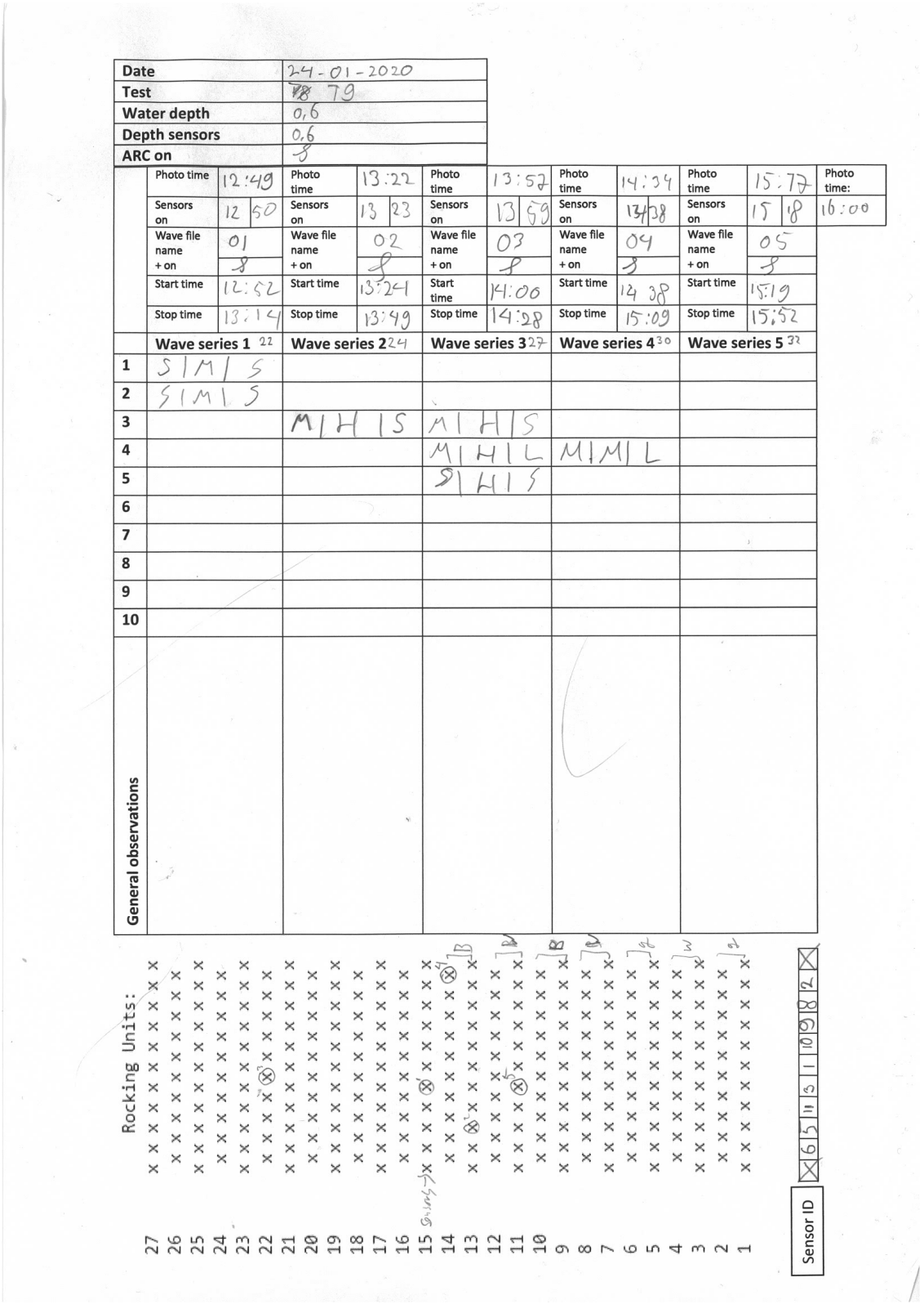

Date	24-01-2020
Test	~~78~~ 79
Water depth	0,6
Depth sensors	0,6
ARC on	S

	Photo time	12:49	Photo time	13:22	Photo time	13:57	Photo time	14:34	Photo time	15:17	Photo time:	
	Sensors on	12 | 50	Sensors on	13 | 23	Sensors on	13 | 59	Sensors on	14 | 38	Sensors on	15 | 18	16:00	
	Wave file name + on	01 S	Wave file name + on	02 S	Wave file name + on	03 S	Wave file name + on	04 S	Wave file name + on	05 S		
	Start time	12:52	Start time	13:24	Start time	14:00	Start time	14:38	Start time	15:19		
	Stop time	13:14	Stop time	13:49	Stop time	14:28	Stop time	15:09	Stop time	15:52		
	Wave series 1 22		**Wave series 2** 24		**Wave series 3** ~~27~~		**Wave series 4** 30		**Wave series 5** 32			
1	S | M | S											
2	S | M | S											
3			M | H | S		M | H | S							
4					M | H | L		M | M | L					
5					S | H | S							
6												
7												
8												
9												
10												
General observations												

Rocking Units:

Sensor ID: ~~6~~ 5 11 13 1 10 9 8 12 ~~X~~

Date	27-01-2020
Test	T10
Water depth	0.6
Depth sensors	ROW 13 0.57
ARC on	~~S~~

	Photo time	13:40		Photo time	14:13		Photo time	14:47		Photo time	15:24		Photo time	16:05		Photo time:					
	Sensors on	13	41	Sensors on	14	14	Sensors on	14	48	Sensors on	15	26	Sensors on	16	06	16:20					
	Wave file name + on	01	S	Wave file name + on	02	S	Wave file name + on	03	~~S~~	Wave file name + on	04	S	Wave file name + on	05	S						
	Start time	13:42		Start time	14:15		Start time	14:40		Start time	15:27		Start time	16:07							
	Stop time	14:03		Stop time	14:40		Stop time	15:10		Stop time	15:52		Stop time	16:29							
	Wave series 1 22			Wave series 2 24			Wave series 3 27			Wave series 4 30			Wave series 5 32								
1	L M M																				
2				M L S																	
3				M L S																	
4				L L S																	
5				S L S																	
6							M L M														
7							M L M														
8							M L ~~M~~			L H M											
9	(Unit 9)						~~S H S~~														
10							M L L			M M L											
General observations							11) S L M			~~11) S L L M~~ 12) L L S 13) L ~~M~~ S 14) S M S 15) L H M 16) L H M			15) M M S 16) M M S 17) M H								

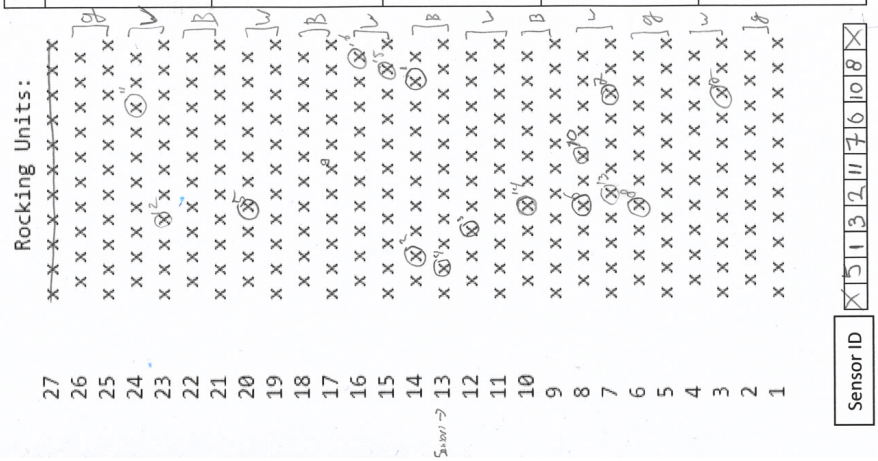

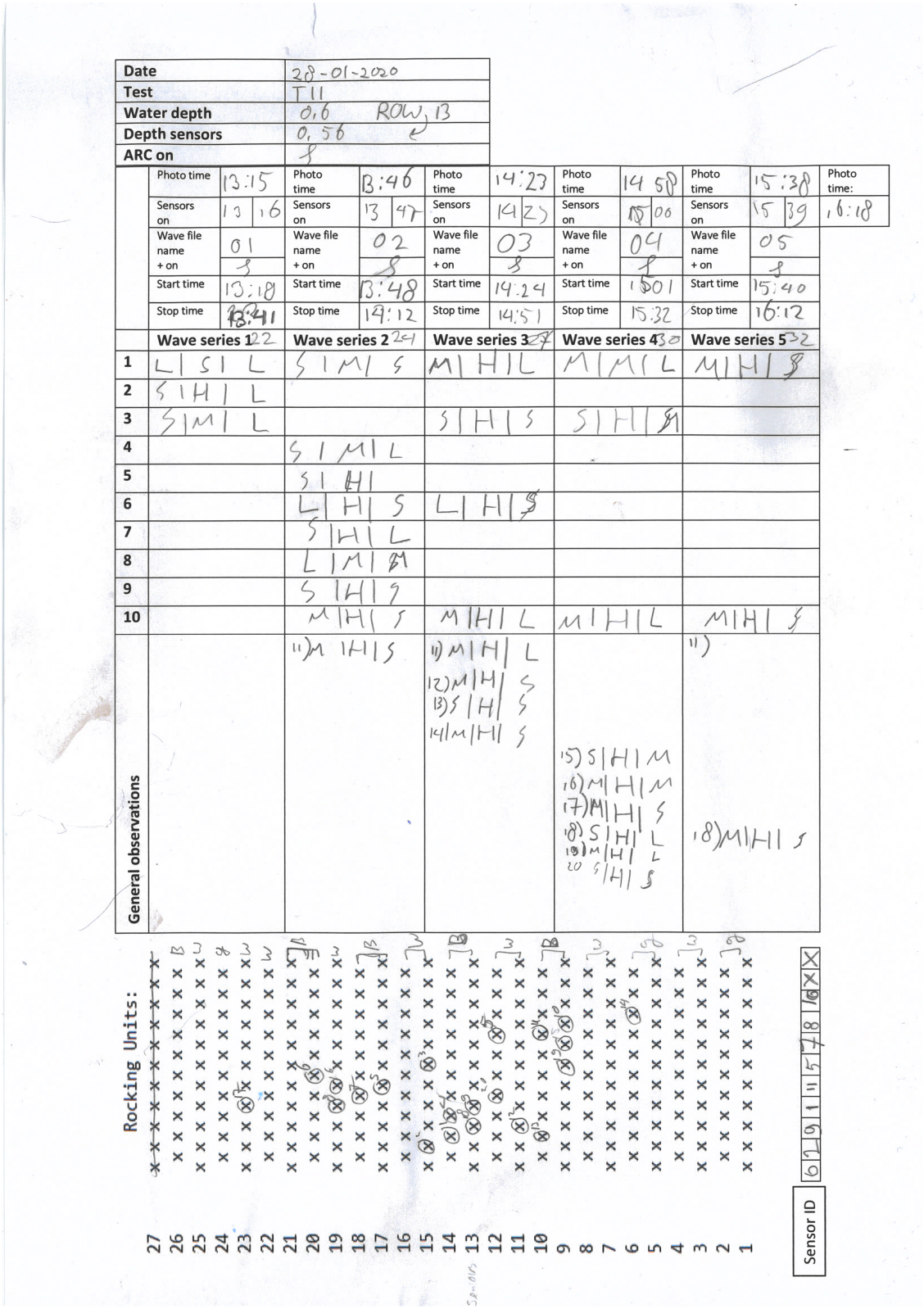

Date	28-01-2020
Test	T11
Water depth	0,6 ROW 13
Depth sensors	0,56
ARC on	S

	Photo time	13:15	Photo time	13:46	Photo time	14:23	Photo time	14 58	Photo time	15:38	Photo time:
	Sensors on	13 16	Sensors on	13 47	Sensors on	14 25	Sensors on	15 00	Sensors on	15 39	16:18
	Wave file name + on	01 S	Wave file name + on	02 S	Wave file name + on	03 S	Wave file name + on	04 S	Wave file name + on	05 S	
	Start time	13:18	Start time	13:48	Start time	14:24	Start time	15:01	Start time	15:40	
	Stop time	13:41	Stop time	14:12	Stop time	14:51	Stop time	15:32	Stop time	16:12	
	Wave series 1 22		**Wave series 2** 24		**Wave series 3** 27		**Wave series 4** 30		**Wave series 5** 32		
1	L S L		S M S		M H L		M M L		M H S		
2	S H L										
3	S M L				S H S		S H S				
4			S M L								
5			S H								
6			L H S		L H S						
7			S H L								
8			L M S								
9			S H S								
10			M H S		M H L		M H L		M H S		
General observations			11) M H S		11) M H L 12) M H S 13) S H S 14) M H S		15) S H M 16) M H M 17) M H S 18) S H L 19) M H L 20 S H S		11) 18) M H S		

Rocking Units:

Sensor ID: 6 12 9 1 11 5 7 8 16 X X

27 26 25 24 23 22 21 20 19 18 17 16 15 14 13 12 11 10 9 8 7 6 5 4 3 2 1

Date	29-01-2020
Test	T12
Water depth	0,8
Depth sensors	0.68 ROW 19
ARC on	S

	Photo time	13:05		Photo time	13:33		Photo time	14:06		Photo time	14 43		Photo time	15:23		Photo time:	16:04
	Sensors on	13	04	Sensors on	13	35	Sensors on	14	07	Sensors on	14	44	Sensors on	15	24		
	Wave file name + on	01	S	Wave file name + on	02	S	Wave file name + on	03	S	Wave file name + on	04	S	Wave file name + on	05	S		
	Start time	17.05		Start time	13:36		Start time	14:09		Start time	14:45		Start time	15:25			
	Stop time	13:28		Stop time	14:00		Stop time	14:36		Stop time	15:16		Stop time	15:57			
	Wave series 1 22			**Wave series 2** 24			**Wave series 3** 27			**Wave series 4** 30			**Wave series 5** 32				
1	S | H | S																
2	S | H | S																
3	M | M | S																
4	M | H | VS																
5	L | M | M			L | M | M														
6				S | H | M														
7				S | M | M			S | H | S			M | H | S						
8							L | S | [illegible]			L | M | M							
9							M | H | M			S | H | M							
10										S | H | S							
General observations										11) S | H | M 12) S | H | M 13) S | H | M 14) M | M | M 15) M | M | S 16 M | H | S			14) L | M | L 16 M | H | S 17 M | H | S 18 S | H | S 19 S | H | S Unit of top row fell of the back			

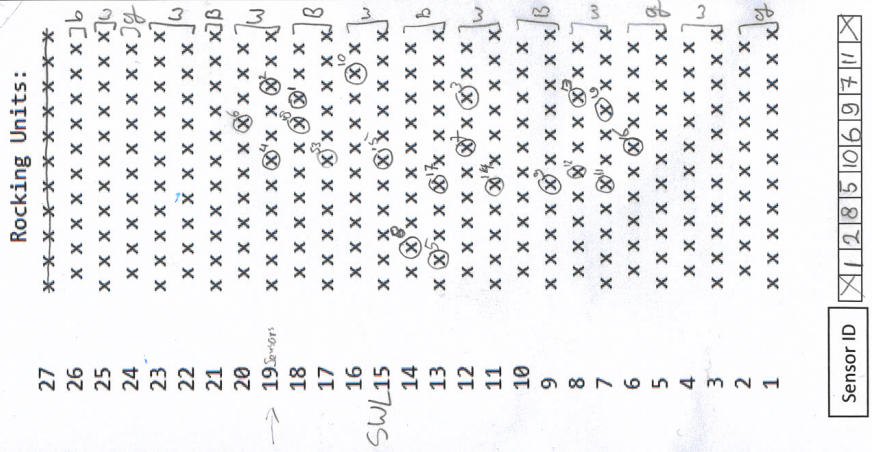

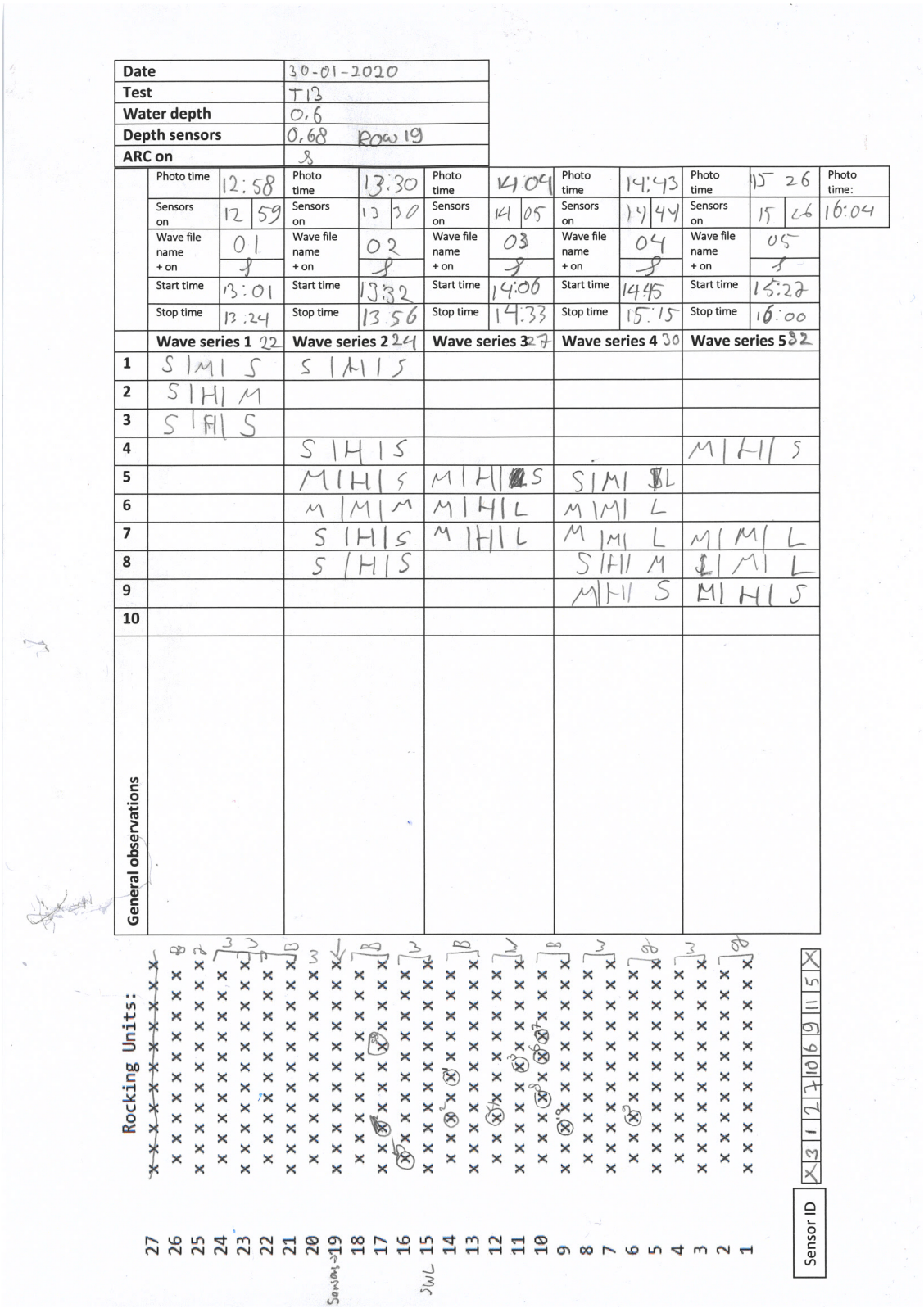

Date	30-01-2020
Test	T13
Water depth	0,6
Depth sensors	0,68 Row 19
ARC on	8

	Photo time	12:58		Photo time	13:30		Photo time	14:09		Photo time	14:43		Photo time	15:26		Photo time:
	Sensors on	12	59	Sensors on	13	30	Sensors on	14	05	Sensors on	14	44	Sensors on	15	26	16:04
	Wave file name + on	01	8	Wave file name + on	02	8	Wave file name + on	03	8	Wave file name + on	04	8	Wave file name + on	05	8	
	Start time	13:01		Start time	13:32		Start time	14:06		Start time	14:45		Start time	15:27		
	Stop time	13:24		Stop time	13:56		Stop time	14:33		Stop time	15:15		Stop time	16:00		
	Wave series 1 22			**Wave series 2** 24			**Wave series 3** 27			**Wave series 4** 30			**Wave series 5** 32			
1	S M S			S H S												
2	S H M															
3	S H S															
4				S H S									M H S			
5				M H S			M H S			S M L						
6				M M M			M H L			M M L						
7				S H S			M H L			M M L			M M L			
8				S H S						S H M			L M L			
9										M H S			M H S			
10																
General observations																

Rocking Units:

Sensor ID

X 13 1 2 7 10 16 9 11 5 X

27 26 25 24 23 22 21 20 19 18 17 16 15 14 13 12 11 10 9 8 7 6 5 4 3 2 1

Date	30-01-2020
Test	T14
Water depth	0,6
Depth sensors	0, 68 (ROW 19)
ARC on	8

	Photo time	12:34	Photo time	13:16	Photo time	13:47	Photo time	14:24	Photo time	15:04	Photo time:	
	Sensors on	12 | 34	Sensors on	13 | 16	Sensors on	13 | 47	Sensors on	14 | 25	Sensors on	15 | 04	15:41	
	Wave file name + on	01 / 8	Wave file name + on	02 / 8	Wave file name + on	03 / 8	Wave file name + on	04 / 8	Wave file name + on	05 / 8		
	Start time	12:37	Start time	13:17	Start time	13:50	Start time	14:27	Start time	15:07		
	Stop time	12:59	Stop time	13:41	Stop time	14:12	Stop time	15:57	Stop time	15:40		
	Wave series 1 22		**Wave series 2** 21		**Wave series 3** 27		**Wave series 4** 30		**Wave series 5** 32			
1	S | M | S											
2	S | M | S											
3	L | H | S											
4			L | M | L		L | M | M							
5			S | H | S									
6			L | M | S									
7					L | H | L							
8					L | H | S							
9					L | H | S		L | H | L		M | H |		
10					L | H | S		M | H | S		M S | H |		
General observations					11) S | H | L		11) M | H | 12) S | H | 13) S | H | 14) S | H |		11 S | H |		

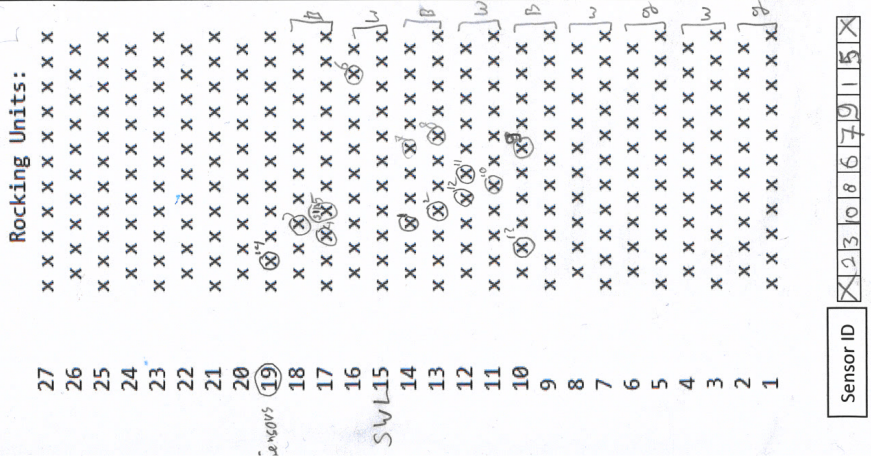

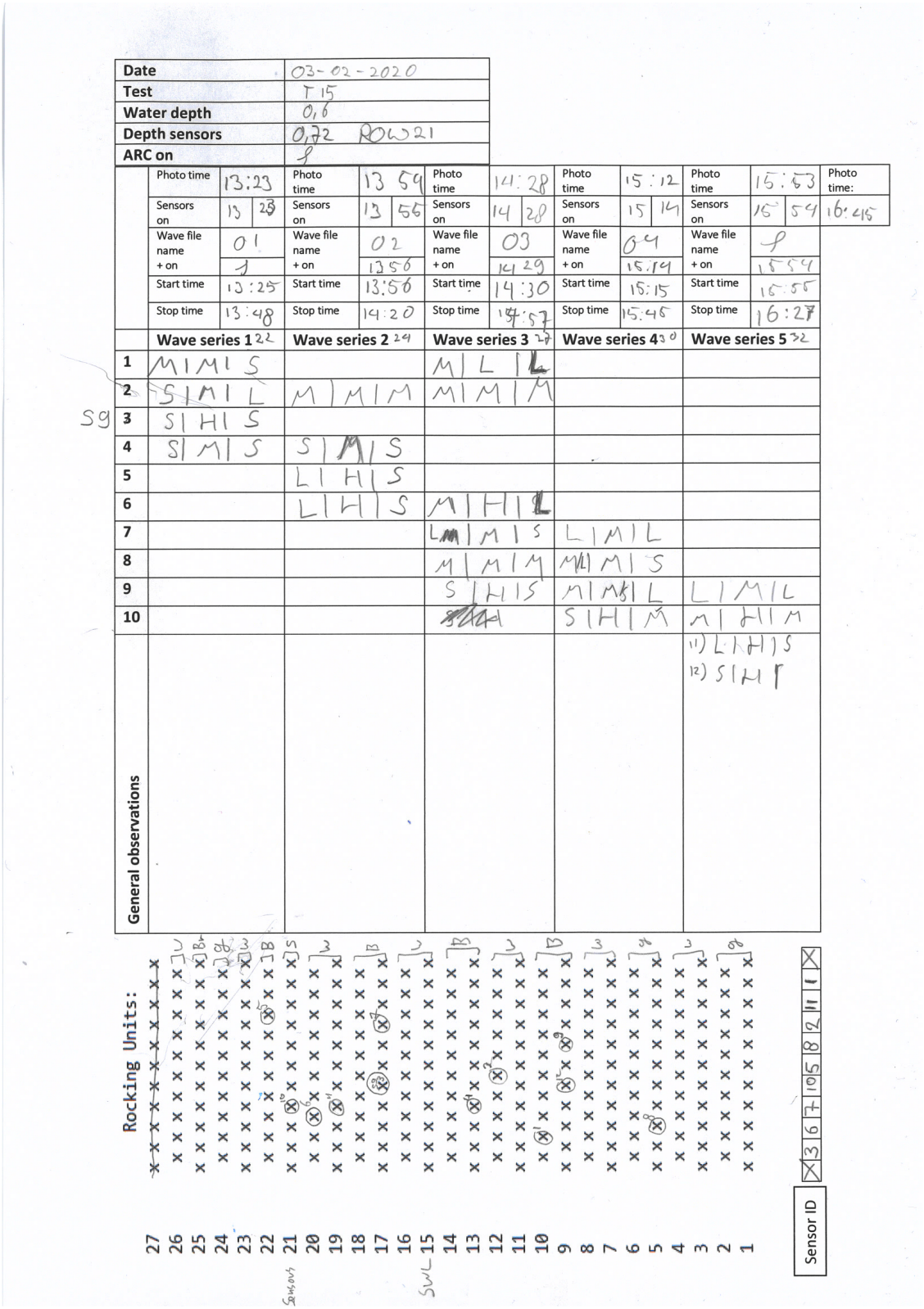

Date	03-02-2020
Test	T 15
Water depth	0,6
Depth sensors	0,72 ROW 21
ARC on	9

	Wave series 1 22	Wave series 2 24	Wave series 3 27	Wave series 4 30	Wave series 5 32
Photo time	13:23	13 59	14:28	15:12	15:53
Sensors on	13 23	13 56	14 28	15 14	15 54
Wave file name + on	01 / 1	02 / 13 56	03 / 14 29	04 / 15:14	9 / 15 54
Start time	13:25	13:56	14:30	15:15	15:55
Stop time	13:48	14:20	14:57	15:45	16:27
1	M I M I S		M I L I L		
2	S I M I L	M I M I M	M I M I M		
3	S I H I S				
4	S I M I S	S I M I S			
5		L I H I S			
6		L I H I S	M I H I L		
7			L M I M I S	L I M I L	
8			M I M I M	M I M I S	
9			S I H I S	M I M I L	L I M I L
10				S I H I M	M I H I M
General observations					11) L I H I S 12) S I M I

Photo time: 16:45

Rocking Units:

Sensor ID

Date	04-02-2020														
Test	T16														
Water depth	0,6														
Depth sensors	0,68 RAW 19														
ARC on	f														
	Photo time	12 30	Photo time	13:06	Photo time	13:38	Photo time	14:14	Photo time	14 56	Photo time:				
	Sensors on	12 34	Sensors on	13 06	Sensors on	13 38	Sensors on	14 15	Sensors on	14 55	15:33				
	Wave file name + on	01 12:35	Wave file name + on	02 13:07	Wave file name + on	03 15:39	Wave file name + on	04 14:16	Wave file name + on	05 14:56					
	Start time	12:36	Start time	13:08	Start time	13:40	Start time	14:18	Start time	14:56					
	Stop time	12:59	Stop time	13:32	Stop time	14:08	Stop time	14:48	Stop time	15:28					
	Wave series 1 22		**Wave series 2** 24		**Wave series 3** 28		**Wave series 4** 30		**Wave series 5** 32						
1	M | H | S		M | M | M		S | M | M		M | H | M		M | H | L						
2	L | M | M		S | H | S												
3	S | H | S				M | H | S										
4	S | H | M														
5			M | M | S												
6			L | M | M		S | M | M										
7					S | M | S										
8					S | M | M										
9							S | H | L		M | H | S						
10							L | H | L								
General observations							11) S | H | M 12 M | H | S 13 M | H | S 14 M | H | S 15 M | H | S		16 M | H | L 17 M | H | S 18 S | H | S						

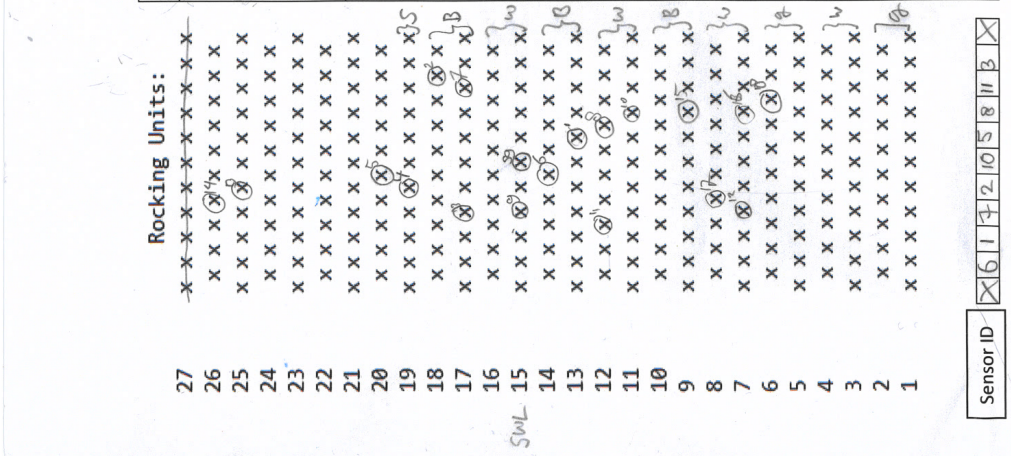

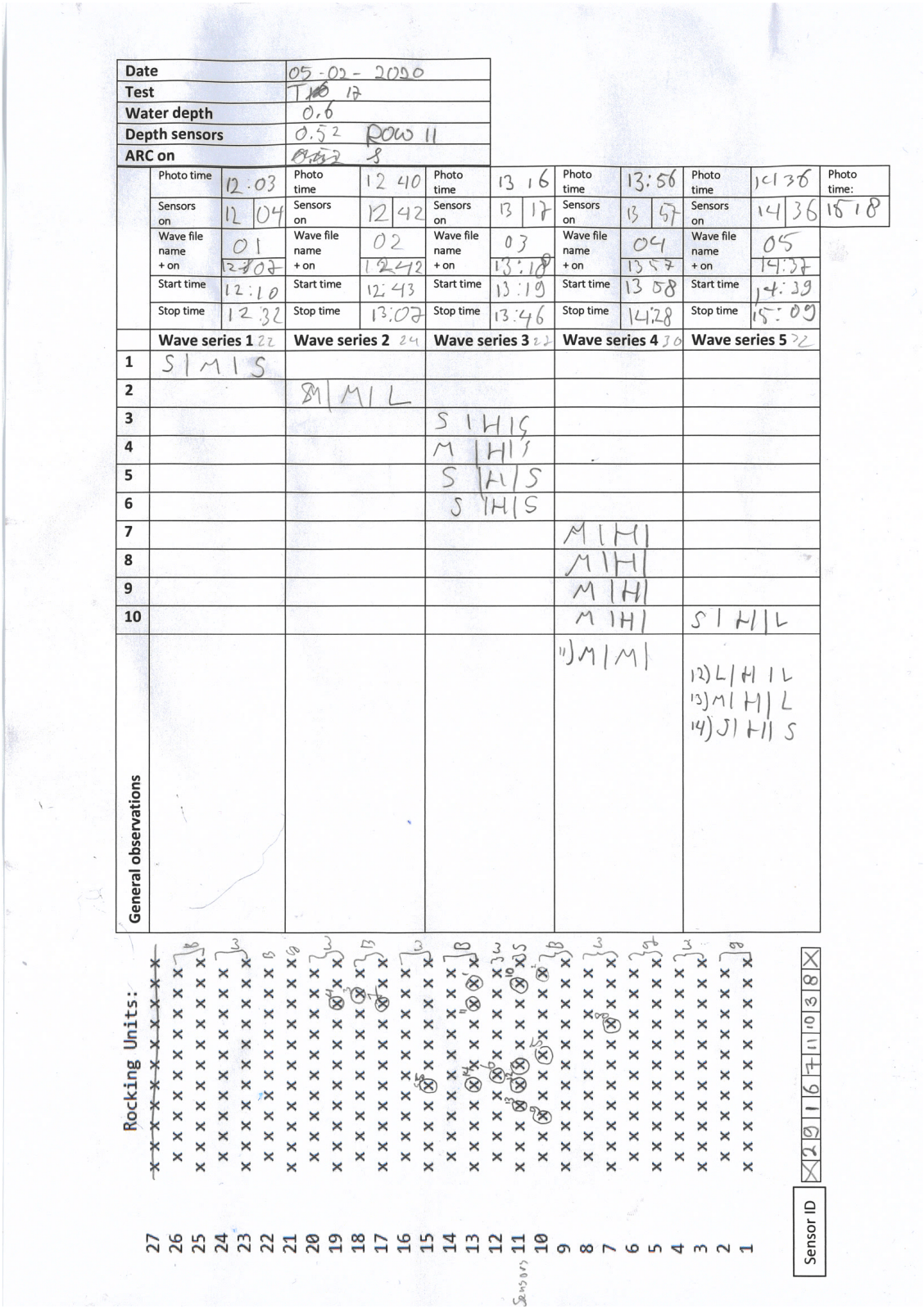

Date	05-02-2020
Test	T 17
Water depth	0,6
Depth sensors	0.52 Row 11
ARC on	8

	Wave series 1 22	Wave series 2 24	Wave series 3 23	Wave series 4 30	Wave series 5 32
Photo time	12:03	12 40	13 16	13:56	14 36
Photo time:					15 18
Sensors on	12 04	12 42	13 17	13 57	14 36
Wave file name + on	01 12:07	02 12:42	03 13:18	04 13:57	05 14:37
Start time	12:10	12:43	13:19	13:58	14:39
Stop time	12:32	13:07	13:46	14:28	15:09
1	S | M | S				
2		M | M | L			
3			S | H | S		
4			M | H | S		
5			S | H | S		
6			S | H | S		
7				M | H |	
8				M | H |	
9				M | H |	
10				M | H |	S | H | L
General observations				11) M | M |	12) L | H | L 13) M | H | L 14) S | H | S

Rocking Units:

Sensor ID

T_1 11:01 = 10°C
T_2 12:00 = 9.3 °C

Date	06-02-2020
Test	T18
Water depth	0,6
Depth sensors	0, 68
ARC on	8

	Photo time	11 18	Photo time	11:52	Photo time	12:24	Photo time	13:09	Photo time	13 40	Photo time:
	Sensors on	11 18	Sensors on	11 53	Sensors on	12 25	Sensors on	13 02	Sensors on	13 42	14:29
	Wave file name + on	01 11:21	Wave file name + on	02 11:53	Wave file name + on	03 12:26	Wave file name + on	04 13:03	Wave file name + on	05 13:42	
	Start time	11:21	Start time	11:54	Start time	12:26	Start time	13:04	Start time	13:43	
	Stop time	11:44	Stop time	12:18	Stop time	12:53	Stop time	13:34	Stop time	14:15	
	Wave series 1		**Wave series 2**		**Wave series 3**		**Wave series 4**		**Wave series 5**		
1	S | H | S										
2	M | H | S										
3	S | H | S										
4			L | H | L								
5			M | M | S								
6			S | M | L		S | M | M						
7			M | M | L								
8					L | H | S						
9					L | H | S						
10					S | M | L		S | M | L		M | M | L		
General observations					11 S | M | M 12 M | H | L		12 M | H | L 13 M | H | M 14 M | M | M 15 L | H | M 16 S | H | M		17 S | M | H | M	

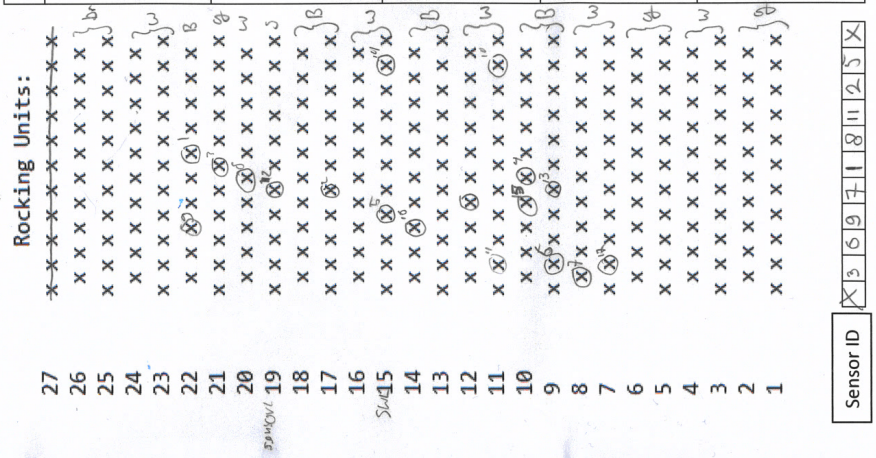

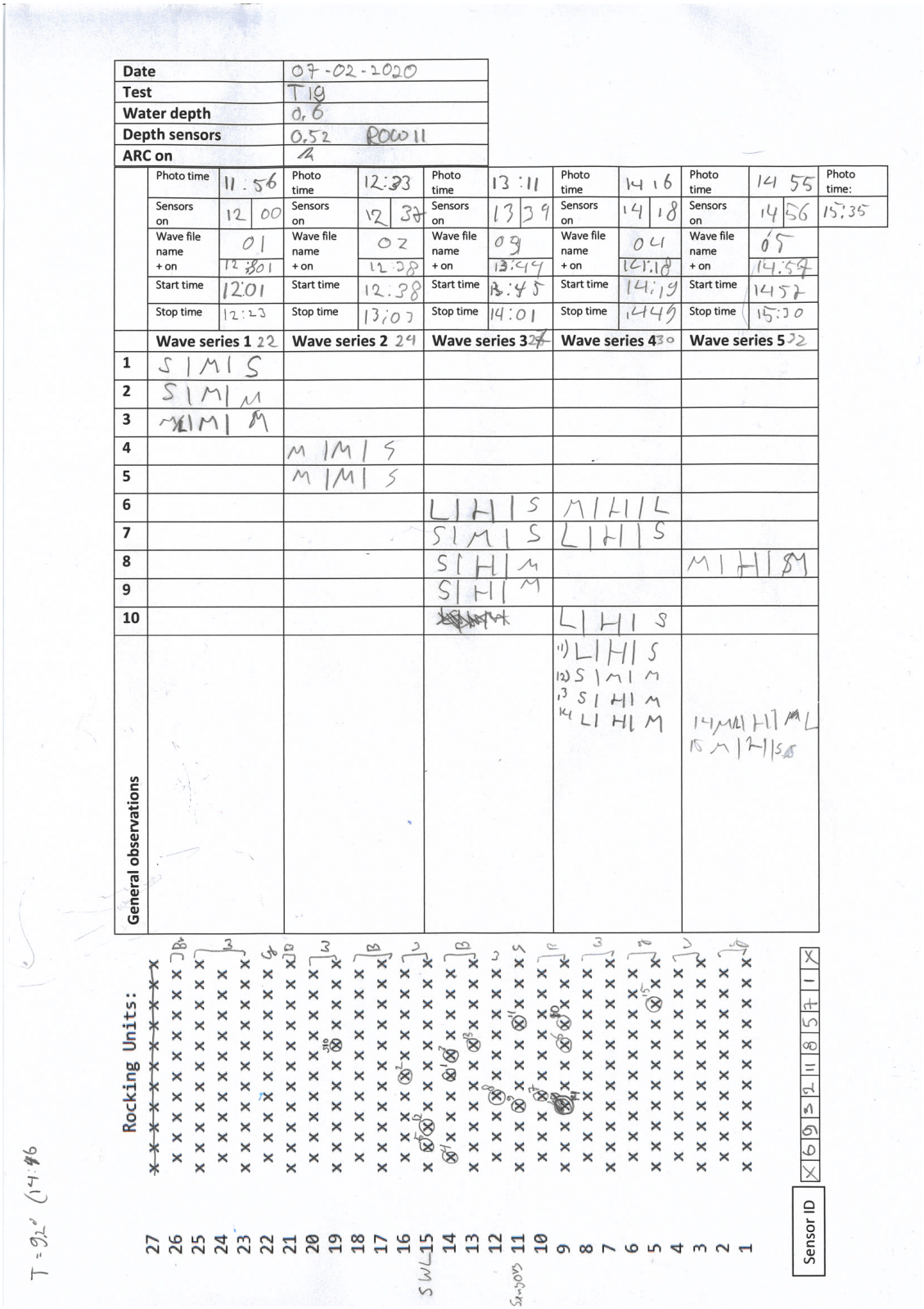

Date	07-02-2020
Test	T19
Water depth	0,6
Depth sensors	0,52 R000111
ARC on	A

	Photo time	11:56	Photo time	12:33	Photo time	13:11	Photo time	14:16	Photo time	14:55	Photo time:	15:35								
	Sensors on	12:00	Sensors on	12:37	Sensors on	13:39	Sensors on	14:18	Sensors on	14:56										
	Wave file name + on	01 12:01	Wave file name + on	02 12:38	Wave file name + on	03 13:45	Wave file name + on	04 14:19	Wave file name + on	05 14:57										
	Start time	12:01	Start time	12:38	Start time	13:45	Start time	14:19	Start time	14:57										
	Stop time	12:23	Stop time	13:07	Stop time	14:01	Stop time	14:49	Stop time	15:30										
	Wave series 1 22		**Wave series 2** 24		**Wave series 3** 27		**Wave series 4** 30		**Wave series 5** 32											
1	S M S																			
2	S M M																			
3	M M M																			
4			M M S																	
5			M M S																	
6					L H S		M H L													
7					S M S		L H S													
8					S H M				M H M											
9					S H M															
10					~~M M M~~		L H S													
General observations							11) L H S 12) S M M 13) S H M 14) L H M		14) M H M L 15) M H S											

Rocking Units:

Sensor ID: X 6 9 3 12 11 8 5 4 1 X

SWL

T = 9.2° (14:46

T = 8°C 12:52
T = 8.5°C 14:16
T = 8.4°C 15:02

Date	10-02-2020
Test	T20
Water depth	0,60
Depth sensors	0,52 ROW 11
ARC on	8

	Photo time	11:49		Photo time	12:26		Photo time	13:04		Photo time	13:41		Photo time	14:25		Photo time:					
	Sensors on	11	50	Sensors on	12	27	Sensors on	13	05	Sensors on	13	41	Sensors on	14	26	15:02					
	Wave file name + on	01	11:51	Wave file name + on	02	12 27	Wave file name + on	03	13 06	Wave file name + on	04	13:42	Wave file name + on	05	14:26						
	Start time	11:52		Start time	12 29		Start time	13:07		Start time	13:43		Start time	14:27							
	Stop time	12 15		Stop time	12:53		Stop time	13:34		Stop time	14:14		Stop time	14:59							
	Wave series 1			**Wave series 2**			**Wave series 3**			**Wave series 4**			**Wave series 5**								
1	S | H | M			M | H | L						M | H | L			M | M | M						
2	M | H | S						L | H | M													
3	L | VH | S			M | H | S																
4				S | H | S																
5				S | H | M																
6				M | H | M																
7				M | H | L																
8							S | H | S														
9							L | H | S														
10							~~L | H | S~~			M | H | S											
General observations													11 L | H | S 12 L | H | S							

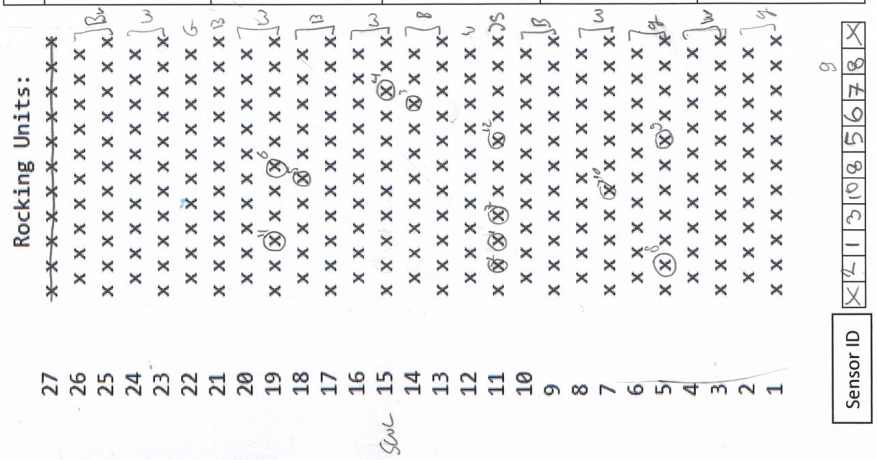

Date	11-02-2020
Test	T21
Water depth	0.6
Depth sensors	0.525 ROW 11
ARC on	S

	Photo time	11:11	Photo time	11:50	Photo time	12 24	Photo time	13;04	Photo time	13:45	Photo time:
	Sensors on	11 10	Sensors on	11 51	Sensors on	12 25	Sensors on	13 06	Sensors on	13 45	14:25
	Wave file name + on	01 11:19	Wave file name + on	02 11.52	Wave file name + on	03 12:26	Wave file name + on	04 13;07	Wave file name + on	05 13:46	
	Start time	11:20	Start time	11:53	Start time	12:27	Start time	13;08	Start time	13 47	
	Stop time	11:42	Stop time	12:18	Stop time	12:54	Stop time	13:38	Stop time	14:18	
	Wave series 1		**Wave series 2**		**Wave series 3**		**Wave series 4**		**Wave series 5**		
1	S | M | S										
2	M | H | S		L | H | M		L | H | M					
3			L | M | M							
4			M | H | L							
5			M | H | L							
6			L | H | M							
7			M | H | S							
8			L | M | S		L | H | S					
9			~~S | H | L~~		S | H | S					
10					L | U | H | S		L | H | L		L | H | M	
General observations			wave gauge not on!				11) M | H | L		11 L | H | S 12 S | H | S 13 M | H | M	

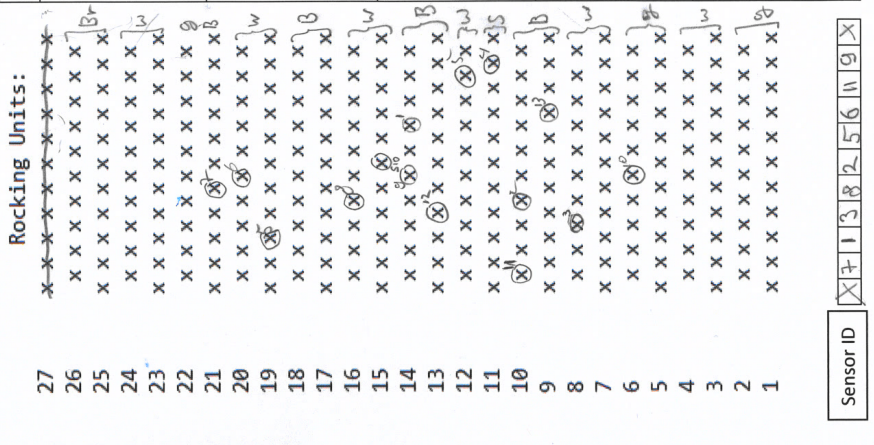

Date	12-02-2020
Test	T22
Water depth	0,6
Depth sensors	0,52
ARC on	8

TU Delft

	Photo time	11:44	Photo time	12 21	Photo time	12:54	Photo time	13:35	Photo time	14:12	Photo time
	Sensors on	11 | 48	Sensors on	12 | 21	Sensors on	12 | 55	Sensors on	13 | 36	Sensors on	14 | 13	14:53
	Wave file name + on	01 11:40	Wave file name + on	02 12:22	Wave file name + on	03 12:56	Wave file name + on	04 13:37	Wave file name + on	05 14:14	
	Start time	11:50	Start time	12.23	Start time	12:57	Start time	13 37	Start time	14:15	
	Stop time	12 12	Stop time	12.50	Stop time	13:23	Stop time	14:02	Stop time	14:48	
	Wave series 1		**Wave series 2**		**Wave series 3**		**Wave series 4**		**Wave series 5**		
1	S | H | L		S | H | S		S | H | S		M | H | L			
2			M | H | S				S | H | S			
3			M | H | S				S | H | S			
4			M | H | S							
5					S | H | S		S		L | H | L		
6							S | H | M			
7							M | H | M			
8							M | H | S			
9							M | H | L		L | H | L		
10											
General observations											

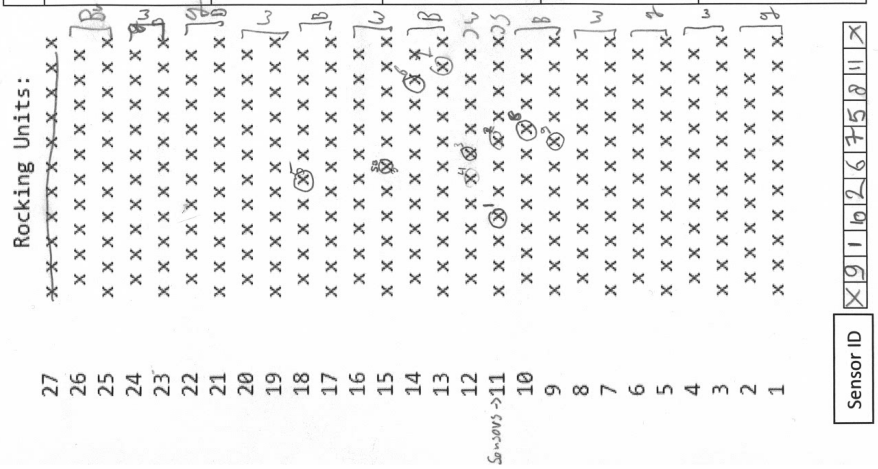

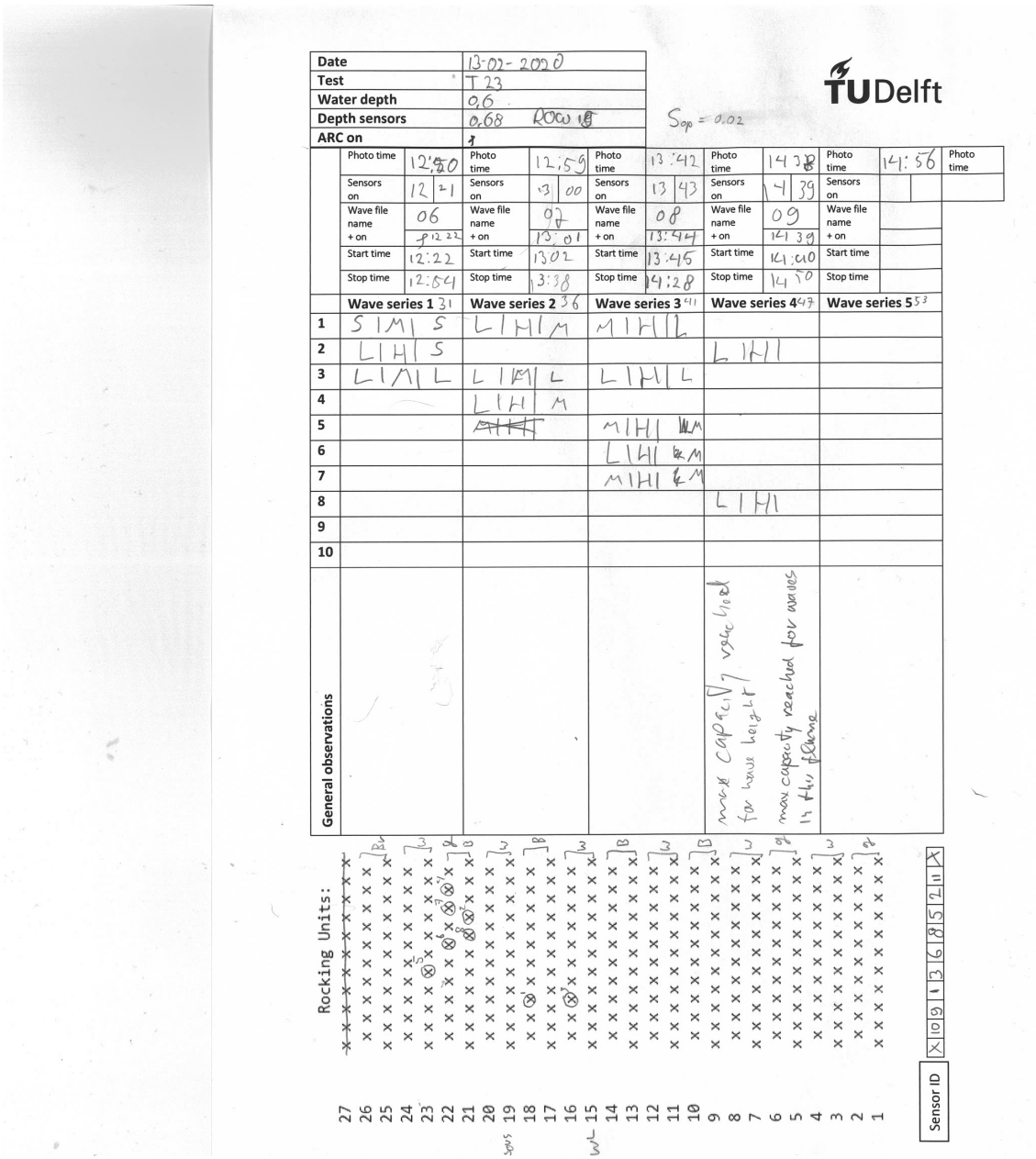

Date	13-02-2020														
Test	T 23														
Water depth	0,6														
Depth sensors	0,68 200 Hz														
ARC on	1														
	Photo time	12:50	Photo time	12:59	Photo time	13:42	Photo time	14:28	Photo time	14:56	Photo time	
	Sensors on	12 21	Sensors on	13 00	Sensors on	13 43	Sensors on	14 39	Sensors on			
	Wave file name + on	06 12:22	Wave file name + on	07 13:01	Wave file name + on	08 13:44	Wave file name + on	09 14:39	Wave file name + on			
	Start time	12:22	Start time	13:02	Start time	13:45	Start time	14:40	Start time			
	Stop time	12:54	Stop time	13:38	Stop time	14:28	Stop time	14:50	Stop time			
	Wave series 1 31		**Wave series 2** 36		**Wave series 3** 41		**Wave series 4** 47		**Wave series 5** 53			
1	S M S		L H M		M H L							
2	L H S						L H					
3	L M L		L M L		L H L							
4			L H M									
5			~~H H~~		M H							
6					L H							
7					M H							
8							L H					
9												
10												
General observations							max capacity V7 vane load for wave height		max capacity reached for waves in this flume			

Rocking Units:

27	~~x~~	~~x~~	~~x~~	~~x~~	~~x~~	~~x~~	~~x~~	~~x~~	~~x~~	~~x~~	~~x~~	~~x~~	~~x~~	~~x~~	~~x~~	~~x~~	~~x~~	~~x~~	~~x~~	~~x~~	~~x~~	~~x~~	~~x~~	~~x~~	~~x~~	~~x~~	~~x~~	~~x~~	~~x~~	~~x~~
26	x	x	x	x	x	x	x	x	x	x	x	x	x	x	x	x	x	x	x	x	x	x	x	x	x	x	x	x	x	x
25	x	x	x	x	x	x	x	x	x	x	x	x	x	x	x	x	x	x	x	x	x	x	x	x	x	x	x	x	x	x
24	x	x	x	x	x	x	x	x	x	x	x	x	x	x	x	x	x	x	x	x	x	x	x	x	x	x	x	x	x	x
23	x	x	x	x	⊗	x	x	x	x	x	x	x	x	x	x	x	x	x	x	x	x	x	x	x	x	x	x	x	x	x
22	x	x	x	x	x	⊗	x	x	x	x	x	x	x	x	x	x	x	x	x	x	x	x	x	x	x	x	x	x	x	x
21	x	x	x	x	x	x	⊗	x	x	x	x	x	x	x	x	x	x	x	x	x	x	x	x	x	x	x	x	x	x	x
20	x	x	x	x	x	x	x	x	x	x	x	x	x	x	x	x	x	x	x	x	x	x	x	x	x	x	x	x	x	x
19	x	x	x	x	x	x	⊗	x	x	x	x	x	x	x	x	x	x	x	x	x	x	x	x	x	x	x	x	x	x	x
18	x	x	x	x	x	x	x	x	x	x	x	x	x	x	x	x	x	x	x	x	x	x	x	x	x	x	x	x	x	x
17	x	x	x	x	x	x	x	x	x	x	x	x	x	x	x	x	x	x	x	x	x	x	x	x	x	x	x	x	x	x
16	x	x	⊗	x	x	x	x	x	x	x	x	x	x	x	x	x	x	x	x	x	x	x	x	x	x	x	x	x	x	x
15	x	x	x	x	x	x	x	x	x	x	x	x	x	x	x	x	x	x	x	x	x	x	x	x	x	x	x	x	x	x
14	x	x	x	x	x	x	x	x	x	x	x	x	x	x	x	x	x	x	x	x	x	x	x	x	x	x	x	x	x	x
13	x	x	x	x	x	x	x	x	x	x	x	x	x	x	x	x	x	x	x	x	x	x	x	x	x	x	x	x	x	x
12	x	x	x	x	x	x	x	x	x	x	x	x	x	x	x	x	x	x	x	x	x	x	x	x	x	x	x	x	x	x
11	x	x	x	x	x	x	x	x	x	x	x	x	x	x	x	x	x	x	x	x	x	x	x	x	x	x	x	x	x	x
10	x	x	x	x	x	x	x	x	x	x	x	x	x	x	x	x	x	x	x	x	x	x	x	x	x	x	x	x	x	x
9	x	x	x	x	x	x	x	x	x	x	x	x	x	x	x	x	x	x	x	x	x	x	x	x	x	x	x	x	x	x
8	x	x	x	x	x	x	x	x	x	x	x	x	x	x	x	x	x	x	x	x	x	x	x	x	x	x	x	x	x	x
7	x	x	x	x	x	x	x	x	x	x	x	x	x	x	x	x	x	x	x	x	x	x	x	x	x	x	x	x	x	x
6	x	x	x	x	x	x	x	x	x	x	x	x	x	x	x	x	x	x	x	x	x	x	x	x	x	x	x	x	x	x
5	x	x	x	x	x	x	x	x	x	x	x	x	x	x	x	x	x	x	x	x	x	x	x	x	x	x	x	x	x	x
4	x	x	x	x	x	x	x	x	x	x	x	x	x	x	x	x	x	x	x	x	x	x	x	x	x	x	x	x	x	x
3	x	x	x	x	x	x	x	x	x	x	x	x	x	x	x	x	x	x	x	x	x	x	x	x	x	x	x	x	x	x
2	x	x	x	x	x	x	x	x	x	x	x	x	x	x	x	x	x	x	x	x	x	x	x	x	x	x	x	x	x	x
1	x	x	x	x	x	x	x	x	x	x	x	x	x	x	x	x	x	x	x	x	x	x	x	x	x	x	x	x	x	x

Sensor ID	X	10	9	4	13	6	8	5	2	11	X

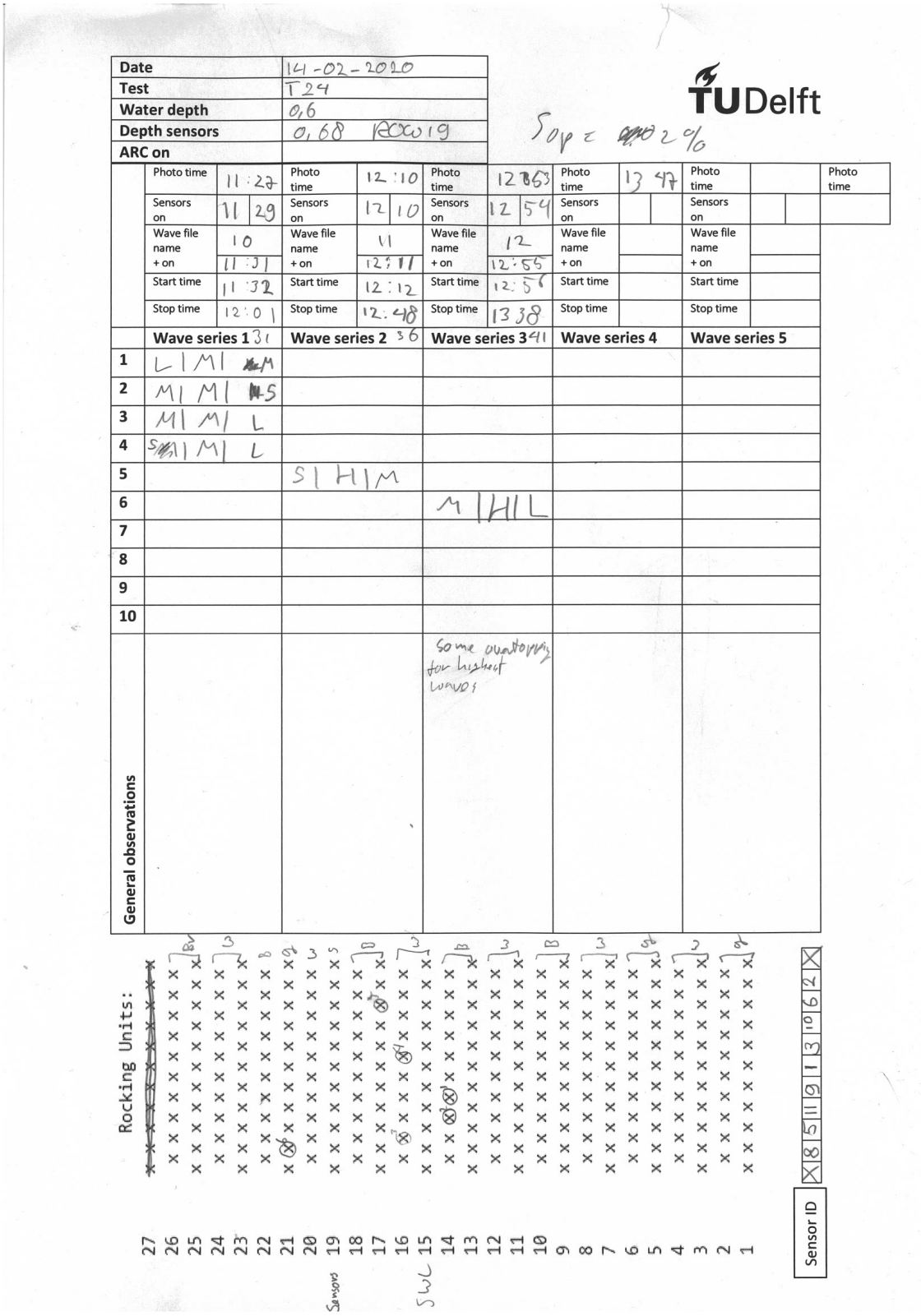

Date		14-02-2020													
Test		T24													
Water depth		0,6													
Depth sensors		0,68													
ARC on															
	Photo time	11:27	Photo time	12:10	Photo time	12 [illegible]	Photo time	13 47	Photo time		Photo time
	Sensors on	11 29	Sensors on	12 10	Sensors on	12 54	Sensors on		Sensors on		Sensors on	
	Wave file name + on	10 11:31	Wave file name + on	11 12:11	Wave file name + on	12 12:55	Wave file name + on		Wave file name + on		Wave file name + on	
	Start time	11:32	Start time	12:12	Start time	12:57	Start time		Start time		Start time	
	Stop time	12:01	Stop time	12:48	Stop time	13 38	Stop time		Stop time		Stop time	
	Wave series 1 31		**Wave series 2** 36		**Wave series 3** 41		**Wave series 4**		**Wave series 5**			
1	L | M | M											
2	M | M | S											
3	M | M | L											
4	S | M | L											
5			S | H | M									
6					M | H | L							
7												
8												
9												
10												
General observations					some overtopping for highest waves							

Sop = 2%

Rocking Units:

Sensors

Sensor ID